MOUNTAIN-PLAINS CONSORTIUM

MPC 19-410 | C. Pantelides, B. Kunwar, and V. McEntee

Seismic Rehabilitation of Reinforced Concrete Bridge Wall Piers

MOUNTAIN-PLAINS CONSORTIUM REGION 8

A University Transportation Center sponsored by the U.S. Department of Transportation serving the Mountain-Plains Region. Consortium members:

Colorado State University
North Dakota State University
South Dakota State University
University of Colorado Denver
University of Denver
University of Utah
Utah State University
University of Wyoming

SEISMIC REHABILITATION OF REINFORCED CONCRETE BRIDGE WALL PIERS

Chris P. Pantelides
Professor

Bhaskar Kunwar
Graduate Student

Vanessa McEntee
Graduate Student

Department of Civil and Environmental Engineering
The University of Utah

December 2019

Acknowledgments

The authors acknowledge the financial support provided by the Mountain-Plains Consortium (MPC) under project MPC-526.

Disclaimer

ABSTRACT

Reinforced concrete bridge wall piers constructed using older codes perform inadequately during strong earthquakes; deficiencies include short reinforcement lap splices, insufficient steel reinforcement ratios in the longitudinal and transverse direction, and inadequate seismic detailing. Three half-scale wall piers were constructed using as-built reinforcement details conforming to older bridge codes; an identical fourth specimen was constructed using current seismic code-compliant reinforcement details. A total of six quasi-static cyclic tests were conducted regarding the weak axis of the wall piers: (i) as-built test of first wall pier, (ii) test of modern code-compliant pier, (iii) retrofit test of second as-built pier using vertical and horizontal CFRP anchors and jackets (R1), (iv) retrofit test of third as-built pier using near surface mounted (NSM) carbon fiber reinforced polymer (CFRP) rods, horizontal CFRP anchors and jackets (R2), (v) repair test of first as-built pier using mild steel NSM bars, horizontal CFRP anchors and jackets (ABRP), and (vi) repair test of code-compliant pier using a CFRP shell with vertical headed steel bars for relocating the plastic hinge (MCRP). The two retrofit methods increased initial stiffness of the as-built pier by 110%, the lateral load-carrying capacity by 73%, and the hysteretic energy dissipation capacity by 67%. The repair method of the as-built pier increased initial stiffness of the as-built pier by 50% and load-carrying capacity by 73% with similar hysteretic energy dissipation. The repair method of the code-compliant pier increased the initial stiffness by 31%, load-carrying capacity by 15%, and hysteretic energy capacity by 55% for lateral displacements that reached a 6% drift ratio.

TABLE OF CONTENTS

LIST OF FIGURES

LIST OF TABLES

EXECUTIVE SUMMARY

The research presented in this report addresses seismic deficiencies found in older reinforced concrete bridge wall piers. These deficiencies include inadequate length of lap spliced bars, low reinforcement ratios for longitudinal and transverse steel reinforcement, and inadequate seismic reinforcement details. Three half-scale wall piers were constructed with older seismic code details and one wall pier with modern code seismic details. One of the piers with older seismic details was tested in the as-built condition and the other two were seismically retrofitted with CFRP rods or vertical CFRP anchors. The retrofits also included CFRP horizontal anchors and CFRP jackets for confinement. The wall pier with modern seismic code details was also tested to failure for comparison. The two retrofitted wall piers increased the initial stiffness, lateral load carrying capacity, and hysteretic energy dissipation of the as-built wall pier. The damaged as-built wall pier was subsequently repaired with steel NSM bars and CFRP anchors and jackets; the damaged modern code wall pier was also repaired using a CFRP donut and headed steel bars. The repairs were successful as they increased the initial stiffness, load carrying capacity, and hysteretic energy of both damaged wall piers.

LIST OF ACRONYMS

AASHTO	American Association of State Highway and Transportation Officials
ACI	American Concrete Institute
ASTM	American Society of Testing and Materials
LRFD	Load Resistance Factor Design
NSM	Near Surface Mounted
FRP	Fiber Reinforced Polymer
CFRP	Carbon Fiber Reinforced Polymer
FEA	Finite Element Analysis
FEM	Finite Element Model
LVDT	Linear Variable Differential Transducer
OpenSEES	Open System for Earthquake Engineering Simulations
SDC	Seismic Design Criteria
UDOT	Utah Department of Transportation

1. INTRODUCTION

This research investigates the seismic performance of bridges constructed with reinforced concrete (RC) wall pier currently in use in southern Utah. These wall piers do not meet the current seismic code. Deficiencies include 14-inch. lap splices located at the interface of footings and wall piers, inadequate reinforcement ratio in longitudinal and horizontal directions, and poor seismic detailing often used in bridge structures prior to 1971. Three half-scale wall piers were constructed using typical as-built inadequate details: one pier was tested in the as-built condition; and two were seismically retrofitted. The three piers were tested under quasi-static cyclic loading to simulate their performance and accumulation of damage during an earthquake. A fourth specimen was built using the current seismic design code and used to compare the performance of the as-built and two retrofitted wall piers.

Six tests were conducted on the four RC wall piers. These included: (i) an as-built control specimen used as reference of the performance of a deficient wall pier, (ii) repair of this control specimen using carbon fiber reinforced polymer (CFRP) sheets and mild steel near-surface mounted (NSM) bars, (iii) retrofit of an as-built wall pier using CFRP NSM bars and CFRP wraps, (iv) retrofit of an as-built wall pier using CFRP sheets and horizontal and vertical CFRP anchors, (v) a current seismic design code-compliant wall pier, and (vi) repair of the code-compliant wall pier using a CFRP donut.

1.1 Background

When a large seismic event occurs, a bridge is required to maintain strength and displacement ductility while being subjected to significant bending and shear forces. In a bridge wall pier, these forces become concentrated at the top and bottom of the member in what is referred to as the plastic hinge region (Wu and Pantelides 2017a). Prior to the San Fernando Earthquake in 1971, and the publication of the first AASHTO Standard Specifications for Highway Bridges, which addressed seismic concerns (AASHTO, 1973), structural members in a bridge were only designed for gravity loads, and a lap-splice of the longitudinal reinforcing steel was often placed in these plastic hinge regions (Hantouche et al. 2015: Kim et al. 2011). These seismically deficient designs also included low-quality concrete, inadequate transverse reinforcement, and deficient lap splice length of longitudinal steel bars (Seifi et al. 2018).

The current seismic bridge design criteria require that wall piers be designed to withstand concrete cracking, cover spalling, yielding of the reinforcing steel, and significant rotational capacity in the plastic hinge region (Jiang et al. 2016). The new AASHTO code (AASHTO 2011) prohibits lap splicing of longitudinal steel bars at the ends of a structural member where a plastic hinge could form. The code also requires seismic detailing of transverse and longitudinal reinforcing steel and increased transverse confinement reinforcement in the plastic hinge region.

Many tall bridges constructed using pre-1971 design criteria exhibited inadequately dimensioned lap splices and transverse reinforcement, which results in weak confinement and insufficient clamping action in the lap splice region to prevent debonding (Elsanadedy and Haroun 2005). During a significant seismic event, the increased drift demand and steel stress reversals cause bond splitting of the lap-spliced longitudinal bars. This bond failure causes flexural and stiffness degradation of the wall pier. Studies following large earthquakes such as Loma Prieta (1989), Northridge (1994), and Kobe (1995) validate this lap splice failure (Priestley et al. 1996). A seismic retrofit is required to improve performance of these deficient bridge wall piers in a strong earthquake.

External confinement is the most common way to increase bond strength of the lap-spliced longitudinal reinforcement. Current retrofit methods to address confinement issues include steel jacketing (Mitchell et al. 1994; Aboutaha et al. 1999; Hantouche et al. 2015) and carbon fiber-reinforced polymer jackets (Priestley et al. 1996; Hawkins et al. 2000; Seible et al. 2002; Harries et al. 2006; Ghosh and Sheikh

2007; Harajli and Dagher 2008; Harajli 2009; Bournas et al. 2015). Most of this research has only been applied to concrete columns, and very little has been studied on jacketing of bridge wall piers.

CFRP jacketing, however, does not typically extend beyond the existing member and into the joint. Thus, the addition of a jacket will not increase flexural resistance and stiffness of the member, but will improve only shear strength, deformation capacity and splicing of longitudinal reinforcement (Bousias et al. 2007). To increase flexural resistance of a member, current retrofit methods include using CFRP vertical anchors (Vrettos et al. 2013; Bournas et al. 2015) or near-surface mounted (NSM) bars, (Bournas and Triantafillou 2009) in conjunction with CFRP jacketing. These (NSM and CFRP vertical anchors) techniques involve placement of reinforcements in the epoxy-filled pre-cut grooves (for NSM) or pre-drilled holes (for CFRP vertical anchors) into the footing.

Recent research on the use of NSM bars and CFRP jacketing shows a significant increase in the flexural capacity (Bousias et al. 2007, Jiang et al. 2016; Seifi et al. 2018). In addition to CFRP jacketing for confinement and vertical anchorage for flexural strengthening, research has shown that the use of horizontal CFRP anchors in conjunction with these methods offers increased confinement, bond strength, shear capacity, and strengthening (Perrone et al. 2009; Kim et al. 2009; Nye et al. 2018). Few studies have been done on the repair of severely damaged concrete wall piers. A plastic hinge relocation technique was developed to repair severely damaged reinforced concrete column specimens by relocation of the plastic hinge to a position slightly higher in the column that remained elastic during the initial test (Priestley et al.1996; Hose et al. 1997; Mahini and Ronagh 2011). A combination of Carbon Fiber Reinforced Polymer (CFRP) wraps and CFRP vertical anchors was one methodused for relocating the plastic hinge (Rutledge et al. 2014). The FRP confinement is more effective for confining circular sections as compared to rectangular or square cross-sections. The flat sides of such cross-sections remain mostly unconfined (Yan and Pantelides 2011). One approach for strengthening rectangular or square columns using FRP confinement is to perform a shape modification of the cross-section into elliptical, oval, or circular sections (Yan and Pantelides 2011).

2. TESTING PROGRAM

2.1 Test Setup

All four of the wall pier specimens were sandblasted; and the corners rounded prior to testing to prevent fiber cutting and ensure optimal bonding. The typical wall pier was anchored to steel beams on the floor of the Civil and Environmental Engineering Structures Laboratory at the University of Utah using 12 1.0 in. (25 mm) 150 ksi (1,034 MPa) threaded bars. The threaded bars were tightened on1 in. (25 mm) plates on the top of the footing to ensure minimal movement of the footings during the test. To run the bars through the footing, 1 ½ in. (38 mm) PVC pipes were embedded into the footing before the concrete was cast. To cyclically test the pier a hydraulic actuator with a 240 kip (1068 kN) capacity was applied at the center of the wall, 12 in. (305 mm) from the top, using a steel collar. The collar consisted of two HSS beams on either side of the wall face bolted together using four 0.75 in. diameter threaded bars. The collar was then connected with a pin to the actuator to ensure that a bending moment was not applied at the top face of the wall. The test set-up is shown in Figure 2.1.

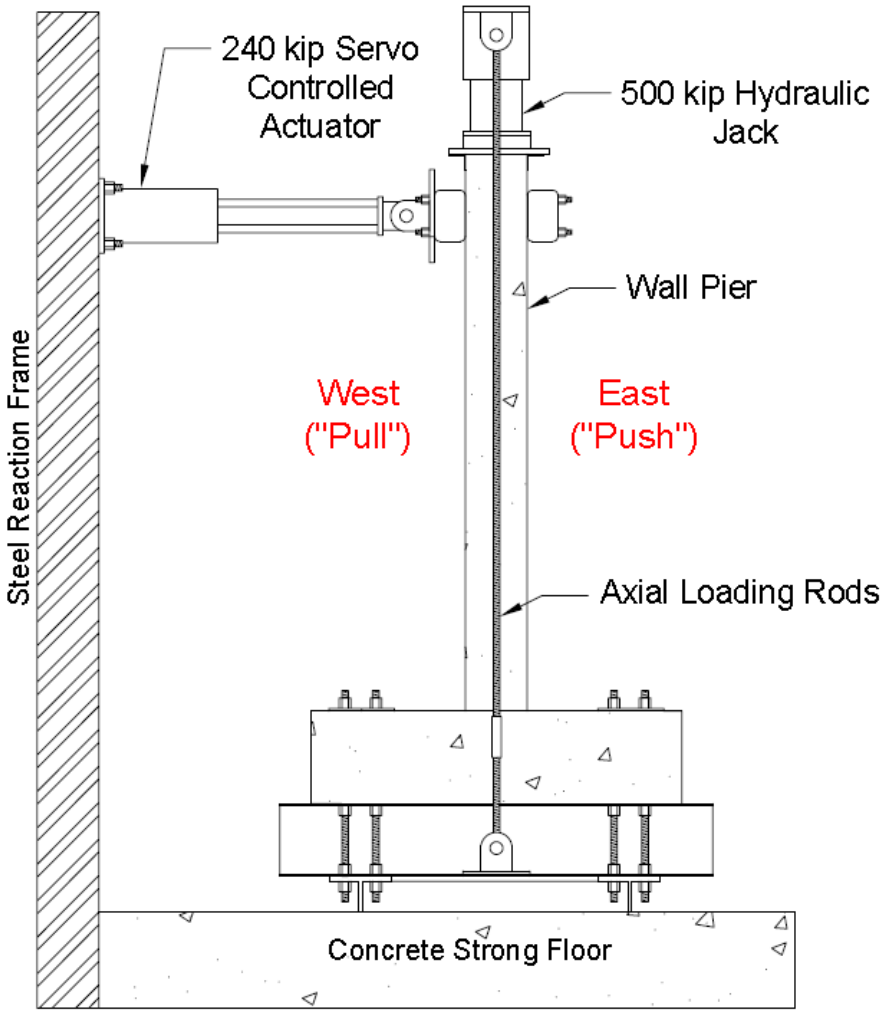

Figure 2.1 Wall test configuration

To simulate a bridge deck and gravity loads, a 500 kip (2,224 kN) hydraulic jack was placed at the top of the wall. This was done by first setting a circular swivel plate on top of the wall, secured by two 3 in. (76 mm) channels welded to the bottom. This plate evenly distributes the load throughout the concrete wall pier. Next, the hydraulic jack was sandwiched between the swivel and a 6 ft (1.83 m) long I-Beam. This I-Beam was attached at both ends to the concrete floor by 15 ft (4.57 m) long and1 in. (25 mm) diameter 150 ksi (1,034 MPa) threaded rods. When engaged, the hydraulic jack pushed against the steel beam and induced an axial load to the specimen via the threaded rods. The axial load was determined to be 6% of the wall pier capacity. The applied axial load was 120 kips (534 kN) and was applied to reproduce the bridge deck gravity effects.

2.2 Loading Protocol

A quasi-static cyclic horizontal load was applied to each wall using displacement control. The loading was based on wall drift and began in increments of 0.5% for the first three drift ratios and then increased by 1% increments. The wall was loaded at a rate of 1.2 in./min (30 mm/min), at two cycles per drift ratio, for the first four drift ratios (i.e. 0.5%, 1%, 1.5%, 2%, and 3%). It was then increased to 4 in./min (102 mm/min) for the remaining cycles (i.e. 4%, 5%, 6%, 7%, 8%, 9%, and 10%). The loading protocol is shown in Figure 2.2. The axial load was applied prior to the beginning of the test and was held constant throughout the entire experiment.

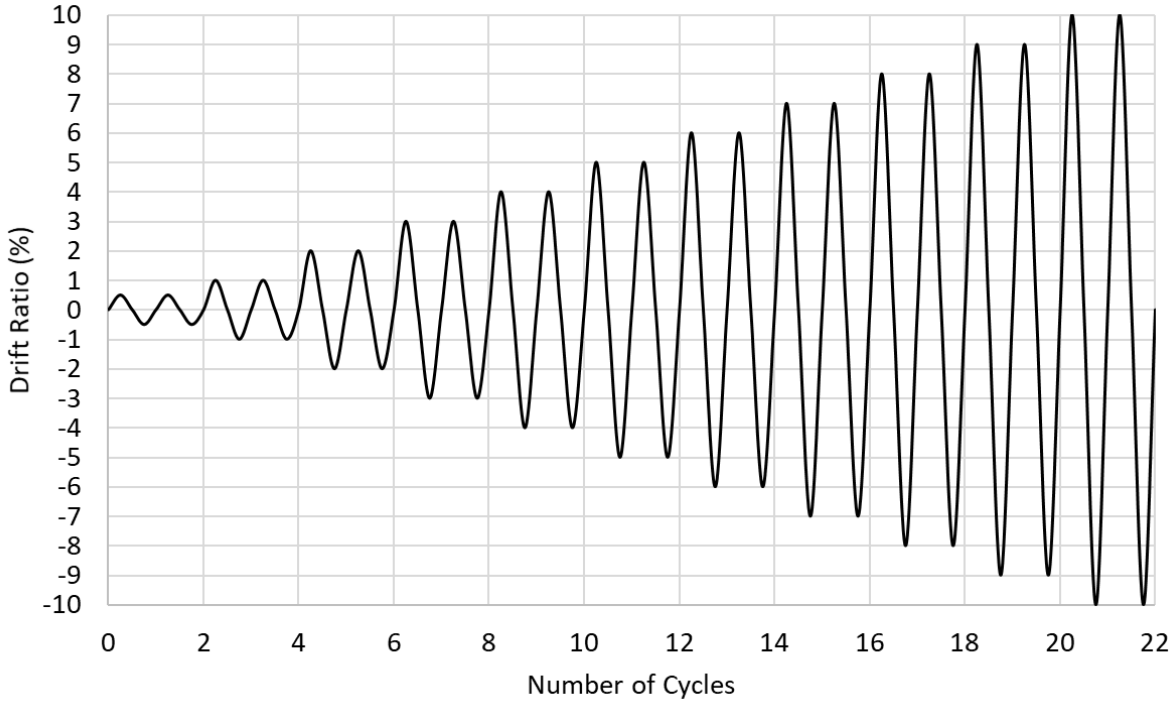

Figure 2.2 Loading protocol

2.3 Material Properties

The 28-day strength of the concrete used was 4,500 psi (31 MPa) and had reached 5,100 psi (35 MPa) on the day of the tests. The concrete mix design is shown in Table 2.1 Grade 60 reinforcing steel was used and tested to determine tensile properties. The average yield stress of the steel was determined as 65 ksi (448 MPa), and the ultimate strength as 103 ksi (710 MPa) from testing.

Table 2.1 Material Properties

Concrete Materials	**Density, lbs./ft3 (kg/m3)**
Cement B	20.46(327.70)
Fly ash	4.55 (72.94)
Fine Aggregate (sand)	65.71 (1052.54)
Coarse Aggregate (chip)	41.13 (658.89)
Water	7.47 (119.70)
High Range Water Reducer	0.046 (0.742)
Air Entrainment	0.0046 (0.0742)

2.4 As-built Wall Pier Design

The wall pier dimensions represent a 1:2 scale of an actual wall pier. The replicated wall dimensions were 9 ft x 4 ft x 1 ft (2.74 m x 1.22 m x 0.30 m) and the footing dimensions were 6 ft x 5 ft x 1.5 ft (1.83 m x 1.52 m x 0.46 m). The wall has two curtains of No. 3 (10 mm) vertical steel rebar spaced at 7.5 in. (190 mm) on each face, and a No. 3 (10 mm) transverse steel bar spaced at 9 in. (229 mm) on center. The top 18 in. (457 mm) of the wall had additional reinforcement to create a beam that could withstand the actuator loading. This included the addition of 10 No. 6 (19 mm) transverse bars in conjunction with No. 4 (13 mm) stirrups spaced at 4 in. (102 mm).

The footing was comprised of No. 5 (16 mm) bars spaced at 6 in. (152 mm) on the top and bottom, confined with 17 No. 3 (10 mm) double stirrup located externally and internally. The lap splices consisted of 14 No. 3 (10 mm) bars 25 in. (635 mm) long and extending 14 in. (356 mm), or 37 bar diameter, $d_{b,}$ above the footing. The lap splices were the only connection between the wall pier and footing. The reinforcement details can be seen in Figure 2.3. The as-built reinforcement during construction can be seen in Figures 2.4-2.6.

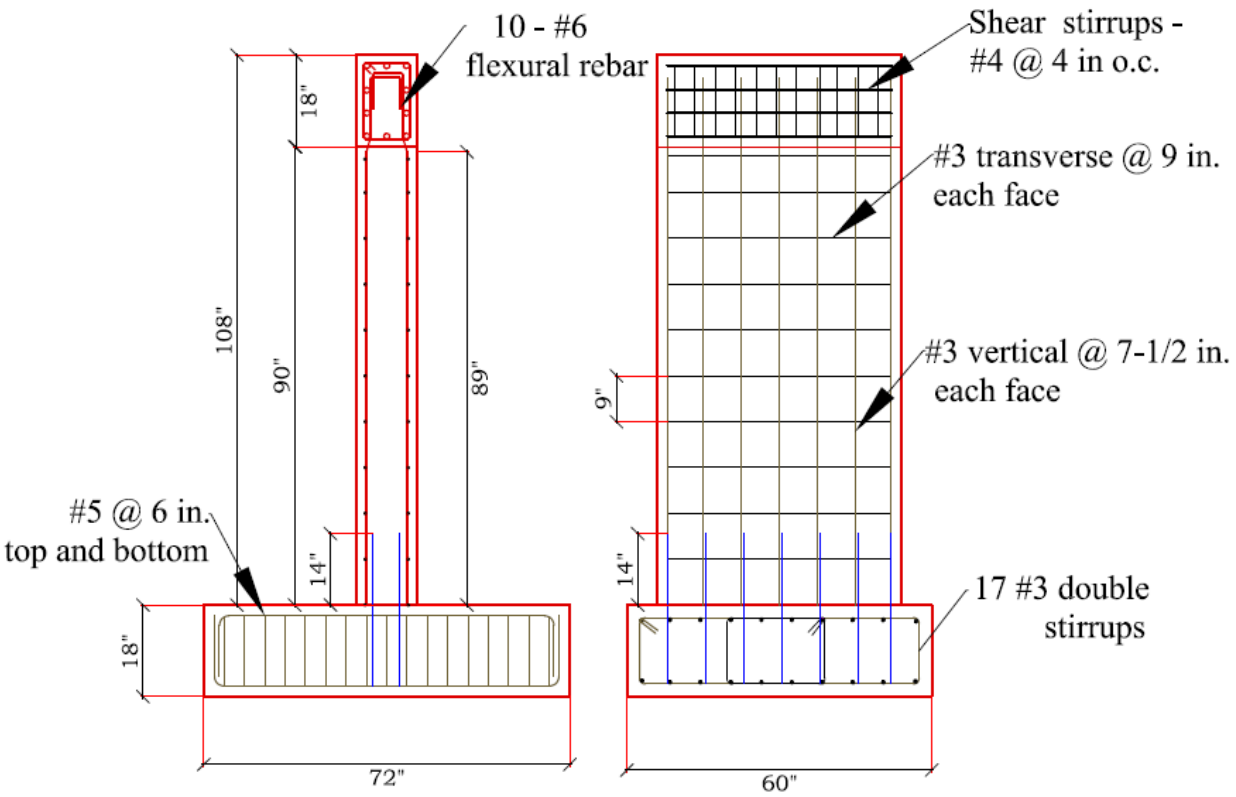

Figure 2.3 As-built wall reinforcement

Figure 2.4 Lap-spliced bars in the footing

Figure 2.5 As-built wall footing reinforcement

Figure 2.6 As-built wall pier reinforcement

2.5 Modern Wall Pier Design

The control test specimen was a half-scale model of a reinforced concrete modern bridge wall pier, which met seismic requirements of newly constructed highway bridges. The wall pier cross-sectional dimensions of the specimen were chosen considering a 1:2 scale of the cross-sectional properties of an actual as-built wall pier. They were identical to those of the as-built pier described in Section 2.4. The longitudinal and transverse steel bars, their configuration, and footing were designed accordingly from the cross-sectional properties. The final height of the specimen was fixed at 9 ft (2.74 m) including a 1 ft (0.30 m) embedded beam in the top section of the wall pier. The beam was designed separately and was heavily reinforced to withstand and effectively transmit the lateral load. The lateral load was applied at a height of 8 ft (2.44 m) from the top of the footing. Two curtains of steel reinforcement were provided. Fourteen #6 (19 mm) steel bars were placed in the longitudinal direction with seven bars on each face. In addition, #4 (13 mm) transverse hoops were provided with a 4 in. (102 mm) spacing in the plastic hinge region and a 9 in. (229 mm) spacing for the remaining height. The longitudinal and transverse reinforcement ratio was 1.07% and 1.7%, respectively. However, outside the plastic hinge region, the transverse reinforcement ratio was 1.07%, which is still higher than 1% as required by the AASHTO (2011) code. The reinforcement layout of the current code-compliant specimen can be seen in Figure 2.7.

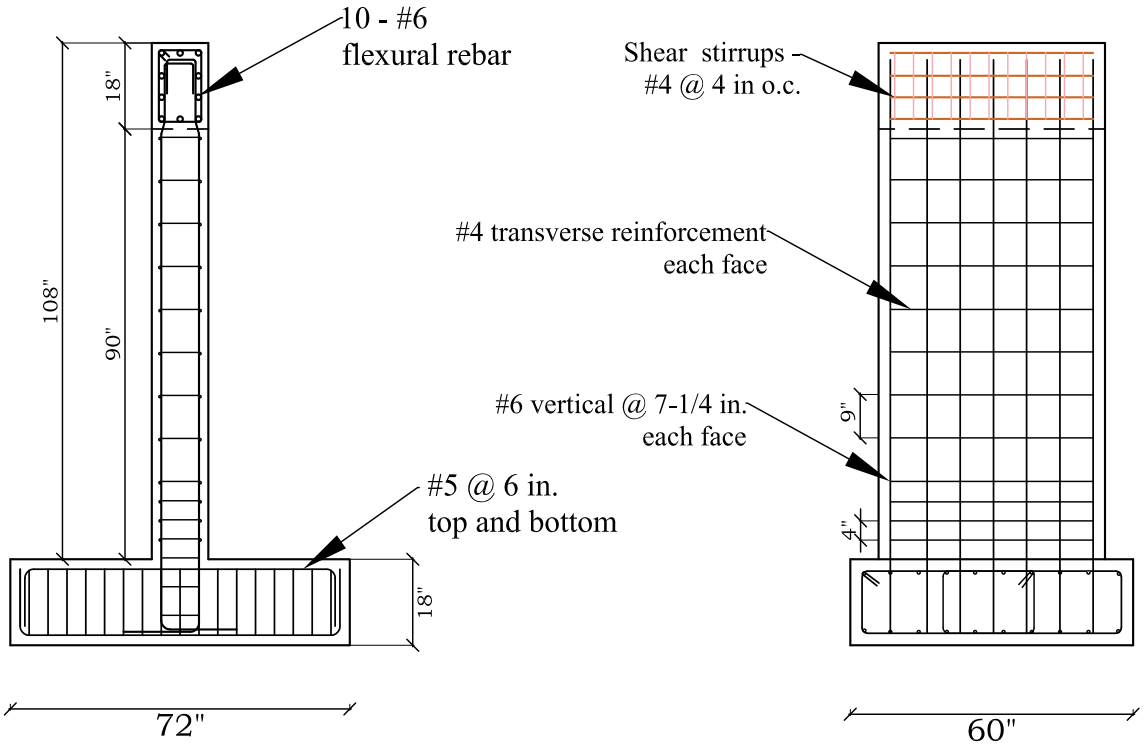

Figure 2.7 Reinforcement details of current code-compliant specimen

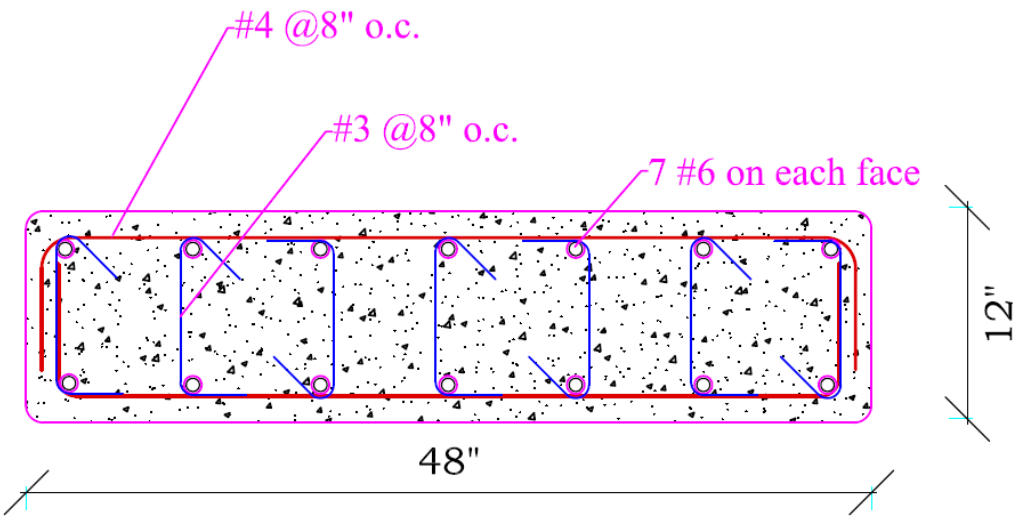

Figure 2.8 Code compliant wall pier cross-section

Figure 2.9 Code compliant wall pier reinforcement

2.6 Pier Wall Instrumentation

Thirty strain gauges were applied to the steel reinforcement in each specimen to measure strain behavior of the bars throughout the test. Twelve gauges were applied on the center two lap-spliced bars to determine potential yielding of the lap-spliced bars at the most critical region of the wall. Three additional gauges were applied to the center of the lowest transverse reinforcing bars to determine strain in the wall pier in the hoop direction. This configuration was repeated for both sides of the wall. The strain gauge layout can be seen in Figure 2.10. For the modern wall pier specimen, 11 strain gauges were applied to steel reinforcement on each steel curtain, as shown in Figure 2.11 for a total of 22 strain gauges.

LVDTs were used to measure the displacement at selected locations. Ten LVDTs mounted with five on each side were used to measure the rotation and relative displacement at the attached point. The LVDT layout is shown in Figure 2.12. Data from the LVDTs was used to study curvature distribution along the wall pier's vertical axis.

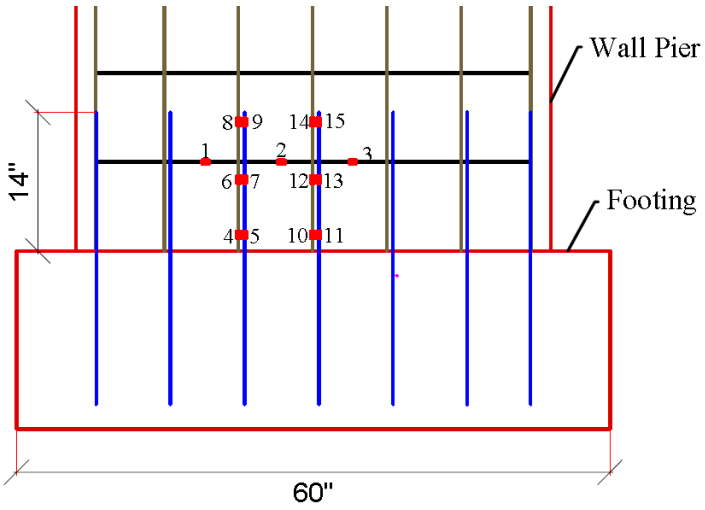

Figure 2.10 As-built wall pier strain gauge set-up

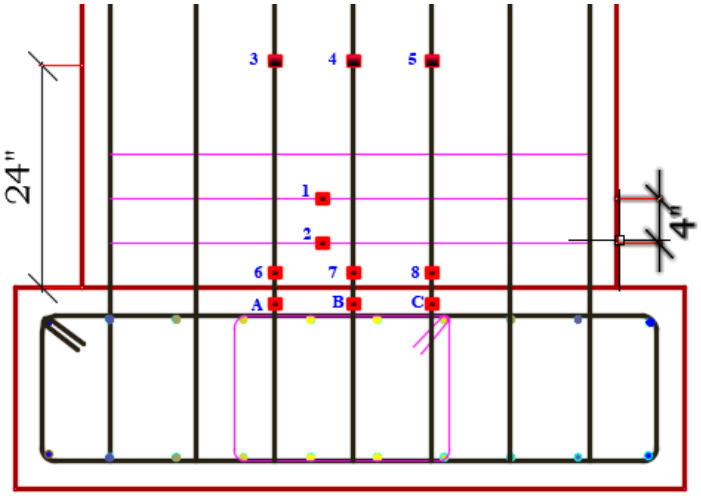

Figure 2.11 Strain gauge set up in modern wall pier

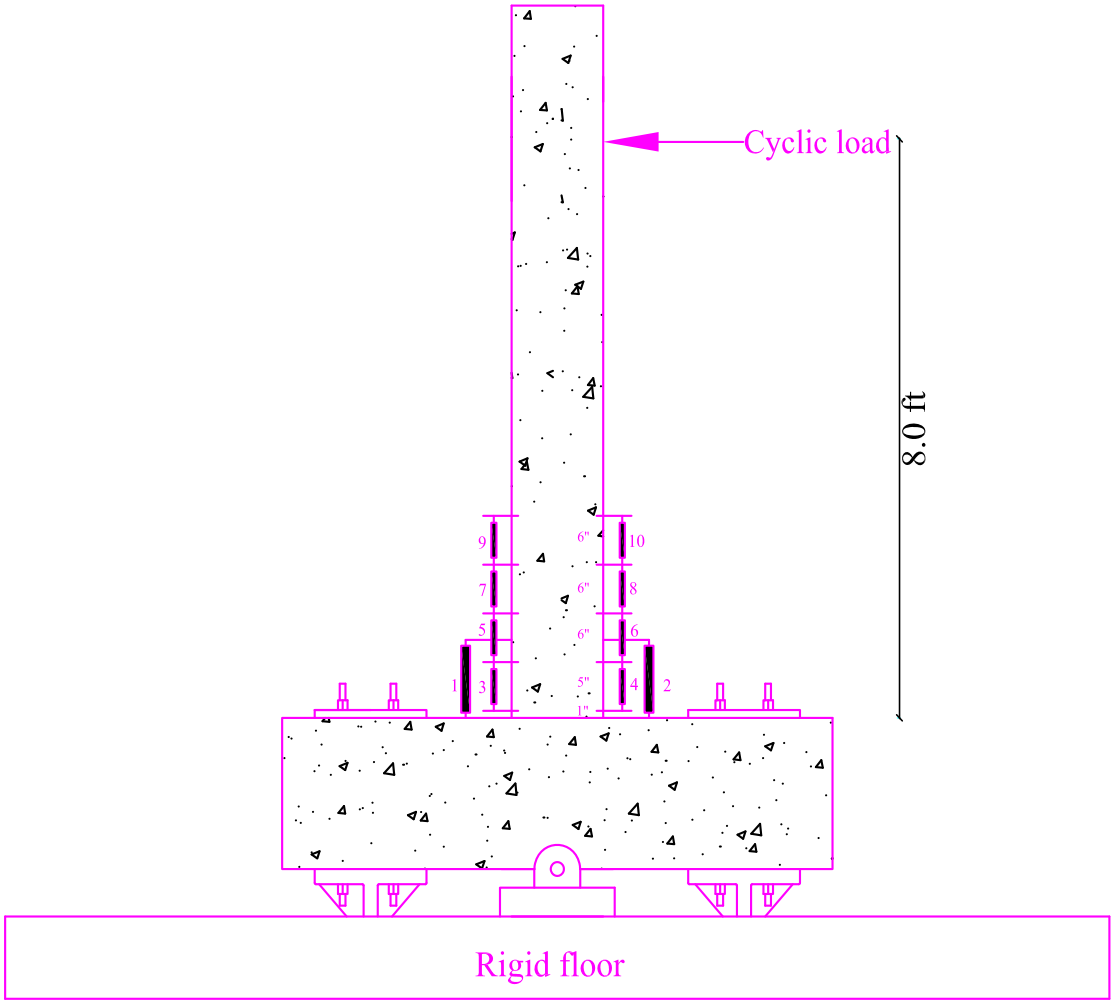

Figure 2.12 General sketch of LVDTs layout

2.7 Wall Pier Performance Evaluation Criteria

2.7.1 Displacement Ductility

The ability of a structure to endure large cyclic deformations without significant strength degradation is represented by the displacement ductility ratio, μ_{Δ}, and is expressed by:

$$\mu_{\Delta} = \frac{\Delta_u}{\Delta_y} \tag{2.1}$$

where Δu represents the ultimate displacement indicated by a 20% drop in the ultimate lateral load strength of the wall pier, and Δy represents the yield displacement. To get this value, the backbone of the experiment was plotted by taking average peak strength value for each load cycle in the "push" and "pull" directions. Then an idealized elastoplastic curve was formulated to have the same energy dissipation as the experimental backbone. The slope of the idealized backbone was found using 50% of the maximum yield force, over the displacement at this location (Wu and Pantelides 2017a). The equal energy rule was applied to find the effective yield displacement of the idealized curve.

2.7.2 Plastic Rotation

The plastic rotation capacity of a structure is the ratio of plastic displacement to height of the specimen. In the case of the wall pier, this height was from the top of the footing to the center of lateral load application. The specimens' plastic rotation capacity (θ_p) was represented by:

$$\theta_p = \frac{\Delta_p}{H} \tag{2.2}$$

$$\Delta_p = \Delta_u - \Delta_y \tag{2.3}$$

where, Δ_p is the difference between the displacement at ultimate lateral load, Δ_u, and the yield displacement, Δ_y. H is defined as the height of the wall pier, which was 96 in. (2.44 m), as shown in Figure 2.12.

2.7.3 Hysteretic Energy Dissipation

Hysteretic energy is the ability of the wall pier to dissipate energy through inelastic deformation. This energy is represented by the area inside the hysteresis loops and is indicative of whether or not the system is ductile and also indicates the combination of strength and displacement ductility performance. The energy dissipation can also be determined by summing the hysteretic energy from each cycle of the hysteretic loops. After each cycle, the energy dissipated by the structure is indicated by the area under the force-displacement curve. The summation of all energy values for all cycles until failure will give the hysteretic energy capacity of the specimen.

2.7.4 Stiffness Degradation

The hysteresis plot indicates stiffness behavior throughout testing of the wall pier. The stiffness, *k*, for each cycle is defined as follows:

$$k = \frac{F_{max}}{\delta_{max}} \tag{2.4}$$

where F_{max} represents the maximum load for a cycle and δ_{max} signifies the corresponding maximum deflection. The hysteretic stiffness is the average value for each "push" and "pull" cycle.

2.7.5 Damage Assessment

The Park and Ang (1985) damage index was used to better categorize the severity of damage exhibited by the wall pierThis comparison plots the drift ratio with a damage indication index. The Park and Ang damage index (Faustino and Chastre 2016, Park and Ang 1985) is found using:

$$PA = \frac{\Delta_i}{\Delta_u} + \frac{\beta}{F_y * \Delta_u} \int^d E \tag{2.5}$$

where Δ_i is the maximum lateral displacement taken at each drift ratio; Δ_u is the ultimate lateral displacement of the specimen; F_y is the yield force found in the backbone curve in Section 2.7.1; *E* is the cumulative hysteretic energy at each increment; and β is the strength deterioration parameter (Faustino and Chastre 2016, Park and Ang 1985).

$$\beta = 0.9^{100\rho_w}(0.37max(\theta, 0.05) + 0.5(w_t - 0.17)^2 \tag{2.6}$$

where ρ_w is the volumetric confinement ratio of the wall; w_t is the longitudinal steel ratio, and θ is the normalized axial stress.

The damage levels were chosen based on previously described damage descriptions mainly for bridge columns. The *PA* damage index levels are indicated in Table 2.2.

Table 2.2 Damage Index Levels

Damage Level	*PA* Damage Index	Description
Minor	0.0 – 0.20	Minor cracks or partial crushing of concrete
Moderate	0.2 – 0.5	Extensive large cracks or spalling of concrete
Severe	0.5 –1.0	Extensive crushing of concrete or visible buckled reinforcement
Collapse	> 1.0	Partial or total collapse

2.8 CFRP Design for As-built Wall Pier Retrofit and Repair

The as-built specimen presented deficiencies that needed to be addressed in the seismic retrofit design. The objective of the retrofit design was to increase the overall seismic performance of the wall pier by increasing the drift ratio capacity, lateral load capacity, initial stiffness, and hysteretic energy dissipation. The first retrofit (R1) was a combination of vertical CFRP anchors and horizontal CFRP anchors confined by layers of unidirectional CFRP sheets placed in the hoop direction. The second retrofit (R2) was a combination of CFRP NSM bars and CFRP jackets oriented in the hoop direction. The repair of the as-built wall (ABRP) consisted of mild steel NSM bars and hoop direction CFRP jacketing as described in Chapter 7. The following subsections will outline the design process for each CFRP geometric form. The design of the modern code wall repair (MCRP) will be addressed in Chapter 8.

2.8.1 CFRP Vertical Anchors and CFRP and Mild Steel NSM Bars

Vertical CFRP anchors were used for retrofitting specimen (R1), CFRP NSM bars were used to retrofit specimen (R2), and mild steel NSM bars were used to repair the as-built wall (ABRP). Each vertical component was implemented to increase flexural capacity and energy dissipation. Since the vertical CFRP layers are terminated at the interface between the footing and wall, their flexural strength and stiffness contribution is negligible (Bousias et al. 2007). An equivalent tension force method was applied to determine the number of vertical anchors needed. The maximum tension force from an AASHTO code-compliant wall pier at the maximum bending moment was set equal to the required tension force resistance of the as-built wall. Due to the seismically deficient lap-splices, and their short lap splice length, their contribution was neglected. The area required by the anchors was found as follows:

$$\{A_s * f_u\}_{code} = C_E * \psi_{f*} C_{f*} \{A_f * f_{fu}\}_{as-built} \quad (2.7)$$

where A_s is the total area of reinforcement in the code compliant wall, 3.08 in^2 (19.87 mm^2); f_u is the ultimate tensile strength of the steel reinforcement in the code compliant wall, 93.5 ksi (645 MPa); C_E is an environmental reduction factor per ACI-440 (2004), equal to 0.85; ψ_f is a reduction factor for the flexural strength contribution of the FRP reinforcement (ACI-440 2004), equal to 0.85; C_f is a reduction factor for FRP under compressive force, equal to 0.8; f_{fu} is the design ultimate tensile strength of the CFRP anchors, equal to 165 ksi (1,138 MPa); A_f is the required area of anchors for the tensile strength requirement.

From Eq. (2.7) we get an A_f equal to 3.02 in^2 (19.5 cm^2). For the retrofit, 0.75 in. (19.05 mm) diameter CFRP vertical anchors were used. The cross-sectional area of one of these anchors is approximately 0.44 in^2 (2.84 cm^2). Thus, a minimum of seven anchors or NSM bars for each side of the wall were needed. Nine vertical anchors were used to prevent flexural failure at ultimate tension force. The anchorage length had to be determined to ensure that the vertical CFRP or mild steel component did not pull out of the footing. The pullout failure can be avoided if anchorage length of the fiber anchors or mild steel bar is 40-60 times the diameter of the fiber anchor (Jiang et al. 2016). This method is developed for CFRP NSM bars; however, it was also considered for application of vertical CFRP anchorage and mild steel NSM bars. The anchorage length obtained using this method is 30 in. (762 mm) to 45 in. (1524 mm) deep. Since the pier wall footing is only 18 in. (457 mm) deep, that was the maximum embedment depth that could be met.

To develop the maximum FRP stress in the given section, the anchorage depth should be larger than the following equation (Hassan and Rizkalla 2004):

$$L_{db} = \frac{d_b}{4*\tau_b} f_{fd} \tag{2.8}$$

where L_{db} is the critical length required to develop effective FRP stress; d_b is the diameter of the CFRP anchor, 0.75 in. (19 mm); τ_b is the average bond strength, which ranges from 500-3,000 psi (3.5–20.7 MPa); τ_b was taken as an average of this range to be conservative, 1,500 psi (10.3 MPa); and f_{fd} is the design stress:

$$f_{fd} = C_E \psi_f C_f f_{fu} \tag{2.9}$$

The variables for the design stress equation are defined in Eq. (2.7). The value of f_{fd} was 95.4 ksi (658 MPa). Using the design stress in Eq. (2.9), the critical development length was equal to 11.92 in. (303 mm). This development length was less than the 40-60 bar diameter suggested by Jiang et al. (2016). The provided length of anchorage in the test was 18 in. (457 mm) or 24d_b, which was the maximum possible and equal to the depth of the footing.

2.8.2 NSM Groove Design

Dimensions of the groove for the CFRP and mild steel NSM bars significantly affects performance of the bond of the NSM bar. It is recommended that the minimum groove dimension is 1.5 times the diameter of the NSM bar (ACI-440 2004; Galati and De Lorenzis 2009; Sharaky et al. 2013). Further studies also recommend that the width to depth ratio for the groove be 1.0. (ACI-440 2004; Galati and De Lorenzis 2009; Jiang et al. 2016; Sharaky et al. 2013). A clear distance between the grooves is suggested as (ACI-440 2004):

$$d_{clear} \geq 2 * d_{groove} \tag{2.10}$$

where d_{groove} is the depth of the NSM bar groove.

Considering these recommendations, a groove dimension of 0.75 in. (19 mm) by 0.75 in. (19 mm) was provided. The spacing of these bars was at a minimum, 5.0 in. (127 mm). Using Eq. (2.10) we had a minimum spacing of 1.5 in. (38.1 mm), thus 5.0 in. (127 mm) met this spacing requirement. The location of these mild steel NSM bars varies across the wall face to avoid the existing wall reinforcement.

2.8.3 CFRP Jacketing

The CFRP wrap adds shear strength and increases energy dissipation of the structural member (Seifi et al. 2018, Pantelides and Gergely 2002). In addition, the jacketing adds confinement and deformation capacity in the lap-splice region (Bousias et al. 2007). The number of CFRP wraps for specimens (R1, R2, and ABRP) was determined using the flexural hinge and shear demand of the lap-splice region. The thickness required for adequate lap splice clamping is as follows (Seible et al. 1997):

$$t_j = 500 \frac{D(f_l - f_h)}{E_j} \tag{2.11}$$

where t_j is the required thickness for lap splice confinement; f_h is the horizontal stress given by the existing mild steel hoop reinforcement, taken here as zero because seismic hooks were not used in the construction; D is the column dimension in the loading direction, taken as the wall thickness of 12 in. (304.5 mm); f_l is the lateral clamping pressure over the lap splice; and E_j is the jacket elastic modulus in the hoop direction, 12.5×10^6 psi (86,100 MPa). The equation for lateral clamping pressure can be found using (Seible et al. 1997):

$$f_l = \frac{A_s f_{sy}}{[\frac{p}{2n} + 2(d_b + cc)]L_s} \tag{2.12}$$

where A_s is the area of one main wall reinforcing bar, 0.11 in^2 (70.96 mm^2); f_{sy} is the yield strength of the lap spliced bar, 65 ksi (448 MPa); p is the perimeter line of the cross-section of the wall pier where the lap splices are located, 108 in. (2743 mm); n is the number of spliced bars along the perimeter, 14; d_b is the diameter of the lap spliced bar, 0.375 in. (9.5 mm); cc is the concrete cover of the main steel bar reinforcement from the edge, 2.063 in. (52.4 mm); and L_s is the length of the lap splice, 14 in. (355.6 mm).

Using Eq. (2.12), the lateral clamping pressure for the retrofit was 59 psi (405 MPa). Substituting this into Eq. (2.11), the required thickness of the jacket was 0.0287 in. (0.729 mm). When divided by the 0.04 in. (102 mm) thickness of the CFRP sheets, it was determined that one sheet is required for confining the lap splice. The required CFRP jacketing thickness for the confinement demand of the wall was determined using the following (Moran and Pantelides 2012):

$$t_{j,sh} = (\frac{f_{co}}{E_j})(\frac{H_c * \lambda_{SH}}{4C_{sh}}) \tag{2.13}$$

where f_{co} is the unconfined compressive strength of the concrete, 4,500 psi (31 MPa); λ_{SH} is the factor that accounts for the aspect ratio (Moran and Pantelides 2012):

$$\lambda_{SH} = 3[1 + {\alpha_{sh}}^2]^2 \tag{2.14}$$

where α_{sh} is the aspect ratio of the CFRP shell, equal to 1.5 (Moran and Pantelides 2012; 2019);

$$\alpha_{sh} = \frac{H_c}{B_c} \tag{2.15}$$

H_c is the effective height of the jacket, 12 in. (304.8 mm); B_c is the effective breadth of the CFRP shell, 8.0 in. (203.2 mm); these values were reduced from the actual dimension of the wall pier because the horizontal anchors in each specimen decreased the effective breadth of the wall; C_{sh} is the jacket confinement ratio coefficient and is defined as (Moran and Pantelides 2012):

$$C_{sh} = \frac{1+\alpha_{sh}}{2} * 1 + \frac{3*(\gamma_{sh})^2}{10+\sqrt{4-3(\gamma_{sh})^2}} \tag{2.16}$$

and,

$$\gamma_{sh} = \frac{\alpha_{sh}-1}{\alpha_{sh}+1} \tag{2.17}$$

Using Eq. (2.13-2.17), it is determined that the required thickness for the shear demand is 0.028 in. (0.711 mm); thus, one layer of fiber was required for confinement.

The thickness of CFRP jacketing to prevent a shear failure was determined by (Seible et al. 1997):

$$t_j = \frac{\frac{V_o}{\phi v}-(V_c+V_s+V_p)}{2*0.004*E_j*D} \tag{2.18}$$

V_o is the unconfined wall shear demand, given as 42.3 kips (188.2 kN) from computer analysis; ϕ_v is the shear capacity reduction factor, 0.85; V_s is the horizontal steel reinforcement contribution, taken as zero; V_p is the axial load contribution, taken as zero; and D is the pier wall dimension in the loading direction, 12 in. (304.8 mm); V_c is the concrete shear contribution found using (ACI-318 2014);

$$V_n = A_{cv}(\alpha\sqrt{f'_c} + \rho_t f_y) \tag{2.19}$$

$$V_{max} = 0.83A_{cv}\sqrt{f'_c}) \tag{2.20}$$

V_n is the nominal shear strength of the wall; A_{cv} is the cross-sectional area of the wall pier, 576 in^2 (0.37 m^2); α is a coefficient corresponding to the height-to-width ratio, 2.0; f'_c is the concrete compressive strength, 5,100 psi (35 MPa); ρ_t is the transverse reinforcement ratio, 0.002; and f_y is the yield strength of the transverse reinforcement, 65 ksi (450 MPa); and V_{max} is the maximum allowable shear contribution. From Eq. (2.19) the nominal shear capacity is 151.4 kips (673.4 kN). However, Eq. (2.20) limits the shear contribution, V_c, of the wall to 34.1 kips (151.9 kN). From Eq. (2.18), we get a jacket thickness of 0.013 in. (0.34 mm), which amounts to one CFRP layer.

From the lap splice shear and confinement equations, three layers of CFRP jacketing were required for the retrofit design. An additional hoop direction layer was added to provide two layers of confinement on the outside of the horizontal anchors and to allow transitions between fiber segments. Two layers of CFRP sheets were also added in the vertical direction to sandwich the vertical anchors. This sandwiching effect contributes to a greater capacity of CFRP anchors (Nye et al. 2018). The height of the jacket above the footing was determined using (Elsanadedy et al. 2005):

$$L_j > (1.0 - \alpha * \frac{M_{u(existing)}}{M_{u(retrofit)}}) \tag{2.21}$$

where L_j is the height of the CFRP jacket, α is the safety factor less than 1.0 (0.85 was used); L_c is the height of the column, 96 in. (2.44 m); $M_{u(existing)}$ is the ultimate lateral force or moment capacity of the existing pier wall, 15.2 kip-in (1.72 kN-m); and $M_{u(retrofit)}$ is the ultimate lateral force or moment capacity of the target retrofit of the wall pier, 31.6 kip-in. (3.6 kN-m). The existing and retrofit moments were

determined using an OpenSees pushover analysis. From Eq. (2.21) we get the height of the jacket for each specimen equal to 57 in. (1.44 m).

2.8.4 CFRP Horizontal Anchors

CFRP Jacketing of a rectangular column is not as effective as jacketing a circular column. This results in an uneven stress distribution with higher confinement near the corners, and less in the middle of the wall (Kim et al. 2011: Moran et al. 2019). To increase efficiency of rectangular jacketing, horizontal CFRP anchors were added near the bottom of the jacketing. These anchors divide the sections of unconfined CFRP jacketing and increase confinement capacity.

The compressive force required by the horizontal anchors to prevent bond-splitting failure is as follows (Hantouche et al. 2015):

$$\mu * F_l = 1.85 * n_s * A_b * f_y \tag{2.22}$$

where μ is the coefficient of friction of steel embedded in concrete, 0.6 (Rabbat and Russell 1985); F_l is the required compression force of the anchorage; n_s is the number of spliced bars on each face, in this case, equal to 14; A_b is the area of one spliced bar, 0.11 in^2 (0.71 cm^2); and f_y is the yield force of a mild steel reinforcing bar from testing, 65 ksi (450 MPa). From Eq. (2.22), we obtained a required anchorage force of 308.6 kips (1,372.7 kN). The diameter of the anchors was obtained using (Hantouche et al. 2015):

$$d_a = \sqrt{\frac{4*LF*F_a}{\pi*\varphi_a*F_{ya}}} \tag{2.23}$$

where LF is the load factor, 1.3; φ_a is the resistance factor for axial tension, 0.9; and F_{ya} is the tensile capacity of one CFRP anchor, 165 ksi (1,138 GPa). F_a is the applied pretension force per anchor, found as the maximum effective tensile force on one horizontal CFRP anchor:

$$F_a = A_f * f_{ya} \tag{2.24}$$

where A_f is the cross-sectional area of an 0.75 in. (19 mm) diameter anchor [0.15 in^2 (98.4 mm^2)]. From Eq. (2.24) we had a maximum effective tensile force of 25.2 kips (111.9 kN).

From Eq. (2.23) we get the required anchor diameter is 0.53 in. (13.5 mm). The diameter of each anchor was rounded up to the nearest 0.25 in. (6.35 mm). Thus, the chosen anchors were 0.75 in. (19.05 mm) in diameter.

When we multiplied the anchor tensile capacity of 165 ksi (1,138 GPa) by the area of the CFRP anchor, taken as 0.44 in^2 (283.9 mm^2), we found that each anchor contributed 72.6 kips (322.9 kN) in tension. We then divided the required anchorage force of 308.6 kips (1372.7 kN) found using in Eq. (2.22), by 72.6 kips (322.9 kN) of force per anchor and found that we needed anchors. To confidently restrain the lap splice region, a total of 10 0.75 in. (19.05 mm) diameter horizontal CFRP anchors were used for each specimen (R1, R2, and ABRP); five anchors were placed at 8 in. (203 mm) above the footing and five anchors were placed 16 in. (406 mm) above the footing.

3. PERFORMANCE OF AS-BUILT BRIDGE WALL PIER

3.1 Introduction

The reinforced concrete bridge wall pier was an as-built half-scale replica of an existing wall pier. Prior to the current seismic code, wall piers were designed only for gravity loads, and lap splices were placed in the base of the footing. The lap splice in this region was suspected to be the failure mode of the reinforced bridge wall pier. This is due to spalling of the concrete at the base of the wall, and subsequent failure of the unconfined steel lap splices. The as-built wall pier was tested to determine the true behavior in a seismic event. The performance was characterized by the lap splice behavior, load versus displacement, and hysteretic energy dissipation of the wall pier.

3.2 Wall Design of As-built Wall Pier

The wall pier reinforcement and design are shown in Figure 2.3. This wall pier was tested without any modifications to the design and without the addition of a retrofit system. The actual wall pier before testing can be seen in Figure 3.1.

Figure 3.1 As-built wall pier

3.3 Comparison of As-built Wall Pier to New Code

The AASHTO LRFD Bridge Design and LRFD Seismic Design (2012) provisions require that a bridge wall pier should be designed and detailed as follows:

a) The longitudinal rebar spacing should not exceed 1.5 times the minimum wall dimension or 18 in. (457 mm)
b) The minimum shear reinforcement ratio ρ_w should exceed 0.4%
c) The longitudinal reinforcement ratio ρ_l should fall between 1% and 4%
d) There should not be any lap-splicing of longitudinal rebar in the plastic hinge region
e) The spacing of transverse reinforcement in the plastic hinge region should not exceed 4 in. (102 mm)
f) U-shaped or closed hoops should be used in the corner regions of the piers
g) A seismic hook should confine the opposite face longitudinal bar together. The bend on one side should be 135° and the other side should have a bend of 90° and should extend a minimum of 6 bar diameters d_b or 3 in. (76 mm)
h) The displacement ductility μ_d of the wall pier in the weak direction should not exceed five

A comparison of the as-built design and the AASHTO seismic design criteria is shown in Table 3.1. From this table, it is clear that the only criteria that the as-built wall pier met was the longitudinal reinforcement spacing of less than 1.5 times the wall thickness or 18 in. (576 mm). Other than that, it did not meet the required reinforcement ratios for either the longitudinal or transverse direction. The as-built wall pier had lap-splices in the plastic hinge region, and the spacing of transverse reinforcement exceeded the 4 in. (102 mm) maximum in this region; therefore, it lacked all required seismic detailing.

Table 3.1 Design criteria comparison

Criteria	AASHTO SDC Wall Pier	As-Built Wall Pier	Meets Requirement
Longitudinal Reinforcement Ratio	18 in. (457 mm)	7.5 in. (191 mm)	Yes
Minimum Shear Reinforcing Ratio	0.40%	0.27%	No
Minimum Longitudinal Reinforcing Ratio	1.00%	0.20%	No
Lap Splicing in Plastic Hinge Region	No	Yes	No
Maximum Transverse Bar Spacing in Plastic Hinge Region	4 in. (102 mm)	9 in. (229 mm)	No
U-Shaped or Closed Hoops	Yes	No	No
Seismic Hoop at Opposite Corners	Yes	No	No
Maximum Displacement Ductility	5	7.1	No

3.4 Test Results for As-built Wall Pier

The as-built control specimen was tested under quasi-static loading with five-minute breaks in-between cycles. An axial load of 120 kips (534 kN) was applied at the top of the wall pier for the duration of the experiment. This load corresponded to 6% of the axial load carrying capacity of the wall pier and simulated a bridge deck. Crack sizes and material degradation were observed throughout the test, with various data collection mechanisms to determine wall pier behavior and damage.

3.4.1 Displacement Ductility of As-built Wall Pier

Following the procedure outlined in Section 2.7.1, the ultimate displacement indicated by a 20% drop in the ultimate lateral load strength of the wall pier was 5.76 in. (146.3 mm), the yield displacement was 0.81 in. (21 mm), resulting in a displacement ductility ratio of 7.1 for the system. Figure 3.2 shows the idealized backbone developed using this procedure. It should be noted that even though the displacement ductility of the wall was high, the lateral load capacity was very low. This resulted in a very weak wall pier that dissipates a relatively small amount of hysteretic energy.

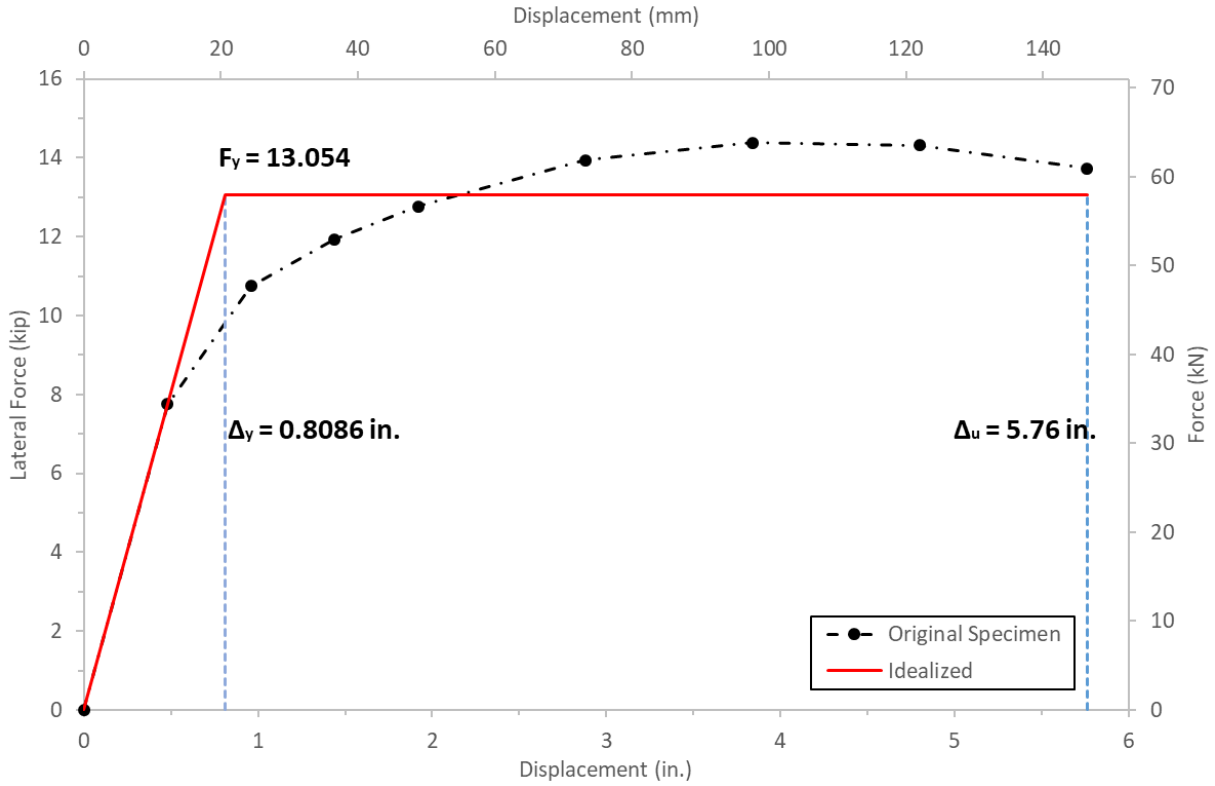

Figure 3.2 As-built displacement ductility

3.4.2 Plastic Rotation of As-built Wall Pier

The plastic rotation capacity of the as-built wall pier was found using the procedure outlined in Section 2.7.2 and can be seen in Figure 3.3. From this plot, it can be seen that the specimen reached 0.05 rad of plastic rotation before its ultimate failure at 6% drift ratio. The plastic rotation of 0.05 rad combined with the displacement ductility ratio of 7.1 signified a large lateral drift ratio. However, when the plastic rotation was compared to the low lateral load resistance, the cyclic performance of the wall pier was not satisfactory.

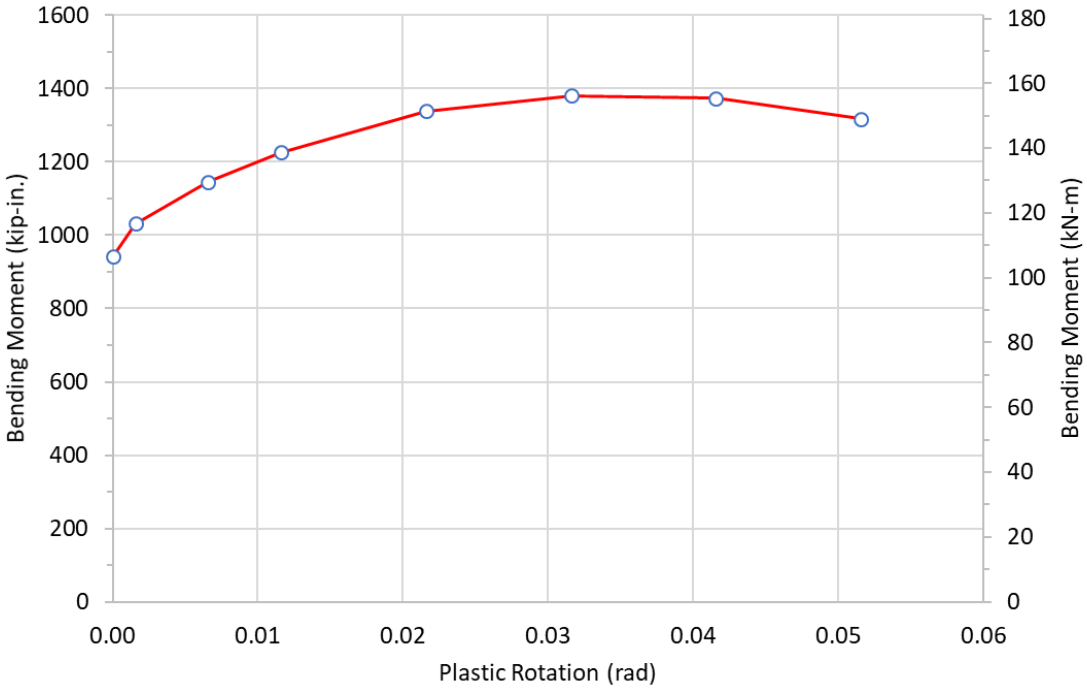

Figure 3.3 Plastic rotation of as-built wall pier

3.4.3 Hysteretic Energy Dissipation of As-built Wall Pier

The specimen hysteresis is shown in Figure 3.4. This plot clearly exhibits the overall behavior of the wall pier during testing. There was pinching in the center, which defined behavior of the plastic hinge formed at the base of the wall pier and the occurrence of lap splice failure in a gradual manner. The hysteresis was seemingly stable throughout the test until the wall pier begin to fail at the 6% drift ratio. Failure of the lap splices could be seen at this point by the significant drop in lateral load in the first cycle of the 6% drift ratio.

The cumulative hysteretic energy dissipation throughout the test is shown in Figure 3.5. Total dissipated energy for the as-built pier wall was 500 kip-in. (56.5 kN-m). From this parameter, it can clearly be seen that the overall performance of the as-built specimen was not satisfactory.

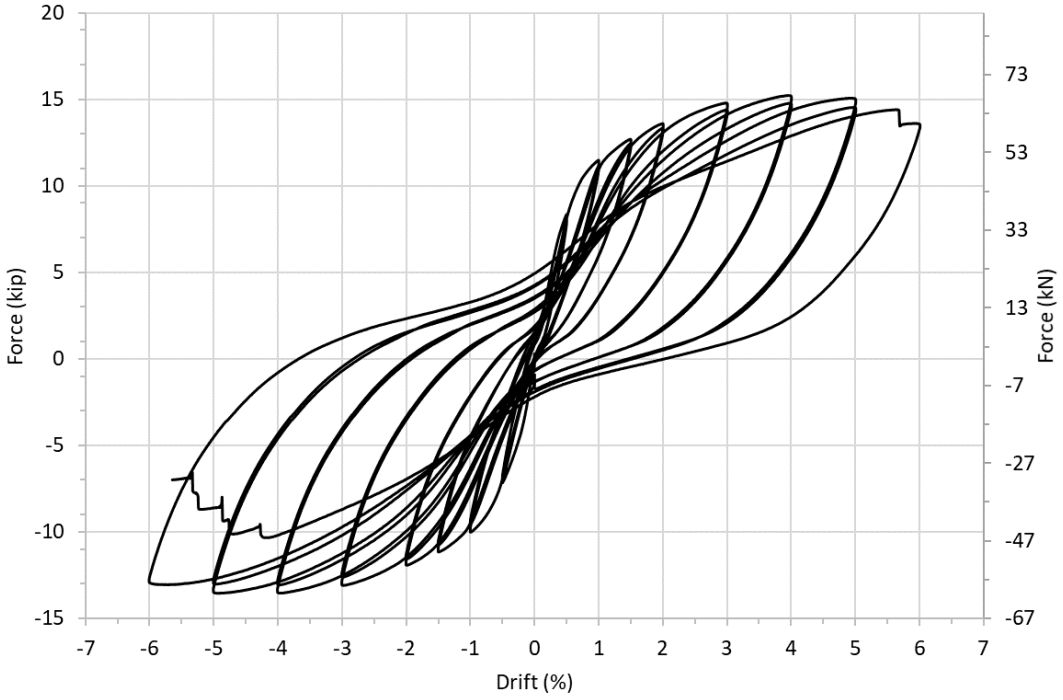

Figure 3.4 Hysteresis of as-built wall pier

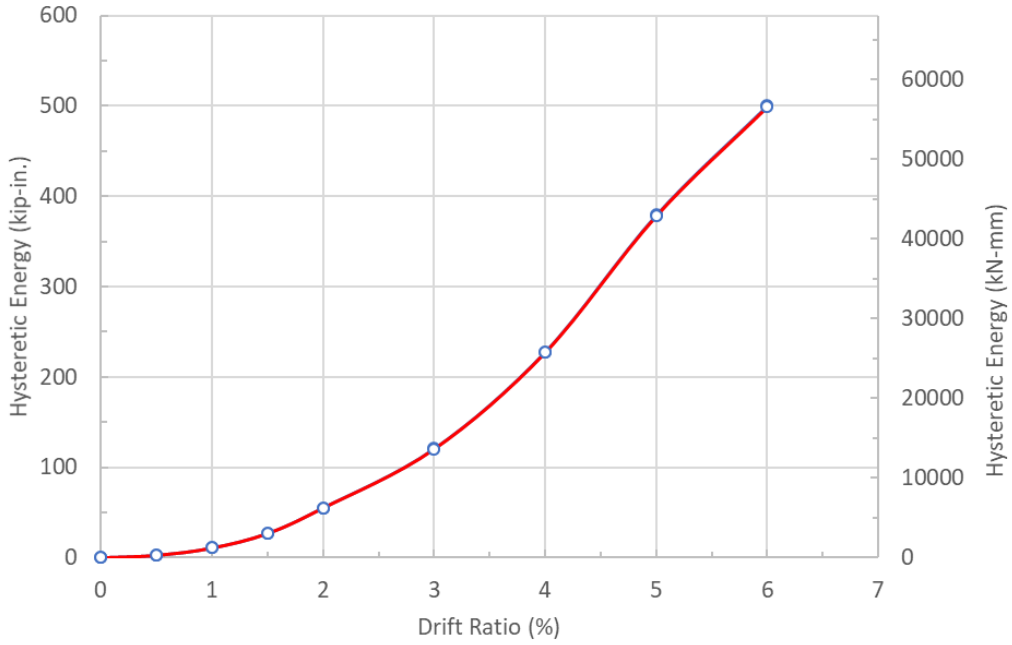

Figure 3.5 Cumulative hysteretic energy dissipation

3.4.4 Stiffness Degradation of As-built Wall Pier

The average hysteretic stiffness was calculated as described in section 2.7.4. Figure 3.6 shows the stiffness values plotted against the drift ratio of the specimen. The as-built specimen exhibits smooth stiffness degradation throughout the test. However, the initial stiffness of the specimen of 16 kips/in. was rather low to start with and the final stiffness of 2 kip/in. was very low.

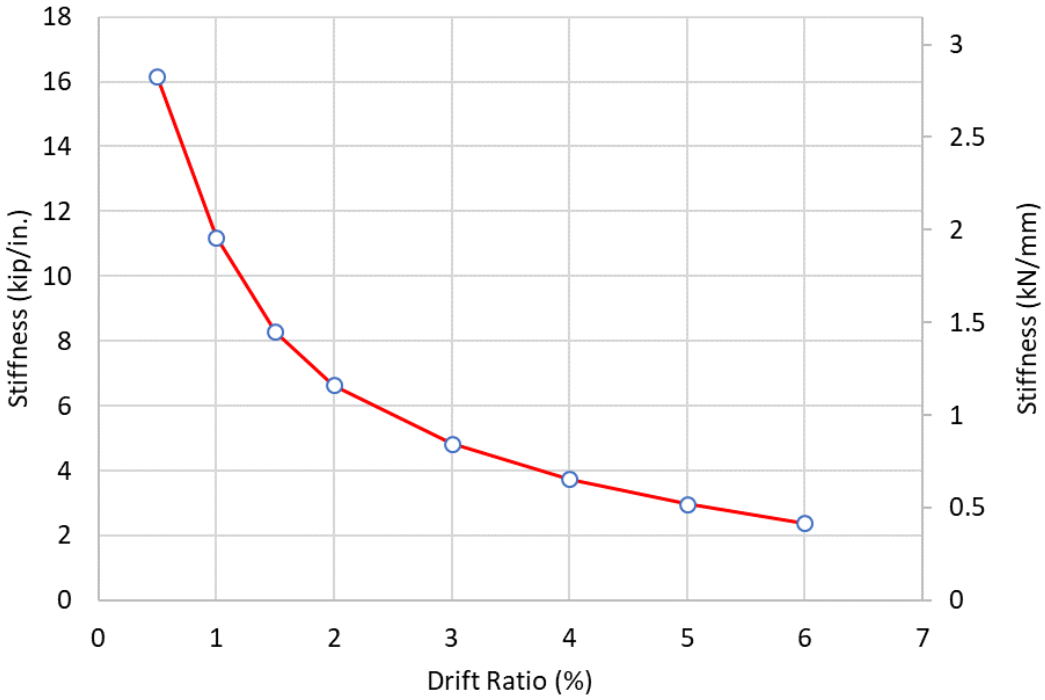

Figure 3.6 Stiffness deterioration of the as-built specimen

3.4.5 Damage Index of As-built Wall Pier

The damage index discussed in Section 2.7.5 was applied to the as-built wall pier test. The index is shown in Figure 3.7. Plotted against the four damage limits described in Table 2.2, the graph shows the damage state of the wall pier at each drift ratio. The specimen reached moderate damage at 1% drift ratio and severe damage at 2% drift ratio. The collapse stage did not occur until the wall pier reached 5% drift ratio. The specimen reached ultimate failure in the first cycle of 6% drift ratio. The plot accurately depicted this failure and the overall performance of the structure under cyclic loads simulating strong earthquakes.

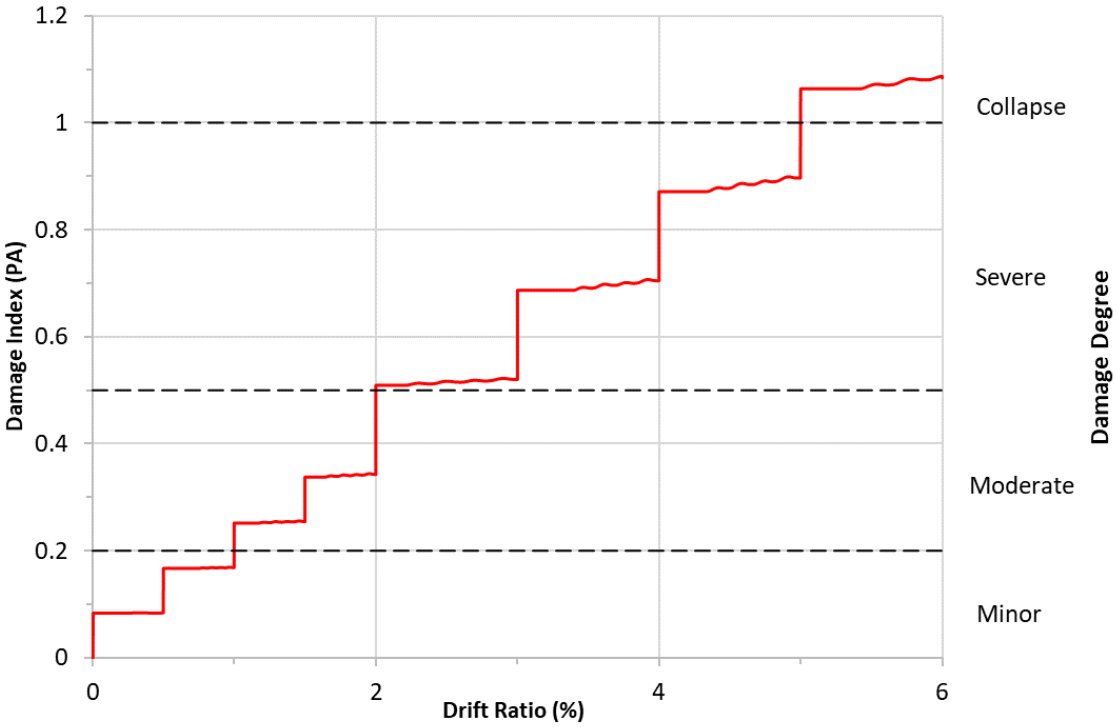

Figure 3.7 Damage index of as-built specimen

3.4.6 Lap Splice Strain of As-built Wall Pier

Figure 3.8 shows the strain in the lap splice bars in the wall pier. The strain from this image was the maximum strain in the lap splices during the test and was located 11 in. (279 mm) above the footing. This figure shows that the lap splices did not develop the yield strain during the test, but actually the lap-spliced bars in the wall reached the yield point. Moreover, the difference in strain values between the bars in the footing and bars in the wall pier was about 1,000 microstrain. This difference in strain indicates lap splice failure occurred.

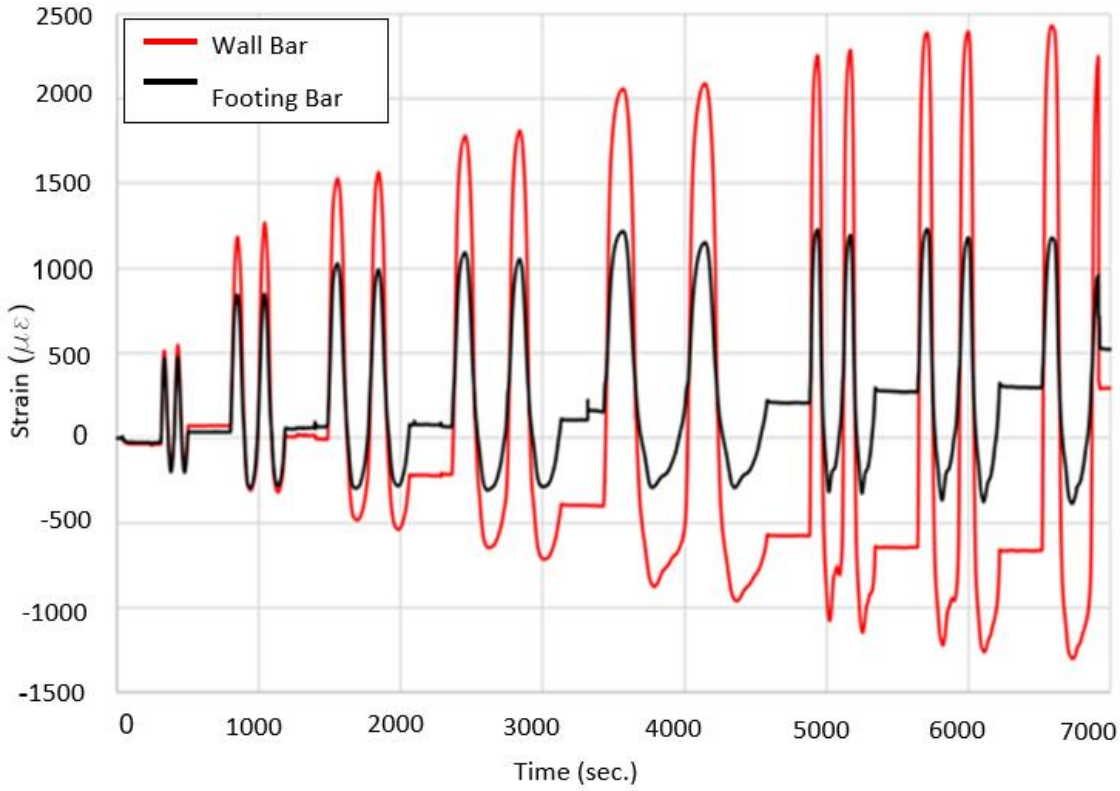

Figure 3.8 As-built wall pier strain in lap-spliced bars

3.4.7 Physical Damage of As-built Wall Pier

Cracks did not begin to develop until the second load step, at 1% drift ratio. At this time, cracks 0.002 in. (0.051 mm) wide began to form 8.0 in. (203 mm) from the top of the footing on both sides of the wall pier. These cracks ran horizontally across the pier and were seen as high as 26 in. (660 mm) above the footing. A small crack at the interface between the footing and wall pier became visible at this time. At the 1.5% drift ratio, more cracks began to develop in the same height range as the 1% drift ratio. At 1.5% drift ratio, cracks also began to lengthen but did not exceed 0.002 in. (0.051 mm) in width. Vertical cracks also began to form, connecting the horizontal cracks. Cracking at 1.5% drift can be seen for both sides of the wall in Figure 3.9(a) and 3.9(b). At 2% drift ratio, the existing cracks measuring 0.013 in. (0.33 mm) began to widen on both sides of the wall pier, but no new damage was seen. During the 3% cycle, the plastic hinge had formed completely. The lateral resisting load reached its maximum for the test of 15.2 kips (68 kN) in the "push" direction, denoted in Figure 2.1. No additional damage accrued on the wall face instead, the plastic hinge crack grew to 0.03 in. (0.76 mm) wide in some locations. By the 4% drift ratio, the plastic hinge crack was 0.125 in. (3.2 mm) wide and large pieces of concrete had begun to spall off as shown in Figure 3.10. The lateral load began decreasing at the 4% drift ratio to a maximum of 15.1 kips (67 kN) and was not recovered. In the first pull sequence of the 6% drift ratio, the wall failed most likely due to a complete loss of the lap splices tension capacity on the east side of the wall. At this point, the load dropped to 6.9 kips (31.1 kN), a decrease of 46% from the maximum wall lateral load capacity.

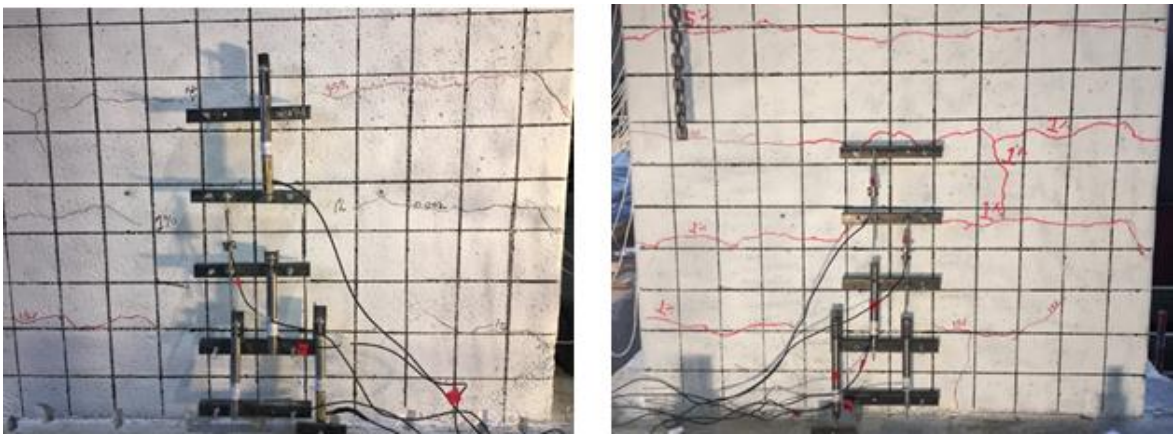

Figure 3.9 Cracking at 1.5% drift: (a) West facing side (b) East facing side

Figure 3.10 Spalling at 4% drift of as-built wall pier

3.5 Analytical Model of As-built Wall Pier

The wall pier and its components were modeled as a fiber section using OpenSees (McKenna et al. 2014). This command allows the object to be composed of fiber-containing UniaxialMaterial with an area and location. Concrete is modeled as confined and unconfined concrete. The strength of confined concrete was manually calculated and taken as the input. The provided transverse reinforcement was not meant to confine the core, so the compressive strength of the confined and unconfined concrete was the same. UniaxialMaterial Concrete 04 was used to construct a uniaxial Popovics (1973) concrete material object with degraded linear unloading/reloading stiffness. The Steel02 material was used to construct a steel material object with isotropic strain hardening. This was a basic model, so the lap splices were not modeled. Pushover analysis was performed for the developed model. Figure 3.11 shows the result of the preliminary pushover analysis performed in OpenSees, which indicated 15.4 kips as the maximum probable lateral force resisting capacity of the specimen. The model failed at a 5.9% drift ratio as a result of concrete crushing and reinforcement failure. As shown in Figure 3.12, the pushover result matched the experimental cyclic test. The wall pier was minimally reinforced with 0.27% of longitudinal

reinforcement. Comparing the test result obtained through the OpenSees and the experiment, the comparison symbolized that the lap splice failure and yielding of the rebar may occur at a similar time. The footing was designed to remain elastic to resist the maximum predicted lateral load without any visible damage.

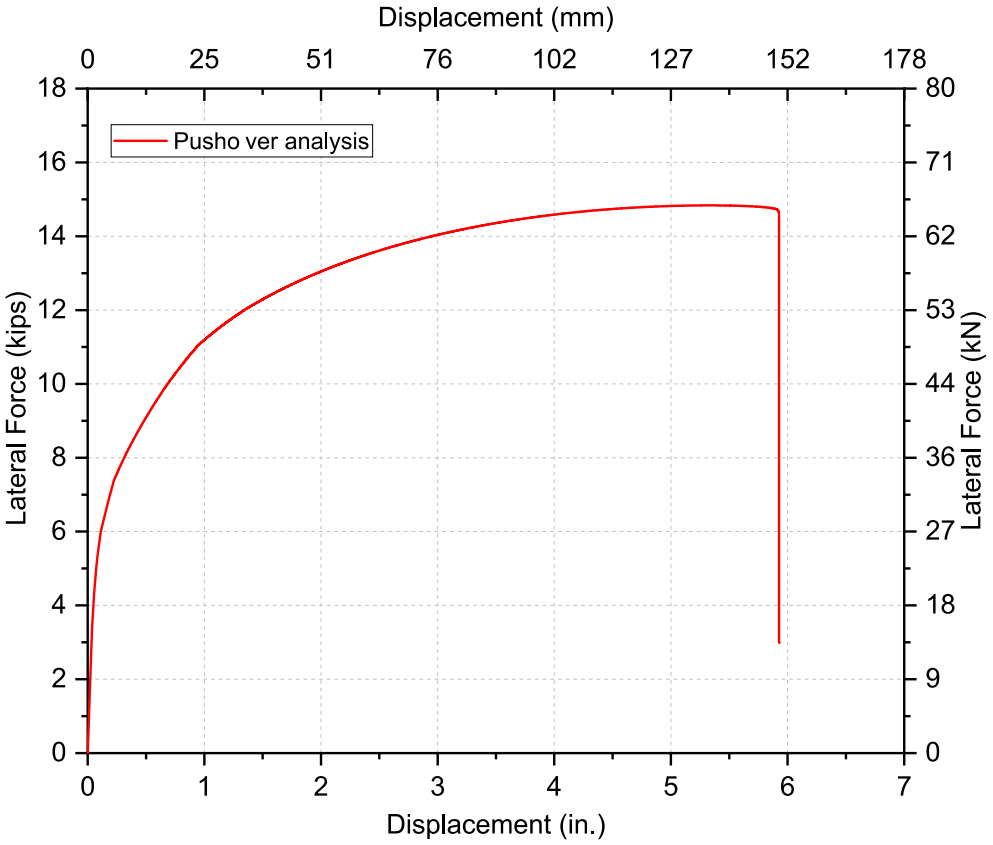

Figure 3.11 Preliminary pushover analysis of the as-built wall pier

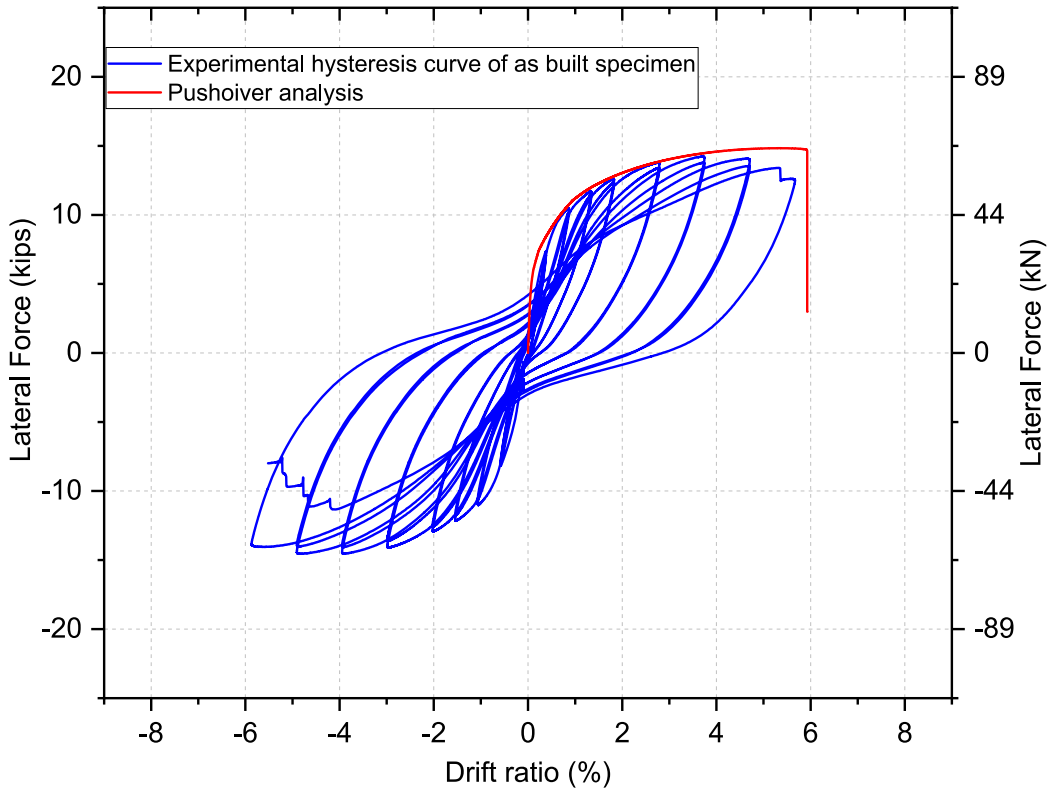

Figure 3.12 Comparison of OpenSees pushover and experimental result for as-built wall pier specimen

3.6 Conclusion for As-built Wall Pier

The as-built reinforced concrete wall pier was tested under quasi-static cyclic loading. The pier failed in the second cycle of the 6% drift ratio due to failure of the lap splices on the east side of the wall. The east side exhibited more damage than the west side of the wall pier because the test began with a pull, stressing the east side of the wall, allowing more damage to accrue on that side throughout the test.

The as-built wall pier behaved poorly, and although it made it completed 15 cycles of testing up to 6% drift, the energy dissipation of 500 kip-in. (56.54 kN-m) was six times less than the modern code-compliant wall pier, which reached 2,857 kip-in (323 kN-m). The lateral load resisting capacity of the wall pier degraded gradually and would have performed poorly in a significant earthquake, potentially collapsing in the case of a strong earthquake. The summary of the as-built wall performance is shown in Table 3.2.

Table 3.2 As-built wall pier test summary

Maximum Force (kip (kN))	15.2 (68)
Drift Ratio at Maximum Force (%)	4.0
Maximum Drift Ratio (%)	6.0
Maximum Displacement (in. (mm))	5.76 (146)
Number of Cycles	15
Energy Dissipation (kip-in. (kN-m))	500.4 (56.5)

4. PERFORMANCE OF MODERN CODE COMPLIANT BRIDGE WALL PIER

4.1 Introduction

The current seismic bridge design code clearly defines the design criteria for designing columns and wall piers. Bridge structures are designed such that under cyclic lateral load, the structural component undergoes concrete cracking, cover spalling, and reinforcement yielding with a significant amount of rotation in the plastic hinge regions without collapse. To facilitate the performance comparison of the old as-built wall pier with the current code-compliant wall pier, a half-scale control specimen was detailed and designed to simulate the performance of modern bridge wall piers with concrete dimensions identical to the as-built wall pier. The steel reinforcement for this specimen was designed based on the AASHTO LRFD Bridge Design Specifications (2012) and AASHTO Guide Specification for LRFD Seismic Bridge Design (2011). This research was performed for seismically active regions such as the State of Utah, where the design falls under Seismic Design Category (SDC) C or D.

To improve the seismic characteristics of the wall pier, the modern AASHTO (2012) code prohibits splicing of longitudinal steel bars at the end regions where plastic hinges may develop during strong earthquakes. The minimum amount of transverse and longitudinal reinforcement was provided with proper seismic detailing for the steel reinforcement outlined in the current codes. The longitudinal steel reinforcement is held together with seismic hooks, and the plastic hinge regions are confined with closely spaced transverse steel ties.

4.2 Wall Design of Modern Wall Pier

The wall pier reinforcement and design were provided in Section 2.5. The modern code compliant wall pier specimen is shown in Fig 4.1.

Figure 4.1 Modern code compliant wall pier

4.3 Test Results for Modern Wall Pier

The modern code compliant wall pier control specimen was tested under reversed cyclic quasi-static lateral load with a constant axial load of 120 kips (534 KN). This load corresponds to 6% of the axial load capacity of the wall pier. The test results include experimental observations while performing the test and analysis of the obtained data to evaluate the hysteretic behavior, ductility capacity, energy dissipation capacity, plastic rotation, and moment-curvature of the specimen.

4.3.1 Displacement Ductility of Modern Wall Pier

Following the procedure outlined in the modern wall pier section 2.7.1, the ultimate displacement indicated by a 20% drop in the ultimate lateral load of the wall pier was 9.62 in. (244.35 mm). Yield displacement was 1.815 in. (46.10 mm), resulting in a displacement ductility ratio of 5.3 for the system. Figure 4.2 shows the idealized backbone developed using this procedure. The figure shows a large amount of dissipated energy in the nonlinear region with good overall performance by the system.

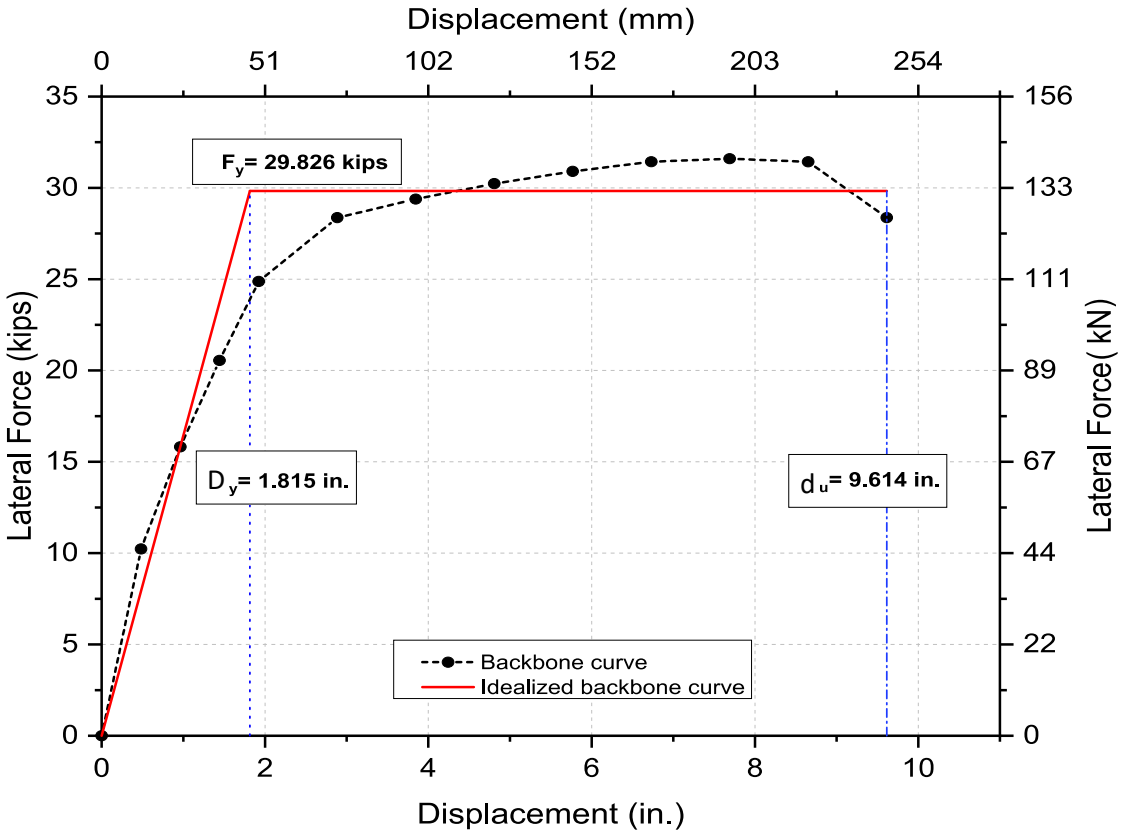

Figure 4.2 Displacement ductility plot for modern code compliant wall pier

4.3.2 Plastic Rotation of Modern Wall Pier

Figure 4.3 shows plastic rotation capacity of the modern code compliant wall pier. The plot shows that the specimen had 0.081 rad of plastic rotation before failure at 10% drift ratio. Hence, from the obtained displacement ductility greater than 5 and plastic rotation of 0.081 rad, the specimen performed very well under the applied lateral cyclic load.

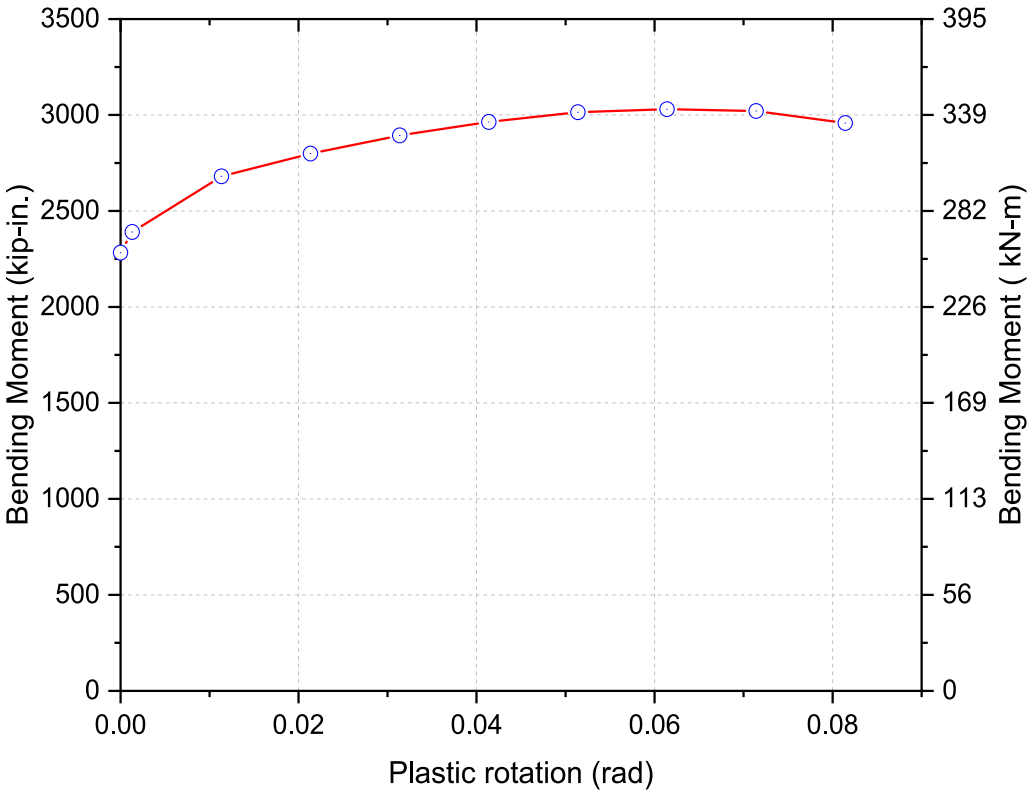

Figure 4.3 Plastic rotation of modern code compliant wall pier

4.3.3 Hysteretic Energy Dissipation of Modern Wall Pier

The specimen dissipated 2,856.7 kip-in. (322 kN-m) of hysteretic energy before failure. While observing the hysteretic cycles in Figure 4.4, the specimen dissipated a large amount of energy through inelastic deformations, which signified good performance by the specimen. The hysteretic cycles are similar in push and pull directions signifying similar performances of the system in both directions. A significant load is resisted without any degradation until the 10% drift ratio. The cumulative hysteretic energy is obtained by adding the calculated hysteretic energy of all cycles and is plotted against the drift ratio, as shown in Figure 4.5. The undulating curve signifies how energy is dissipated in each cycle.

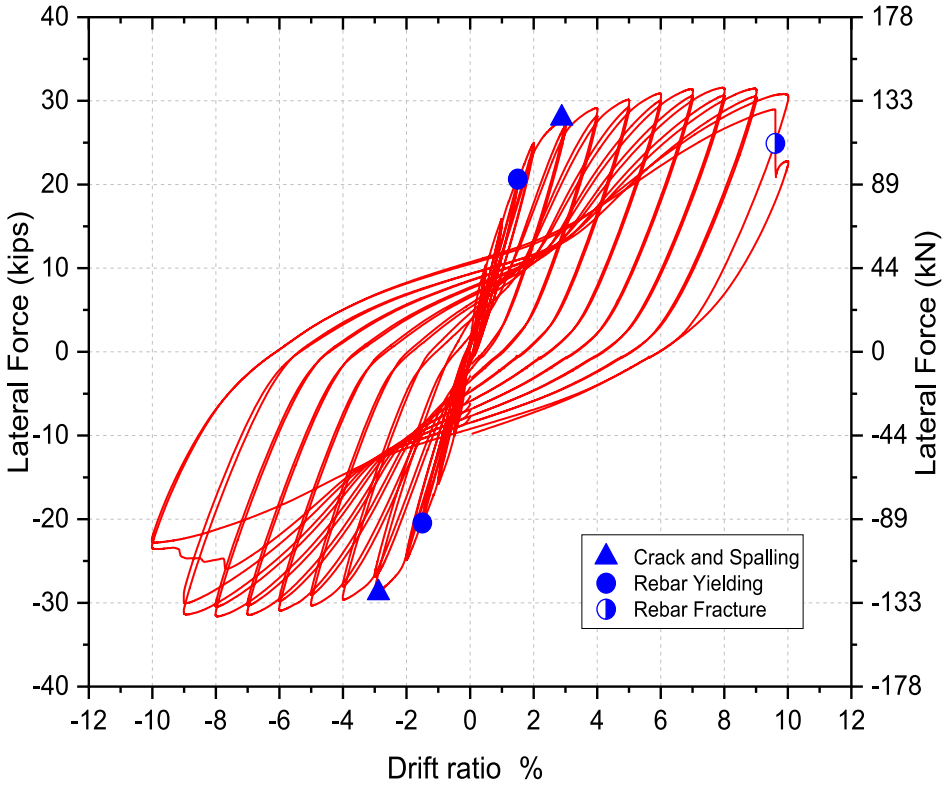

Figure 4.4 Hysteresis of modern code compliant specimen

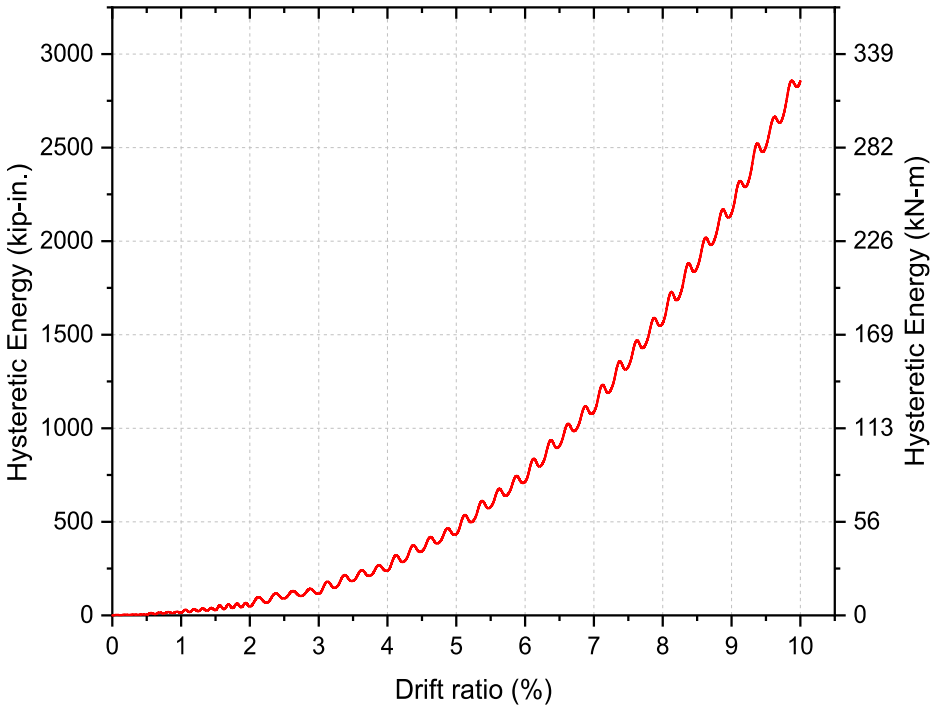

Figure 4.5 Cumulative energy dissipation of modern code compliant specimen

4.3.4 Stiffness Degradation of Modern Wall Pier

The average hysteretic stiffness of the specimen was obtained as described in section 2.7.4. The obtained stiffness deterioration is plotted against drift ratio (%), as shown in Figure 4.6. The plot shows smooth degradation of stiffness, as expected, for the current code-compliant specimen.

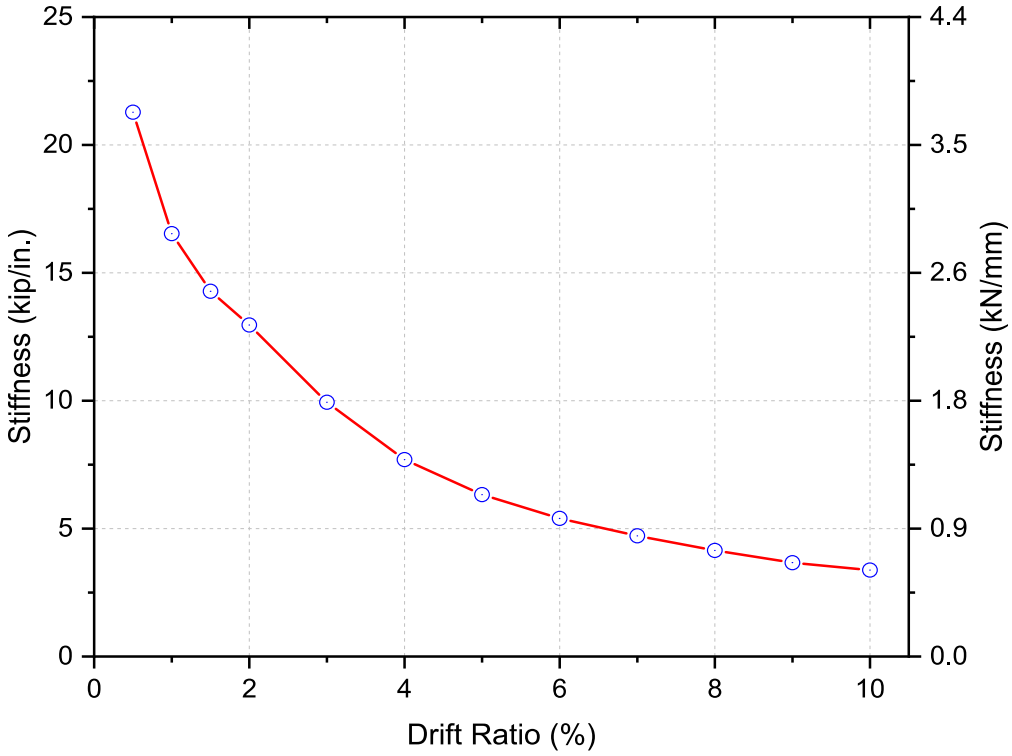

Figure 4.6 Stiffness deterioration of modern code compliant specimen

4.3.5 Damage Index of Modern Wall Pier

Damage assessment and the four damage levels based on the PA damage index was developed, as shown in Figure 4.7. The specimen reached the moderate and severe damage stage in the 2% and 4% drift ratio, respectively. The specimen reached the collapse stage at 8% drift ratio and failed on the first cycle of the 10% drift ratio. Hence, from the plot, one could predict a near collapse value for the specimen.

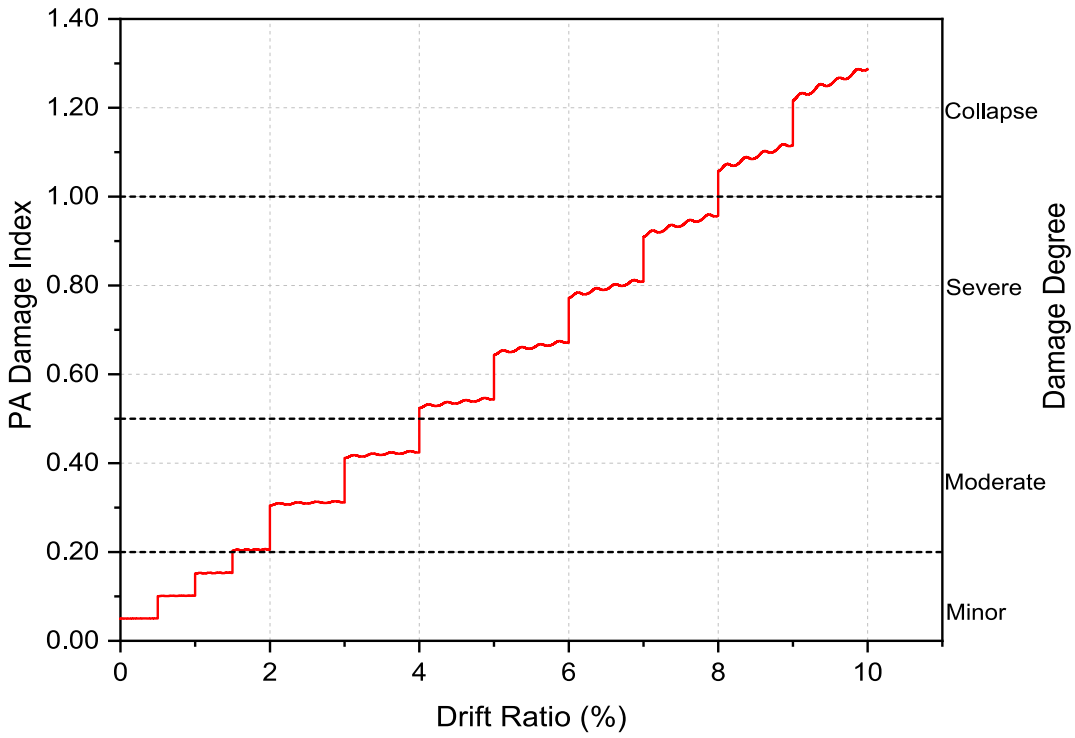

Figure 4.7 Damage index of modern code compliant specimen

4.3.6 Curvature Profile of Modern Wall Pier

A symmetrically distributed curvature profile, as shown in Figure 4.8, was obtained from LVDT data. The curvature was highest in the first curvature segment closest to the footing, which decreased up the wall. This can be considered a desirable distribution of plasticity within a given plastic hinge region. Strain gauges were placed on the longitudinal bars at the top and bottom portion of the plastic hinge region. The strain gauge readings show that the bottom region of the longitudinal bars yield far earlier in comparison to the top region showing the higher flexural demand near the footing.

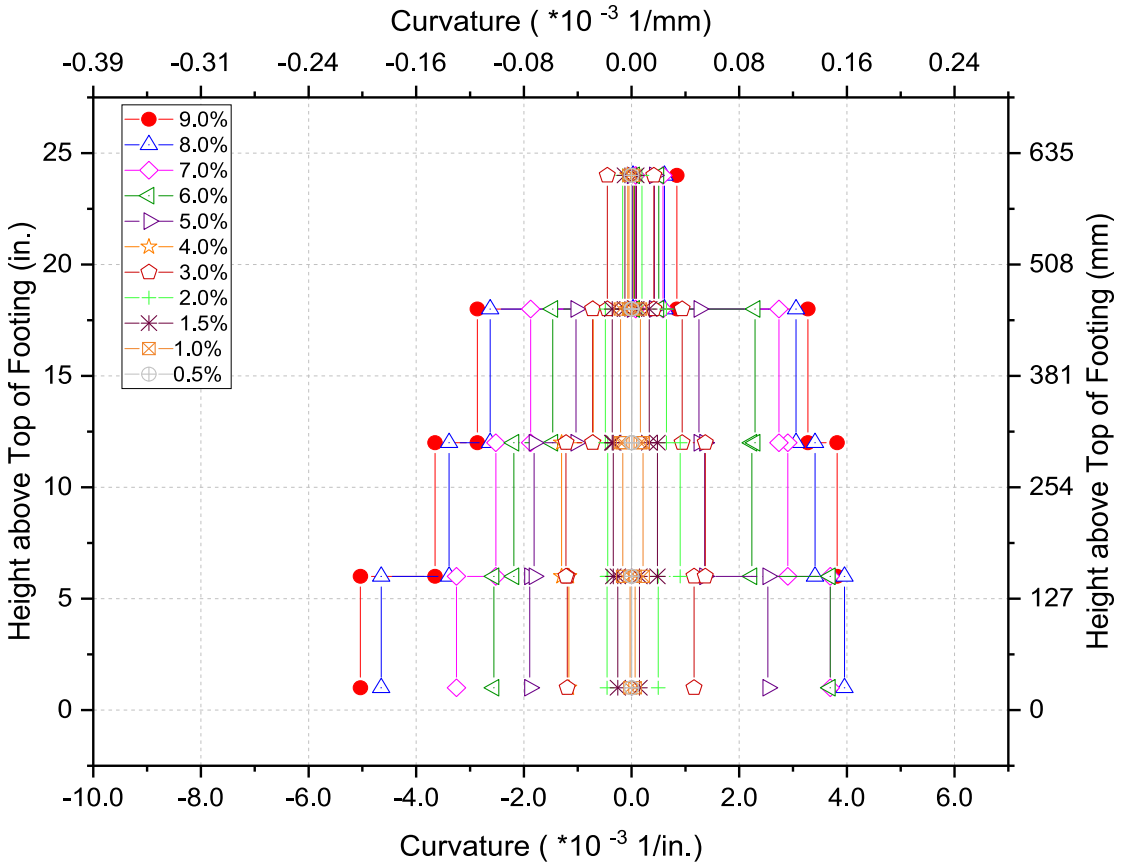

Figure 4.8 Curvature profile of the modern code-compliant specimen

4.3.7 Physical Damage of Modern Wall Pier

For better crack observation, the test specimen was painted white; square grid lines at 4 in. spacing were drawn. No crack was developed during the first (0.5%) drift ratio. Hairline cracks developed at a 20 in. and 36 in. height in the third (1.5%) and fourth (2%) drift ratio, respectively. The bottom hairline cracks widened up to 0.009 in. during the 3% drift ratio. The cracks previously mentioned increased in size to 0.02 in. and 0.03 in., respectively, at the 4% and 5% drift ratio. Similarly, the cracks formed at 20 in. increased in size to 0.009 in. during the 5% drift ratio. Above the footing concrete, spalling started in the west direction during the first cycle of the 6%, drift ratio. All major cracks developed during the 6% drift ratio.

The wall pier began to respond differently in the push and pull direction as more damage was observed in the west direction. The cracks increased to 0.04 in. in the west direction while in the east direction their size increased to 0.03 in. During the 7% drift ratio, spalling started in the east direction, whereas new diagonal cracks were observed in the west direction.

Concrete spalling progressed over the wall height up to 24 in., with more spalling over the sides of the wall at the 8% drift ratio. During the 9% drift ratio, shown in Fig 4.9, spalling was severe and was transmitted to the inner part of the wall. The major flexural cracks were joined over the periphery of the wall. In the first cycle of the last (10%) drift ratio, shown in Fig 4.10, a slight drop in strength was observed in the west (pull) direction. In the second cycle of the 10% drift ratio, one of the bars on the

west face fractured when the wall was displaced in the east (push) direction. This resulted in a significant 24% drop in strength at which point the test was terminated.

The fracture of the longitudinal steel bar occurred in the wall pier approximately 4 in. above the top of the footing due to low cycle fatigue. The severely spalled region was restricted to 12 in. and 6 in. in the west and east direction, respectively. However, the major structural cracks extended for a height of 22 in. above the top of the footing. Observations made after the test confirmed that damage was more severe in the pull direction (west face). No damage or yield penetration was observed in the footing as the strain gauges placed on the longitudinal rebar 1 in. below the top of the footing show that the footing remained elastic during the whole process. The specimen failed with a maximum lateral load of 31.6 kips (141 kN) at a 9.61 in. (244 mm) displacement.

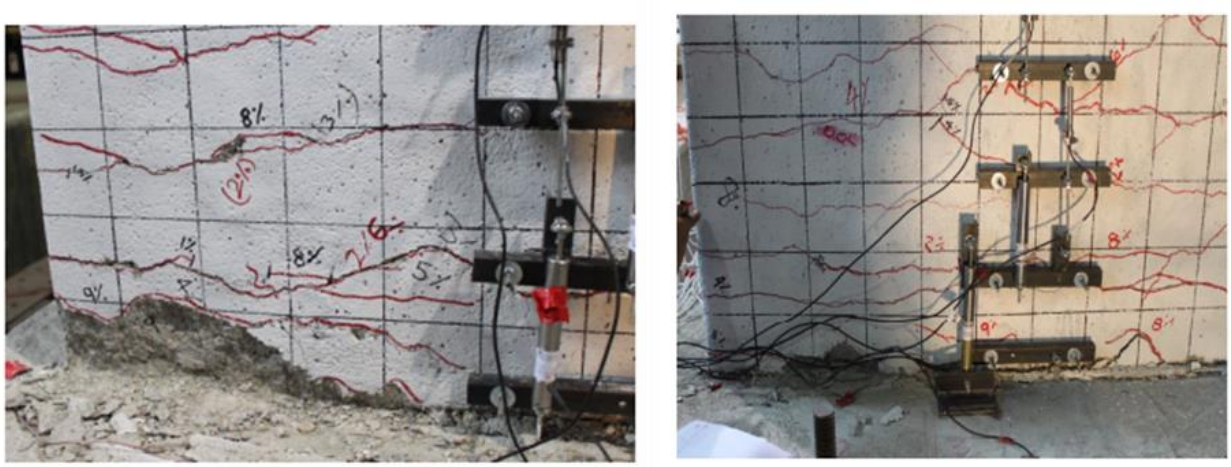

Figure 4.9 Damage state at 9% drift ratio showing cracks and spalling: (a) east face, (b) west face

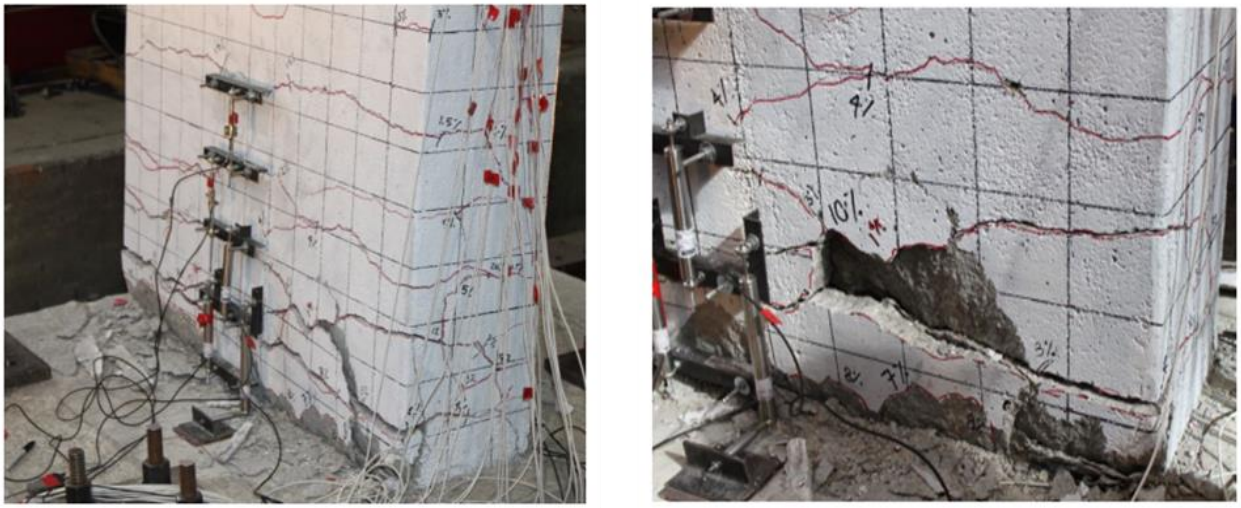

Figure 4.10 Damage state at 10% drift ratio showing cracks and spalling and rebar fracture: (a) east face, (b) west face

4.4 Numerical Analysis of Modern Wall Pier

Numerical analysis was performed using the OpenSees (Open System for Earthquake Engineering Simulation) software. This is an open-source software framework that allows the user to create a finite element model to simulate the response of the structural system subjected to predefined force. The reinforced concrete bridge wall pier was modeled as a single nonlinearBeamColumn element with a 3-integration point. This element encompassed distributed plasticity and plastic hinge integration. The nonlinearBeamColumn element section was discretized with uniaxial fiber element (Yao and Wu 2016). The wall pier cross-section consisting of longitudinal steel and concrete were defined using fiber elements with the corresponding measured material properties. The fiber section command was used to create a fiber section object. Each section object was composed of fibers with each fiber containing a uniaxial material, an area, and a specific location. Figure 4.11 shows the section of the fiber model with different described materials.

The wall pier is analyzed with the fully fixed support condition at the base. The self-weight and the axial load were applied as the vertical load at the top of the wall pier. Similar to the performed experiment, the lateral load was applied at a height of 8 ft from the top of the fixed footing. The lateral load application rate was slow and in a certain proportion of the wall pier's height. The axial load application system was applied in such a way that the applied load was always in the same axial line as the axial line of the wall. Therefore, P- Delta effects were ignored for this analysis.

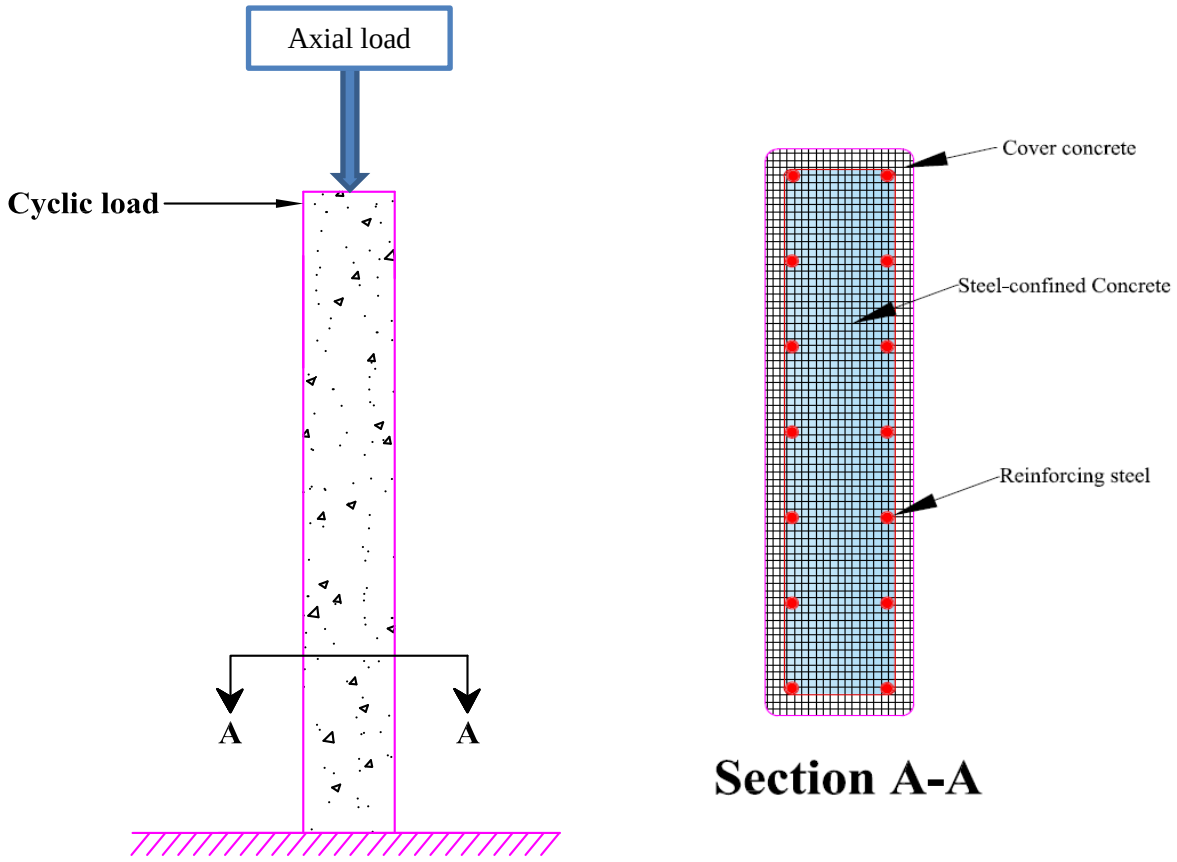

Figure 4.11 OpenSees fiber model of modern code compliant wall pier

4.4.1 Pushover Analysis of Modern Wall Pier

In the OpenSees model, *Concrete04* material model was used to define the cover and confined concrete of the wall pier. The Popovics model (Popovics 1973) defines the compressive stress-strain response until concrete crushing strength is achieved. However, the envelope curve is identical to the curve proposed by Mander (Mander and Priestley 1989). The concrete is modeled using two different groups as confined and unconfined concrete. Concrete outside the transverse reinforcements is defined as unconfined while concrete within the transverse reinforcement is defined as confined concrete. The confined concrete strength and ultimate strain provided by the transverse reinforcement are manually calculated and implemented in the model. The unconfined compressive strength was obtained through a series of compressive strength tests of concrete cylinders in the laboratory. For this model, the unconfined concrete strength used was 5,150 psi.

The reinforcing steel material object was used to model the longitudinal steel reinforcing material in the reinforced concrete section of the wall pier. This uniaxial material object gives added options such as buckling, fatigue, hardening, and curve parameters. The experimental data obtained through the tensile test were used as input in the model. For this model, the yield strength of the longitudinal bar was considered as 65 ksi. The nonlinear pushover analysis with the developed model was analyzed using the OpenSees framework. The model failed, gaining 32.4 kips lateral load capacity at 10.4% drift ratio. The longitudinal steel rebar went up to 82 ksi ultimate strength at 2% strain. Figure 4.12 shows the comparison between the obtained pushover and the cyclic experimental result. From Figure 4.12, looking at the initial stiffness, maximum load-carrying capacity, and failure point, it can be said that the pushover model agrees with the obtained experimental results.

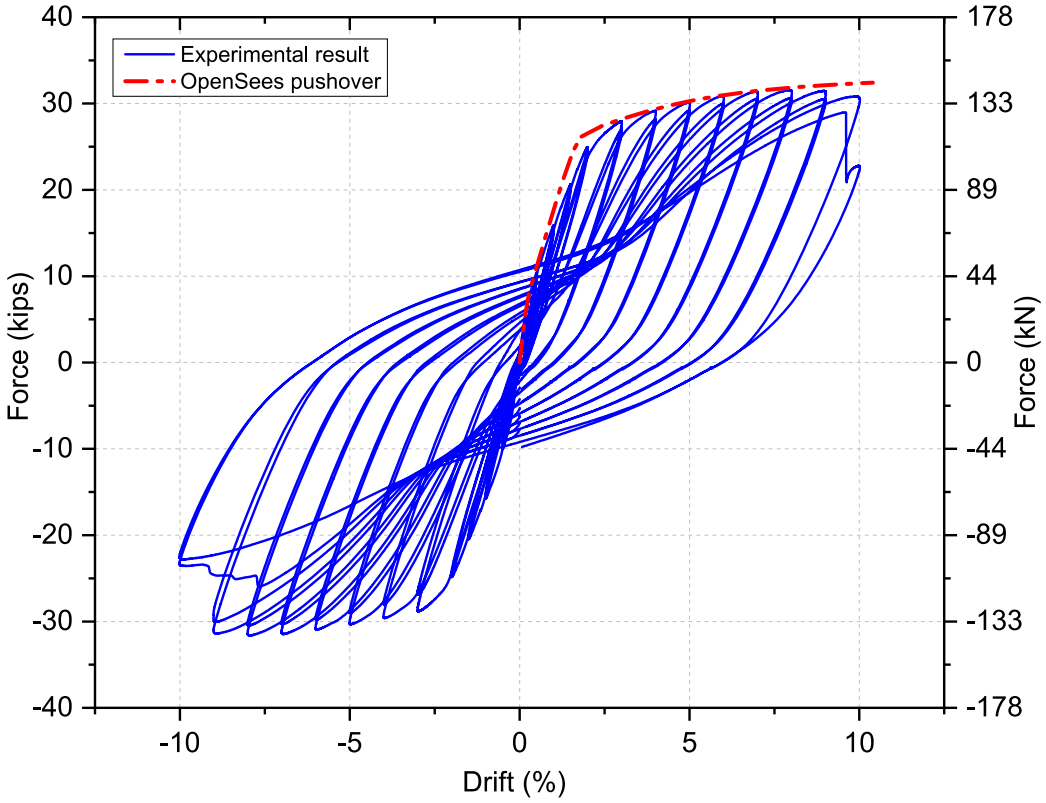

Figure 4.12 Comparison of the analytical pushover with the obtained experimental result

4.4.2 Cyclic Numerical Analysis of Modern Wall Pier

For the cyclic numerical analysis, the *Concrete02* material command was used to define the cover and confined concrete of the wall pier. This command constructs a uniaxial concrete material object with tensile strength and linear tension softening. As described earlier concrete is modeled as confined and unconfined concrete, depending on its location. The unconfined compressive strength of the concrete was obtained through the series of compressive strength tests on test day. The unconfined compressive strength used for the model was 5,150 psi obtained from the compressive strength test of a concrete cylinder on test day. The *Hysteretic material* in OpenSees was used to model the longitudinal steel bars in the reinforced concrete section of the wall pier. This command provides the option to define a uniaxial bilinear hysteretic material with pinching, damage due to ductility and energy, and degraded unloading stiffness. The experimental data obtained through the tensile test of steel bars were used to define the hysteretic material.

Yield strength and ultimate strength of the longitudinal bars were considered as 65 ksi and 106 ksi, respectively. The nonlinear beam-column command was used to construct a nonlinear beam-column element object. This command is based on the iterative force-based formulation, considering distributed plasticity. The cyclic analysis with the developed model was analyzed using the OpenSees framework. The model was stopped after a 10% drift ratio with the maximum force of 30.5 kips and 30.6 kips of force in the push and pull direction, respectively. Figure 4.13 shows a comparison between the OpenSees cyclic analysis result and the cyclic experimental result.

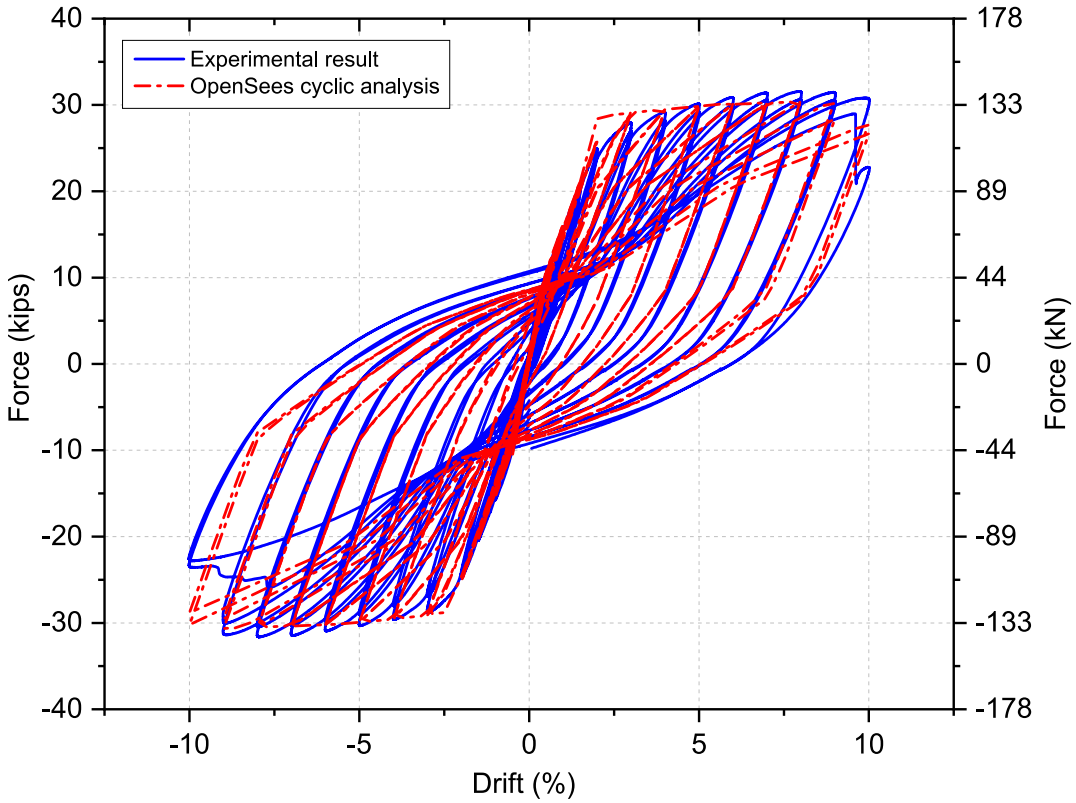

Figure 4.13 Hysteresis comparison between the experimental results and the obtained OpenSees analysis

The figure shows that the stiffness and hysteresis loops obtained from the OpenSees analysis matched the result obtained from the experiment. Figure 4.14 shows the cumulative hysteretic energy dissipated in the experiment and the OpenSees model. In the experiment, the specimen dissipated 2,857 kip-in. of hysteretic energy, whereas in the analytical model it dissipated 3,000 kip-in. of energy, which is 1.5% greater than the experimental results.

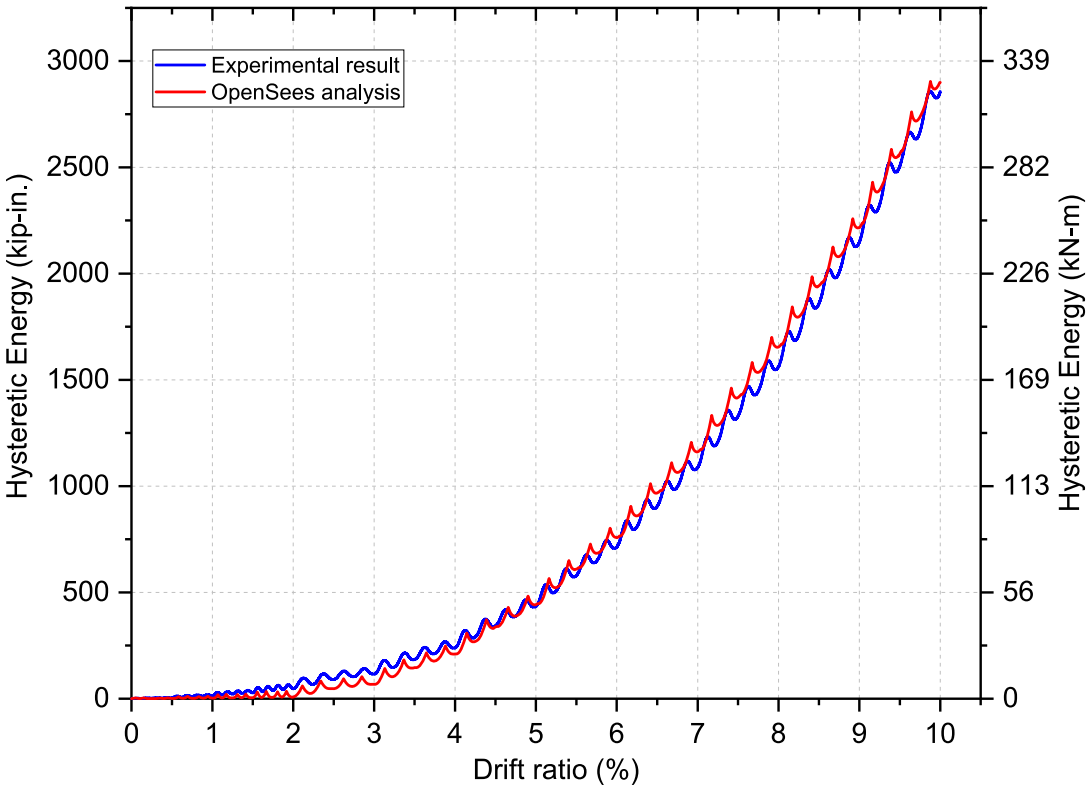

Figure 4.14 Hysteretic energy dissipation comparison between OpenSees and experimental results

4.5 Conclusion for Modern Wall Pier

The code compliant or modern bridge wall pier was tested under reversed cyclic quasi-static lateral load with an axial load of 120 kips (534 kN) corresponding to 6% of the axial load capacity of the wall pier. The specimen failed on the first cycle of the 10% drift ratio due to concrete crushing and spalling which was followed by fracture of a single longitudinal steel bar in the push direction. The specimen dissipated a large amount of hysteretic energy in the inelastic region and had a ductile failure. Table 4.1 summarizes the overall excellent performance of the modern code-compliant wall pier.

Table 4.1 Modern code compliant specimen test summary

Maximum Force (kip (kN))	32 (141)
Drift Ratio at Maximum Force (%)	9
Maximum Drift Ratio (%)	10
Maximum Displacement (in. (mm))	9.6 (244)
Number of Cycles	24
Energy Dissipation (kip-in. (kN-m))	2,857 (322.8)

5. RETROFIT OF AS-BUILT WALL PIER USING CFRP ANCHORS AND WRAPS – SPECIMEN R1

5.1 Introduction

The second as-built specimen was retrofitted using a combination of CFRP systems before testing. This included the use of CFRP sheets in the hoop and vertical directions and vertical and horizontal CFRP anchors. The specimen was tested under the same loading conditions as specified in Section 2.2. The retrofit aimed at improving the seismic performance of the wall pier so that it could achieve code compliance and dissipate significant hysteretic energy.

5.2 Retrofit Design for Specimen R1

The retrofit for Specimen R1 was designed using nine V-wrap HM 0.625 in. (15.8 mm) diameter vertical CFRP anchors on each side of the wall. They were embedded into the footing 12 in. (305 mm) and extended 18 in. (457 mm) up the face of the wall, above the footing. The vertical CFRP anchors were used to create a positive connection between the footing and wall pier under the assumption of failure of the steel lap splices inside the wall pier. Ten V-wrap HM 0.75 in. (19 mm) diameter horizontal CFRP anchors were also placed through the wall to add confinement and shear friction capacity to the lap spliced region of the wall pier. Two layers of vertically oriented V-wrap C200H were applied first to the wall for flexural strengthening. The CFRP anchors and vertical layers were confined with unidirectional V-wrap C200H CFRP wraps oriented in the hoop direction. These included three layers of 24 in. (610 mm) high segments at the base, two layers of 12 in. (305 mm) segments above that, and one layer of another 48 in. (1.22 m) high segments above that. The design of the CFRP composite retrofit is shown in Figure 5.1.

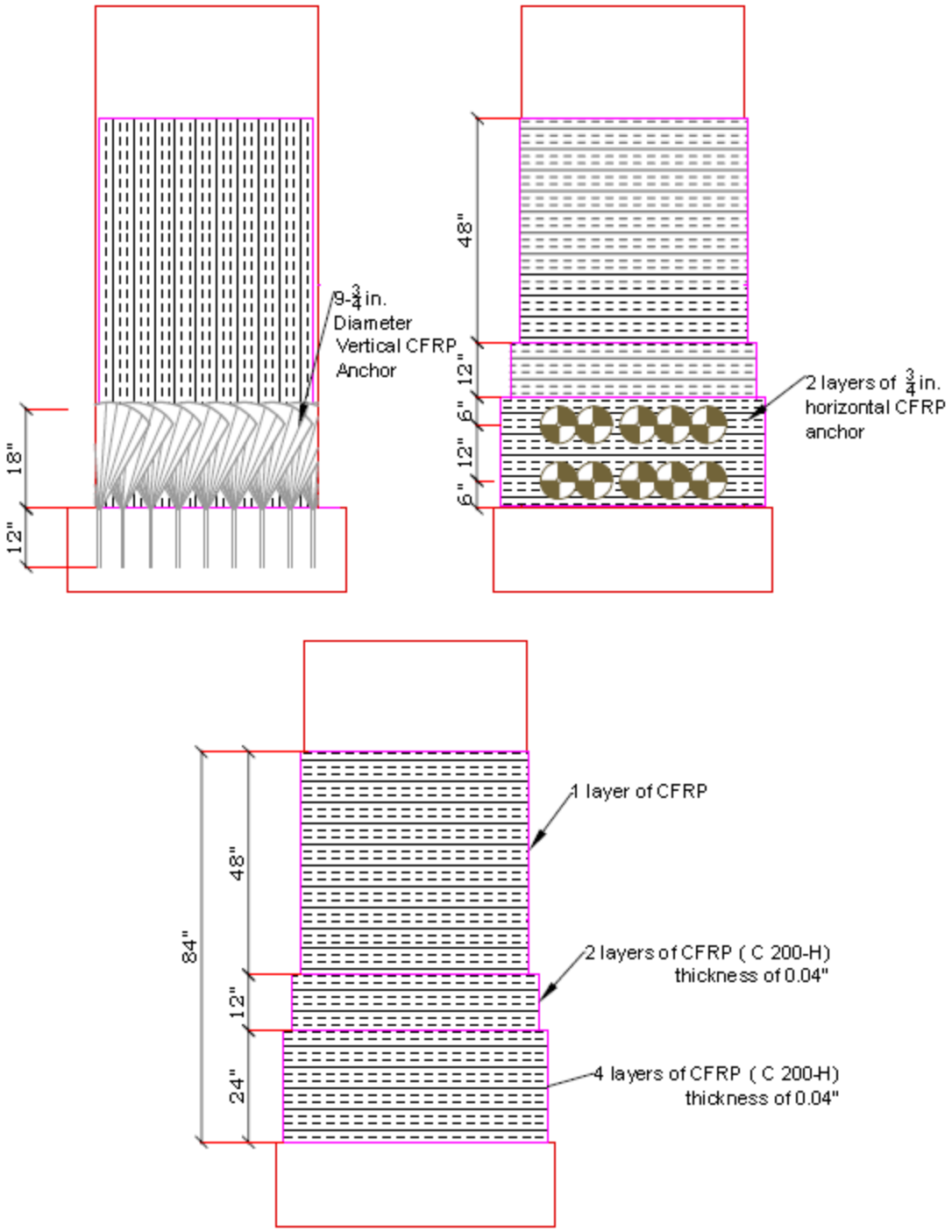

Figure 5.1 Retrofit design; (a) Vertical CFRP sheet and CFRP anchors, (b) Horizontal CFRP anchors, (c) Hoop direction CFRP wraps

5.3 Retrofit Procedure for Specimen R1

The wall pier was first prepared by drilling 10 0.75 in. (19 mm) diameter holes horizontally through the wall face for the placement of the horizontal CFRP anchors. Next, 18 holes total, with nine 0.75 in. (19 mm) diameter holes were drilled into the footing on both sides of the wall to accommodate the vertical CFRP anchors. To begin the application process, the wall was painted with a thin layer of V-wrap 770, a two-part epoxy resin, to saturate the concrete. Part of the epoxy resin mixture was then combined with silica fume to thicken the resin. This thickened paste was also applied to the wall in a thin layer to help keep the fibers in place before they cured. The CFRP sheets of V-wrap and vertical and horizontal CFRP anchors were saturated with the original epoxy resin mixture.

The vertical CFRP layers were applied to the wall first. The holes for the vertical anchors were then filled with epoxy resin, and the CFRP anchors were placed using wooden dowels to set them into place. Next the bottom two layers of hoop direction CFRP wraps were added. Each layer was carefully applied to the wall using metal rollers to ensure no air pockets would form under the CFRP composite. On completion of each CFRP layer application, the fibers were again covered in a thin layer of the thickened epoxy mixture. Then 10 horizontal CFRP anchors were pulled through the wall and set in place in two layers as shown in Figure 5.1. Finally, the remaining CFRP sheets were applied up against the wall face and left to cure. Figure 5.2 shows the application process.

(a)

(b)

Figure 5.2 Fiber application: (a) application of vertical CFRP sheets, (b) vertical CFRP anchors

5.4 Test Results of Specimen R1

The retrofitted specimen was tested under quasi-static loading with five-minute breaks between cycles. An axial load of 120 kips (534 kN) was applied at the top of the wall for the duration of the experiment. This load corresponds to 6% of the load-carrying capacity of the wall pier and simulates a bridge deck. Crack sizes and material degradation were observed throughout the test, with various measured data, which was collected to determine wall behavior. The hysteretic curve from the test can be seen in Figure 5.5. The hysteresis exhibited general stability throughout the entire test until the first cycle of 5% drift when the maximum force dropped by 34%. The rough edges of the hysteresis loops can be attributed to the brittle nature of the CFRP sheets. The larger drops in force are the loss of NSM CFRP bars, which failed due to debonding and tensile failure.

5.4.1 Displacement Ductility of Specimen R1

The ductility of the wall pier was found following the procedure outlined in Section 2.7.1. The ultimate displacement indicated by a 20% drop of the ultimate lateral load strength of the wall pier was 3.84 in. (97.5 mm); the yield displacement was found to be 0.70 in. (17.8 mm), resulting in a displacement ductility ratio of 5.5 for the system. Figure 5.3 shows the systems actual backbone and idealized backbone curves developed using this procedure. It should be noted that this ductility is at a higher lateral load capacity compared to the as-built specimen.

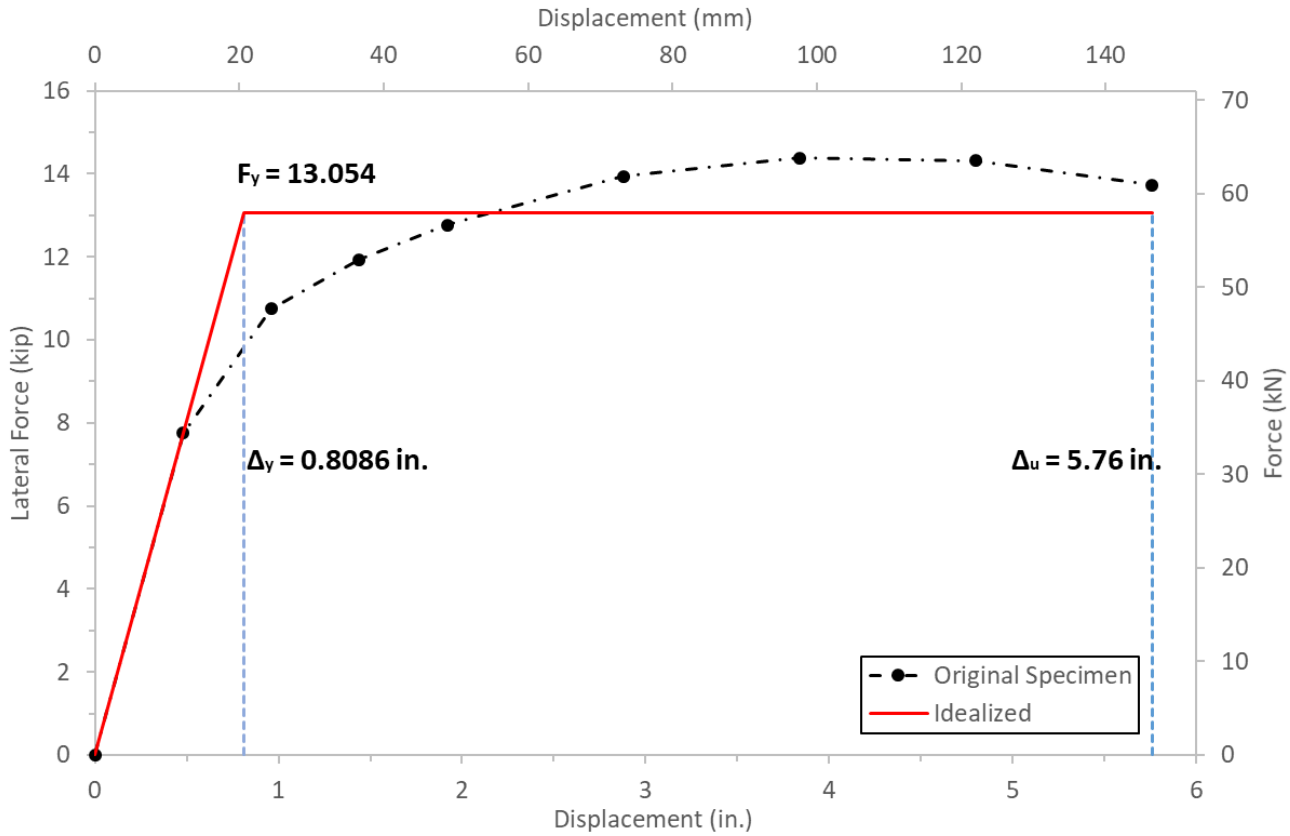

Figure 5.3 Displacement ductility for specimen R1

5.4.2 Plastic Rotation of Specimen R1

A plot of the plastic rotation of the seismically retrofitted pier wall was created using the procedure in Section 2.7.2. This plot is shown in Figure 5.4. From this plot, it can be seen that the specimen reached 0.02 rad of plastic rotation before its ultimate failure at 3% drift. The plastic rotation of 0.02 rad combined with the displacement ductility ratio of 5.5 signifies improved performance when compared to the as-built wall pier.

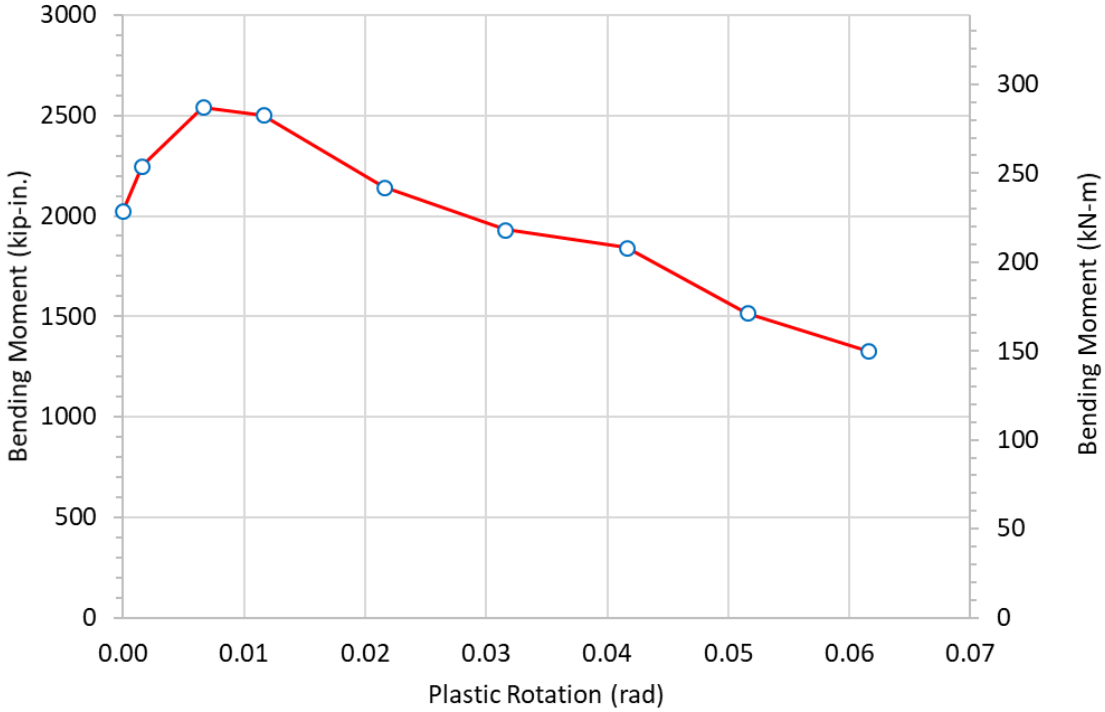

Figure 5.4 Plastic rotation plot for Specimen R1

5.4.3 Hysteretic Energy Dissipation of Specimen R1

The specimen hysteresis can be seen in Figure 5.5. This plot exhibits the overall behavior of the wall pier during testing. There is pinching in the center, which defines the behavior of the plastic hinge formed at the base of the wall pier. The hysteretic curve displays the brittle nature of the CFRP system used on the wall, where large sporadic drops of force occur at various loading increments throughout the test. The significant drop in lateral force resistance indicates fracture of one or more CFRP vertical anchors, while the more gradual loss of lateral force displays that the anchors partially fracture rather than losing strength all at once.

The cumulative hysteretic energy dissipation throughout the test is shown in Figure 5.6. The total dissipated energy for the retrofitted wall pier R1 was 816 kip-in. (92.2 kN-m). This energy dissipation is 1.6 times larger than the energy dissipated by the as-built wall, which was 500.4 kip-in. (56.54 kN-m).

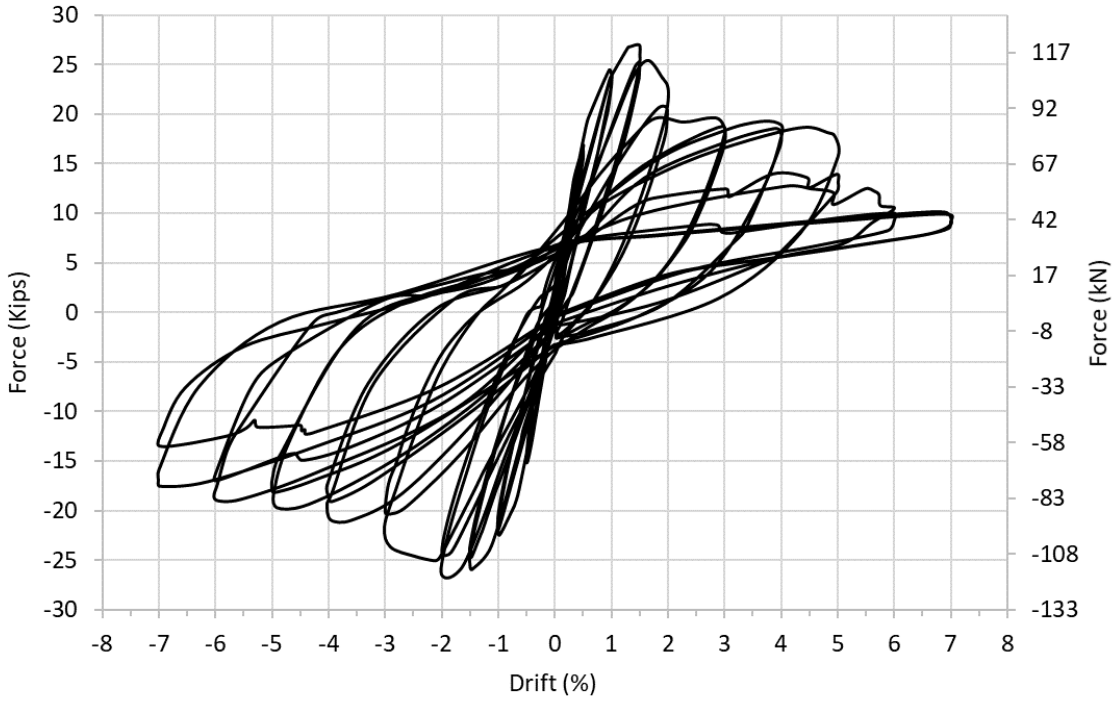

Figure 5.5 Hysteresis of retrofitted wall pier for Specimen R1

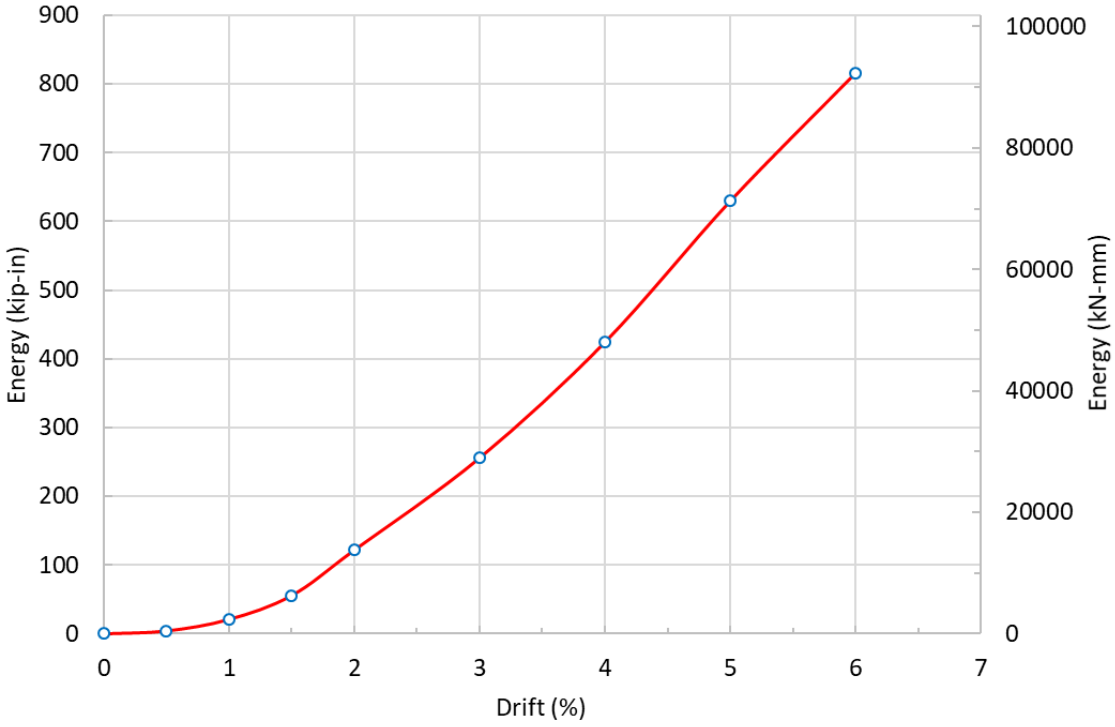

Figure 5.6 Cumulative hysteretic energy dissipation for retrofitted specimen R1

5.4.4 Stiffness Degradation of Specimen R1

The average hysteretic stiffness was calculated as described in Section 2.7.4. Figure 5.7 shows the stiffness values plotted against the drift ratio of the specimen. The retrofit specimen exhibits exponential stiffness degradation throughout the test. The initial stiffness of retrofitted specimen R1 of 34 kips/in. was more than doubled from the 16 kips/in. of the as-built wall pier specimen.

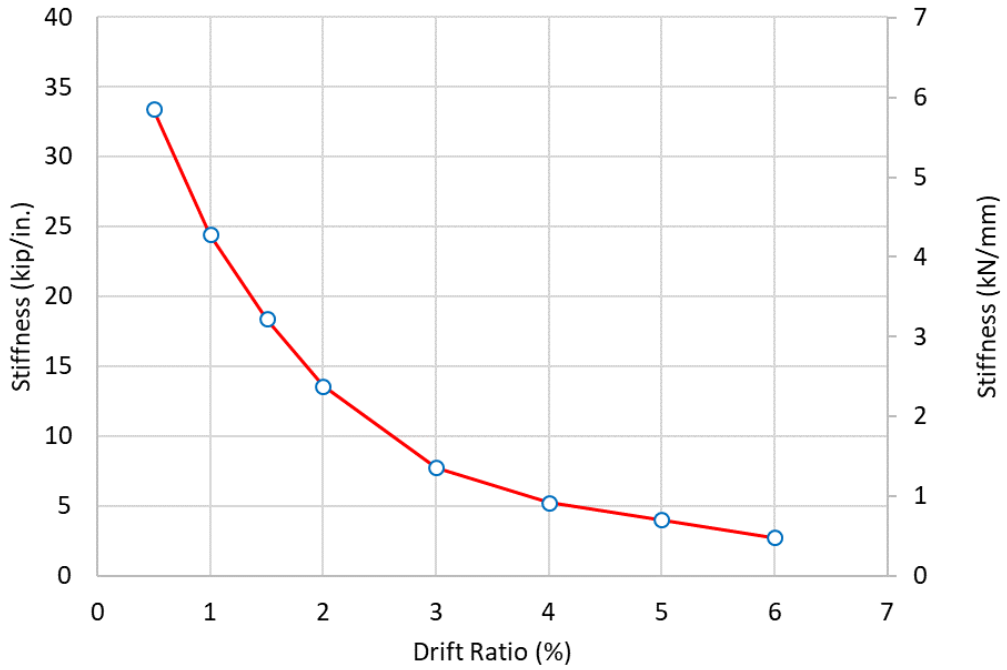

Figure 5.7 Stiffness deterioration for retrofitted specimen R1

5.4.5 Damage Index of Specimen R1

The Damage Index discussed in section 2.7.5 was applied to the as-built wall pier, and the plot is shown in Figure 5.8. Plotted against the four damage limits described in Table 2.2, the graph shows the damage state of the wall pier at each drift ratio. The specimen reached moderate damage at the 0.5% drift ratio, and severe damage was seen at the 1.5% drift ratio. The collapse stage occurred when the wall reached 3% drift ratio. The specimen reached ultimate load capacity on the first cycle of the 2% drift ratio. The plot accurately depicted performance of the retrofitted specimen R1.

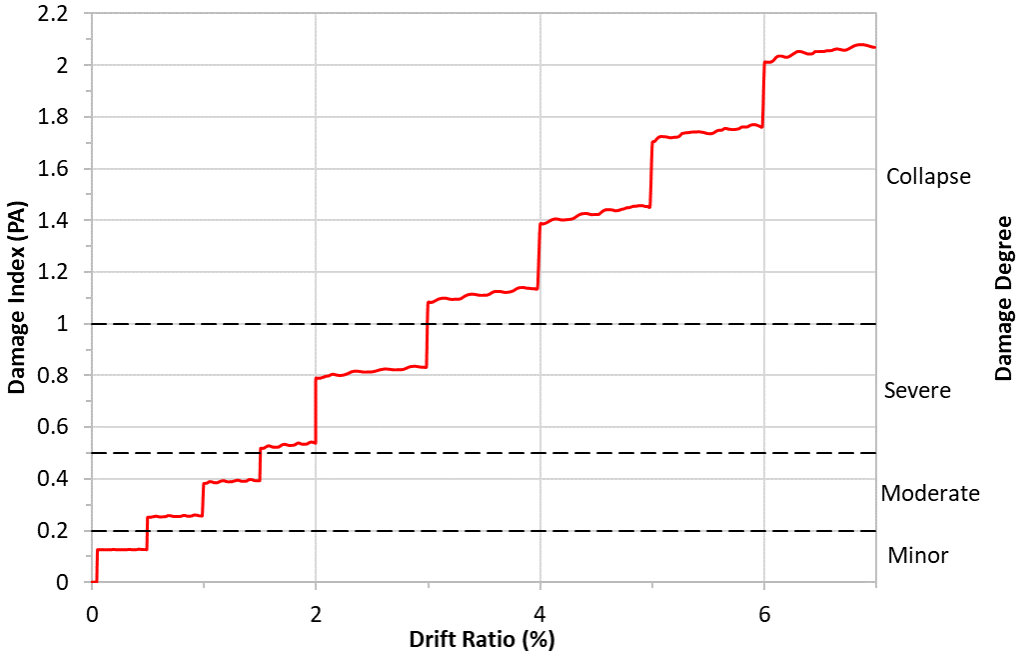

Figure 5.8 Damage Index of specimen R1

5.4.6 Lap Splice Strain for Specimen R1

The lap splice strain was also documented throughout the test. A comparison between the footing bar strain and the wall bar strain can be seen in Figure 5.9. This strain value is measured on the footing lap splice bar, 11 in. (279.4 mm) above the footing. Figure 5.9 clearly shows the reduction in lap splice strain from the addition of the CFRP retrofit. In the as-built test, the lap splices were increasingly strained throughout the test, reaching up to 1,200 microstrain at 5% drift. However, in the retrofit specimen R1, the lap splice strain ceased increasing after the 2% drift ratio and was at a maximum of 830 microstrain at this drift ratio; that is 76% of the strain equal to 1,088 microstrain exhibited at the 2% drift ratio in the as-built test. It is also clear that there was not a large difference in strain between footing bars and wall bars. In addition, none of the spliced bars yielded, which implies there was no lap-splice failure.

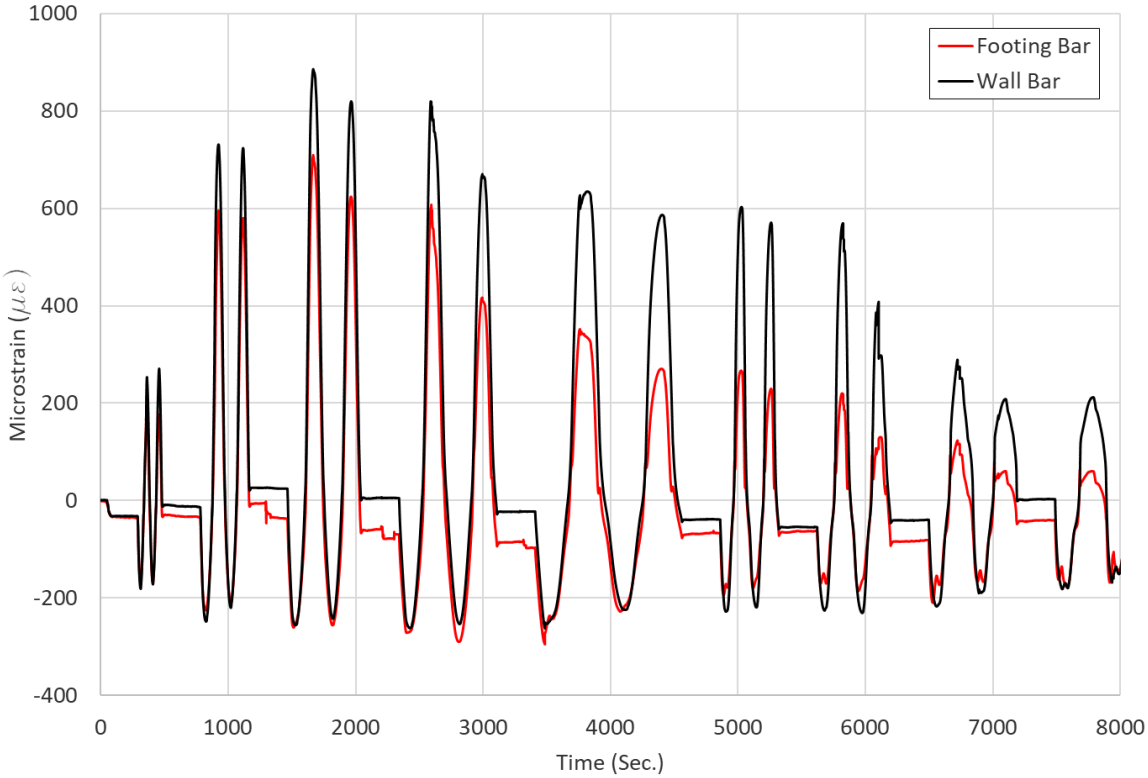

Figure 5.9 Retrofitted R1 wall pier lap-splice strain in footing and wall bar

5.4.7 Physical Damage of Specimen R1

Debonding of the CFRP composite did not occur until the 1% drift ratio. These regions began to form 10 in. (25.4 cm) above the footing, and the largest of these debonded regions measured about 3.0 in^2 (19.4 mm^2). At the 1.5% drift ratio, debonded areas grew larger and more small bubbles were present on the CFRP composite surface. The debonding can be seen in Figure 5.10. A peak load of 27.0 kips (120.1 kN) was reached at this drift ratio.

Figure 5.10 CFRP jacket debonding at 1.5% drift ratio for specimen R1

During the first cycle of the 2% drift ratio, CFRP anchorage failure was observed. A loss of 4.8 kips (21.2 kN) was seen in the lateral load. Based on the geometry of the wall we determined the vertical force lost in the anchors using the sum of bending moments equation:

$$\sum M_o = F_{lateral}(8\,ft) - F_{vertical}(1\,ft) = 0 \tag{5.1}$$

$$F_{vertical} = F_{lateral}(8) \tag{5.2}$$

We then simplified Eq. (5.1) to Eq. (5.2) and determined that a decrease of 38.4 kips (170.8 kN) in the vertical direction of the anchors occurred. Since the tensile capacity of a 0.75 in. (19.05 mm) diameter CFRP anchor is 25 kips (111.2 kN), it was assumed that two anchors partially fractured on the West side of the wall at this time. This fracture was confirmed by inspecting the wall after the test. A partial anchor fracture is shown in Figure 5.11.

Figure 5.11 Partial anchor fracture for Specimen R1

At the 3% drift ratio, a large crack measuring 0.25 in. (6.35 mm) wide, opened on the east face of the wall and portions of the concrete began to spall at the base of the footing. After the 3% ratio, no more debonding of the CFRP occurred on the wall surface, and all damage for the remainder of the test occurred in the footing. At 4% drift ratio, the footing crack became larger than 1.0 in. (2.54 cm). This crack is shown in Figure 5.12.

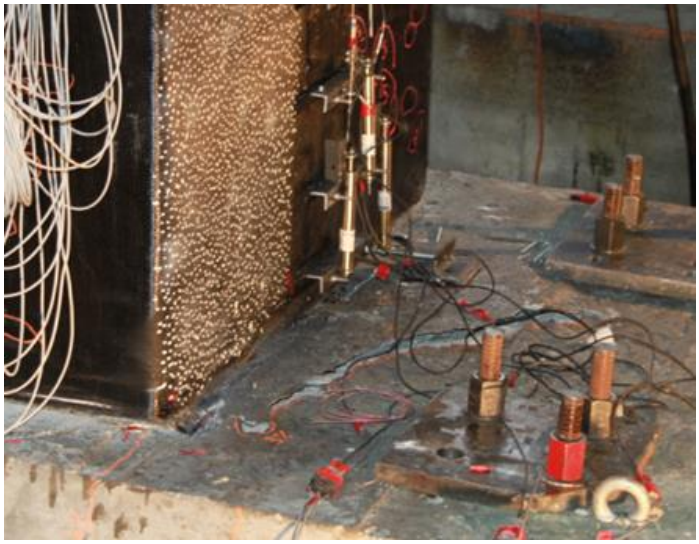

Figure 5.12 East side footing crack at 4% drift ratio for specimen R1

At the 5% drift ratio, during the "pull" cycle, the lateral load dropped. At this point, 5.5 kips (24.5 kN) of horizontal load was lost, and another two vertical anchors partially fractured based on Eq. (5.1-5.2), which was visually confirmed. The rebar also became exposed in the footing due to spalling of concrete at the base of the pier. The test was continued until the end of the 6% drift cycle without further significant reduction in strength. The wall damage at the end of the test is shown in Figure 5.13.

Figure 5.13 Footing damage at the end of the test for specimen R1

5.5 Conclusion for Specimen R1

The seismic retrofitted reinforced concrete wall pier specimen R1 was tested under quasi-static cyclic loading. The pier lost load in the second cycle of the 2% drift ratio due to fracture of multiple CFRP vertical anchors on the west side of the wall. The east side exhibited more physical damage than the west side of the wall pier because the anchor failures began on the east side, which transferred stress to the west side and allowed more damage to accrue throughout the remainder of the test.

The retrofit specimen R1 performed better than the as-built, although it lost 20% of its lateral force resistance after the 2% drift ratio. The energy dissipation of 816 kip-in. (92.2 kN-m) is 1.6 times that of the as-built wall pier, which only reached 500 kip-in (56.5 kN-m). The wall reached the 2% drift ratio with 2.1 times the initial stiffness, 1.6 times the energy dissipation and 2.0 times the lateral force resistance. Overall, the retrofitted wall pier specimen R1 performed well compared to the as-built wall pier. The retrofit results are shown in Table 5.1.

Table 5.1 CFRP anchor retrofit test summary for Specimen R1

Maximum Force (kip (kN))	27.0 (120.0)
Drift Ratio at Maximum Force (%)	1.5
Maximum Drift Ratio (%)	7.0
Maximum Displacement (in. (mm))	6.72 (171)
Number of Cycles	16
Energy Dissipation (kip-in. (kN-m))	815.6 (92.1)

6. RETROFIT OF AS-BUILT WALL PIER USING CFRP NSM RODS AND CFRP WRAPS – SPECIMEN R2

6.1 Introduction

The third as-built specimen was retrofitted using a combination of CFRP systems. This included the use of CFRP Near Surface Mounted (NSM) rods, CFRP horizontal anchors, and CFRP sheets in the horizontal and vertical direction. The primary objective of this retrofit was to sufficiently strengthen the as-built specimen so that its performance, load carrying capacity and stiffness would be comparable to that of modern code-compliant wall piers. The specimen was tested under the same loading conditions as specified in Section 2.2.1 and 2.2.2.

6.2 Retrofit Design for Specimen R2

The retrofit involved the design of the concrete groove depth, the number of CFRP NSM rods, the number of horizontal CFRP anchors, and thickness of CFRP jackets. The groove dimension has a major role in the bond performance of the NSM CFRP rod. A square groove of a dimension of 0.75 in. (19 mm) by 0.75 in. (19 mm), which is at least 1.5 times the diameter of the CFRP rod, was provided. The CFRP jackets do not extend beyond the wall and footing joint interface; thus, they were ignored in considering the flexural strength. To provide flexural strength and a smooth transition of applied lateral force from the wall to the footing, CFRP NSM rods were provided. By using the tension equivalence method, nine #4 (13 mm) V-Wrap, CFRP NSM rods were provided on each face of the wall pier for a total of 18 rods. To prevent pullout failure and to develop a high effective tensile stress at a given section, a 15 in. (381 mm) or 32 d_b anchorage length was provided.

The confinement provided by CFRP jacketing of a square and rectangular column or wall pier is not as efficient as it is for a circular column. The horizontal anchors divide the cross-sectional area into multiple equal cross-sections, increasing the confinement efficiency of CFRP jackets. In the lap-spliced region of the longitudinal steel bars, CFRP horizontal anchors provide confinement and shear friction capacity to avoid bond-splitting failure. Using the shear friction principle, 10 V-wrap HM 0.75 in. (19 mm) diameter carbon fiber anchors were provided in the plastic hinge region. To provide shear strength and confinement in the plastic hinge region, CFRP wraps with unidirectional V-wrap C200H fibers oriented in the hoop direction were provided. Considering shear confinement, strain hardening, and lap splice length, four layers of 24 in. (610 mm) segments at the base, two layers of 12 in. (305 mm) segments above that, and one layer for another 48 in. (1.22 m) above that provided. The design of the CFRP composite retrofit is shown in Figure 6.1.

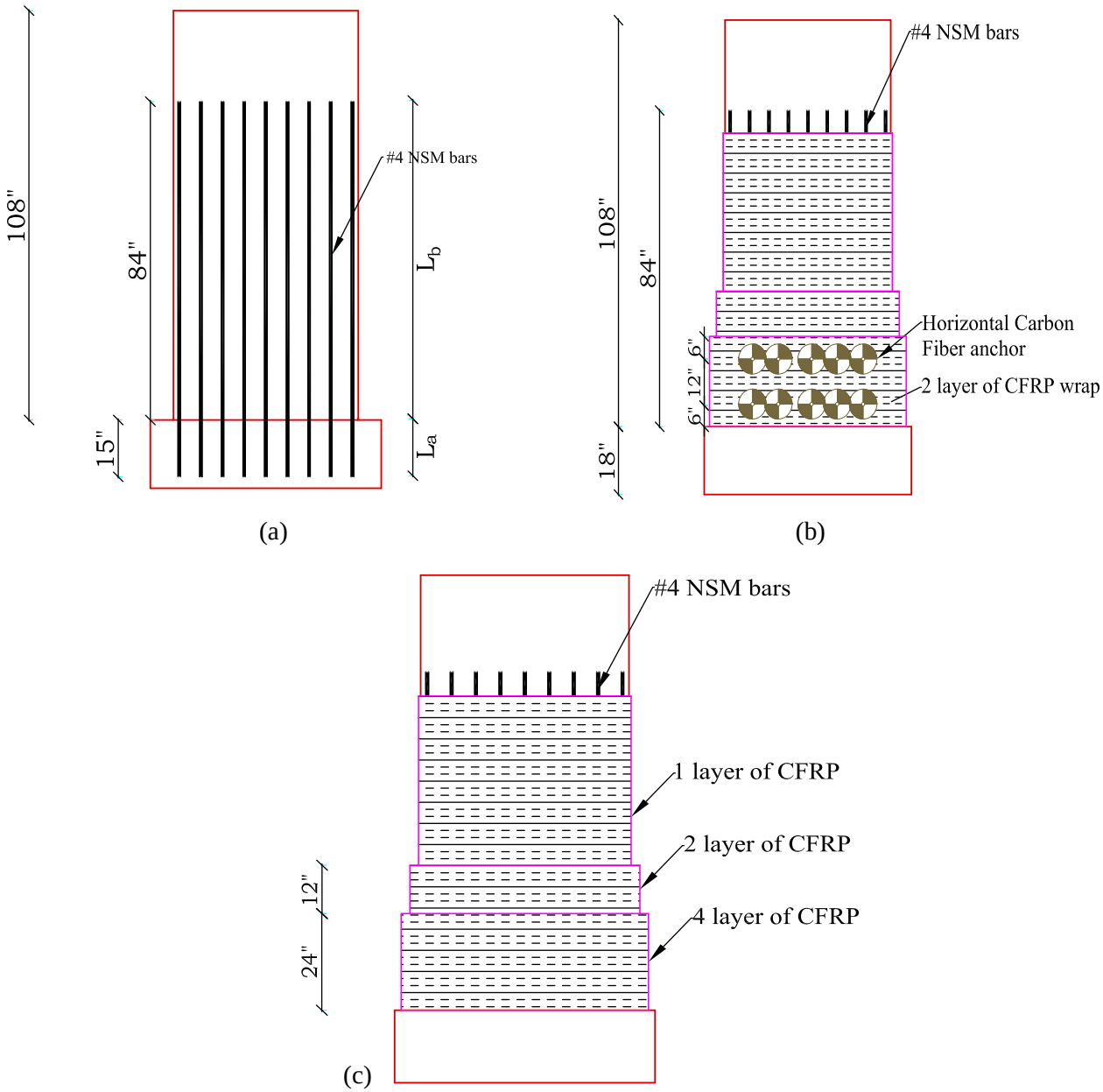

Figure 6.1 Retrofit design of as-built wall pier using NSM CFRP rods for Specimen R2

The nine grooves sized as 0.75 in. (19 mm) depth by 0.75 in. (19 mm) width for NSM fiber rods were first cut and chiseled on both faces of the as-built wall pier at the designed spacing. Cut grooves on both sides of the wall were continued in the footing with drilled holes of 0.75 in. diameter. In addition, 10 0.75 in. (19 mm) diameter holes were drilled horizontally through the wall face for placement of the horizontal carbon fiber anchors at the two elevations of 6 in. (152 mm) and 18 in. (457 mm) above the surface of the footing, as shown in Figure 6.1(b). The wall surfaces were roughened using the sandblasting procedure, and the corners of the wall were chiseled, providing a 0.5 in. (13 mm) corner radius.

To begin the application process, one coat of each of the premixed epoxy and silica fume slurry paste was applied over the wall surface, grooves, and drilled holes. The grooves and drilled holes were filled manually using the silica fume slurry paste. The NSM CFRP fiber rods were placed in their designated position. The precut unidirectional V-wrap C200H carbon fiber wraps were saturated with premixed epoxy resin. The CFRP wraps were wrapped around the prepared wall surface in the hoop direction. The gradual decrease in the number of CFRP wraps are shown in the design in Figure 6.1(c). The bottom layers consist of four wraps. The 10 cured horizontal anchors were applied at the given location after application of two layers of horizontal CFRP wraps. This region was again wrapped with two additional CFRP wraps after the horizontal CFRP anchors were placed, thus providing a sandwiching effect. On completion of each layer, the fiber was again covered in a thin layer of the thickened epoxy mixture. Figure 6.2 shows the retrofit process, and Figure 6.3 shows specimen R2 after the final retrofit application.

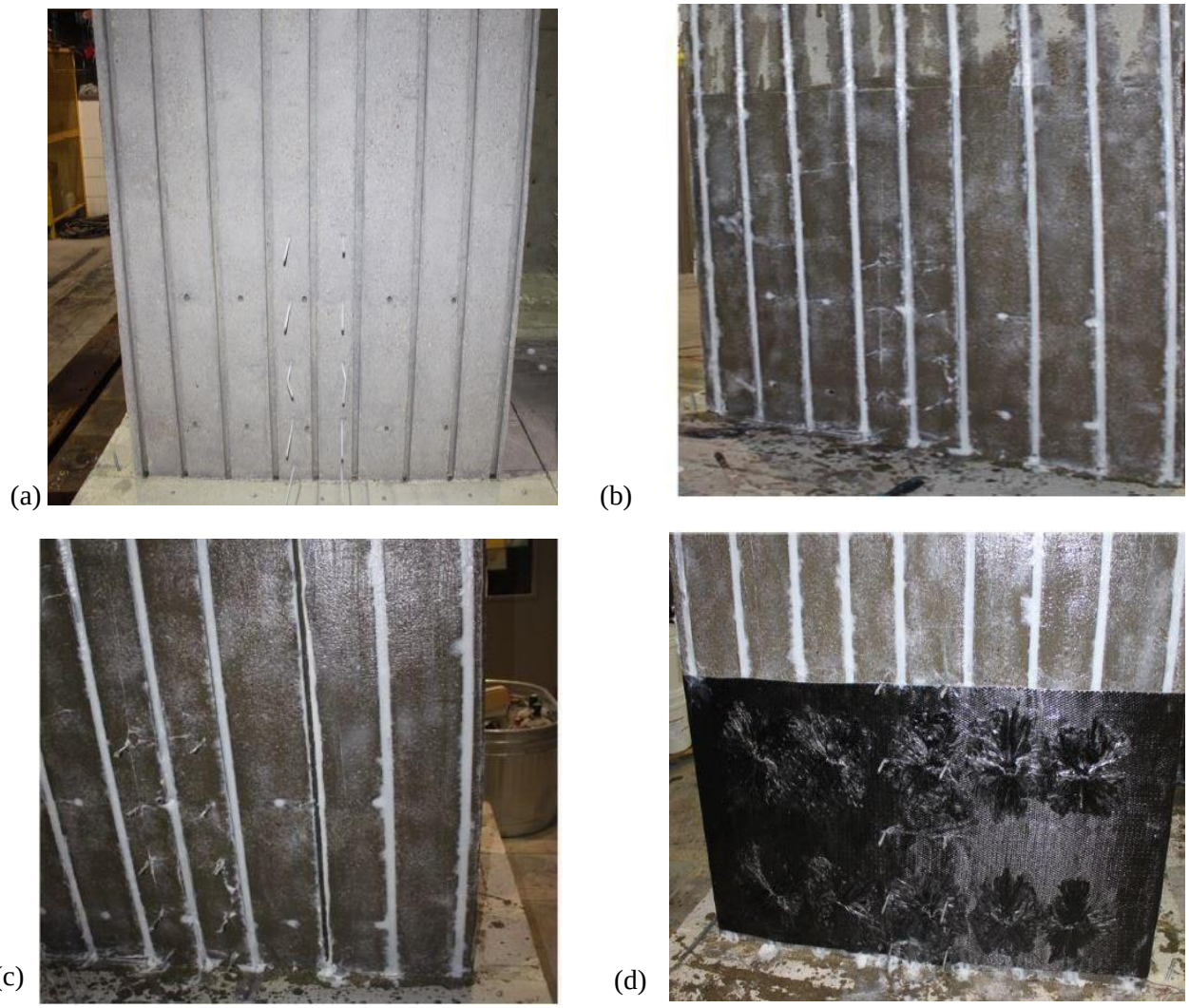

Figure 6.2 Retrofit process for specimen R2: (a) sandblasted surface, (b) application of premixed epoxy, (c) installation of CFRP NSM rods, (d) CFRP wrap and installation of CFRP horizontal anchors

Figure 6.3 Specimen R2 with the final retrofit application

6.3 Test Results for Specimen R2

Retrofitted specimen R2 was tested under reversed cyclic quasi-static lateral load with a constant axial load. An axial load of 120 kips (534 kN) was applied at the top of the wall for the duration of the experiment. This load corresponds to 6% of the load-carrying capacity of the wall pier simulating the dead load due to the bridge deck. The specimen was monitored for formation of any new air bubbles in the CFRP wrap and material degradation throughout the test. Various measured data were also used to monitor wall behavior. The hysteresis curve from the test can be seen in Figure 6.4. The hysteresis curve shows that the specimen continued to resist lateral force until 1.5% drift ratio where a sharp loss in the lateral load-carrying capacity is observed in the push direction. Through the video documentation and experimental observation, premature debonding failure of two of the NSM CFRP rods was observed, resulting in significant loss of lateral load-carrying capacity of the specimen. Figure 6.5 shows the images of premature bond failure of the CFRP bars. The retrofitted specimen had enough strength to resist the applied lateral force in the pull direction. This premature bond failure at 1.5% drift ratio, resulted in the eventual failure of the specimen at a 5% drift ratio, at which point the lateral force dropped by 19.5%.

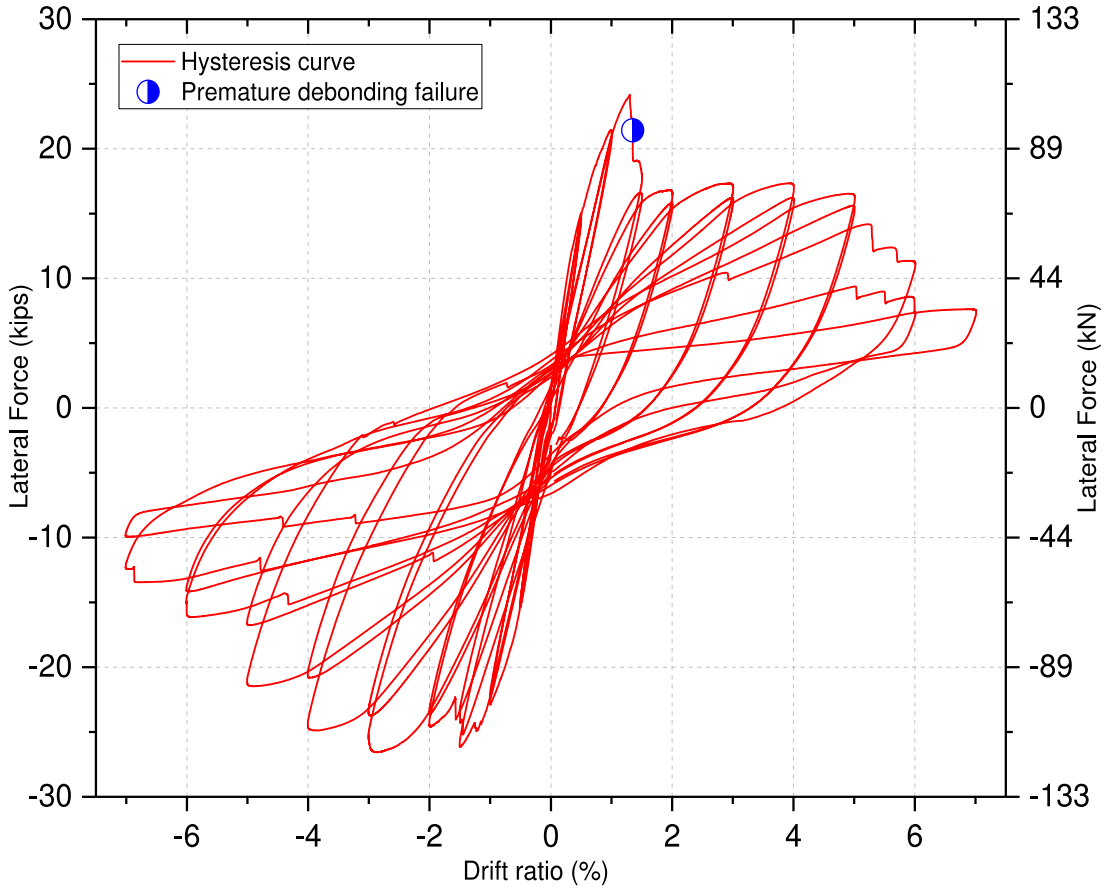

Figure 6.4 Hysteresis from test of the CFRP NSM retrofitted specimen R2

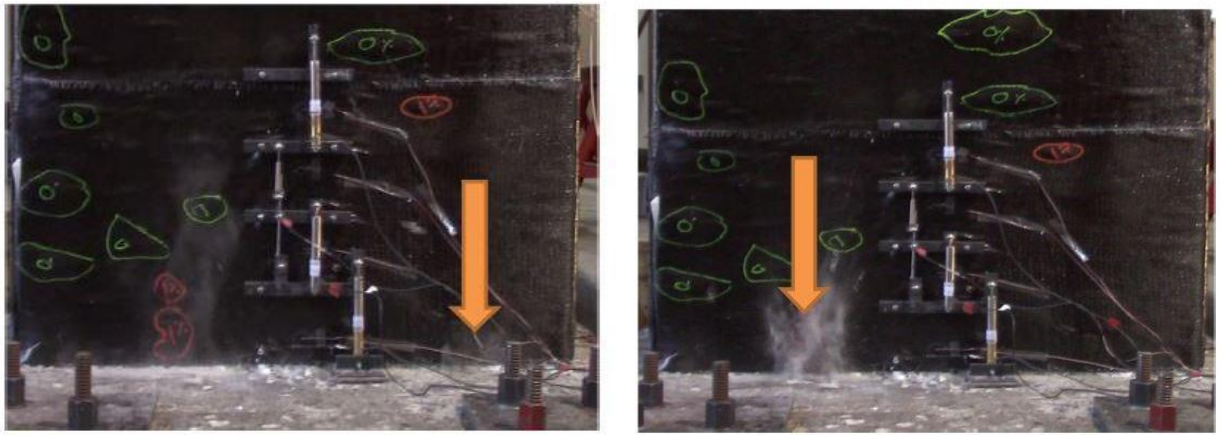

Figure 6.5 Bond Failure of CFRP NSM rods: (a) debonding of first bar, and (b) debonding of second bar at 1.5% drift ratio

6.3.1 Displacement Ductility of Specimen R2

An idealized elastoplastic curve was obtained through the method described in Section 2.7.1 and was plotted with the average backbone curve, as shown in Figure 6.6. The yield displacement obtained was 0.625 in. with a corresponding yield force of 21.3 kips. The ultimate displacement was 4.81 in. From Fig. 6.6, we can see that the lateral force resistance capacity dropped sharply after debonding failure of the NSM bars.

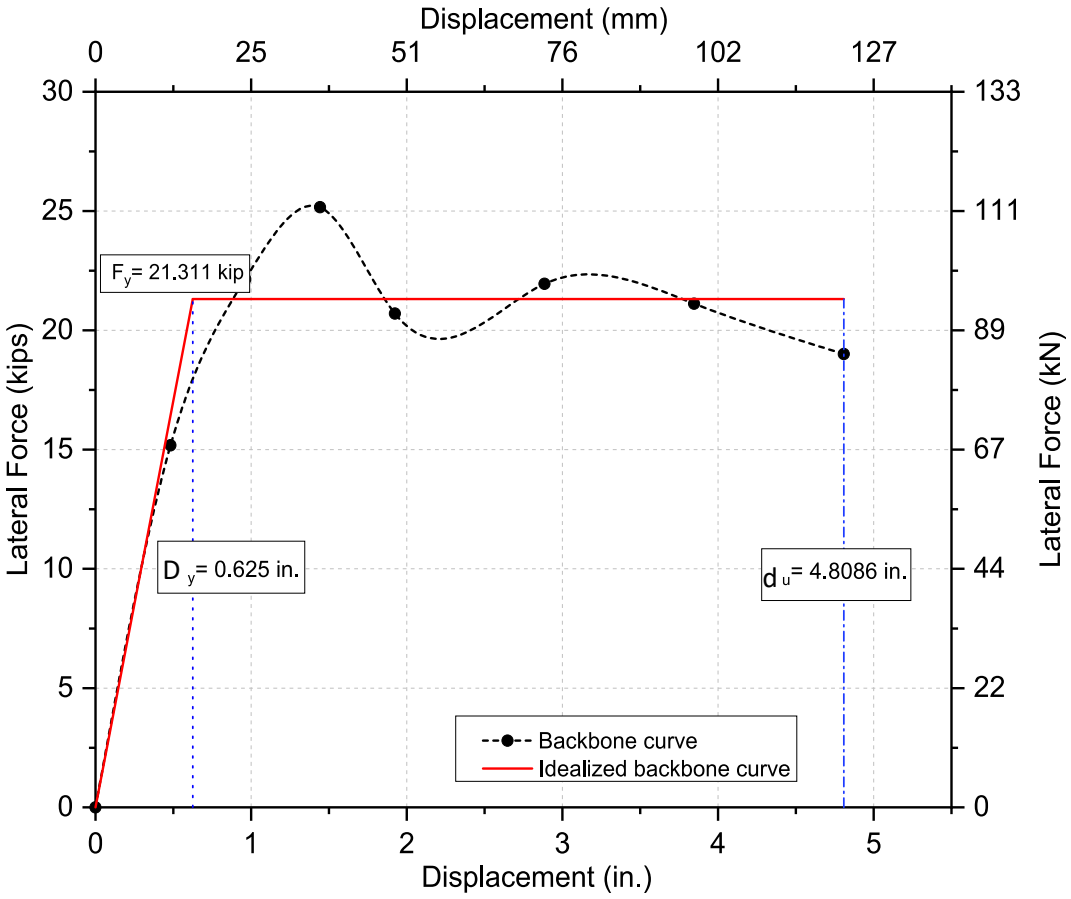

Figure 6.6 Backbone curve of the CFRP NSM bar retrofitted specimen R2

6.3.2 Plastic Rotation of Specimen R2

The plot of plastic rotation of the NSM retrofitted wall pier specimen was found using the procedure outlined in Section 2.7.2 and is shown in Figure 6.7. The plot shows the specimen has 0.06 rad of plastic rotation before ultimate failure at a 7% drift ratio.

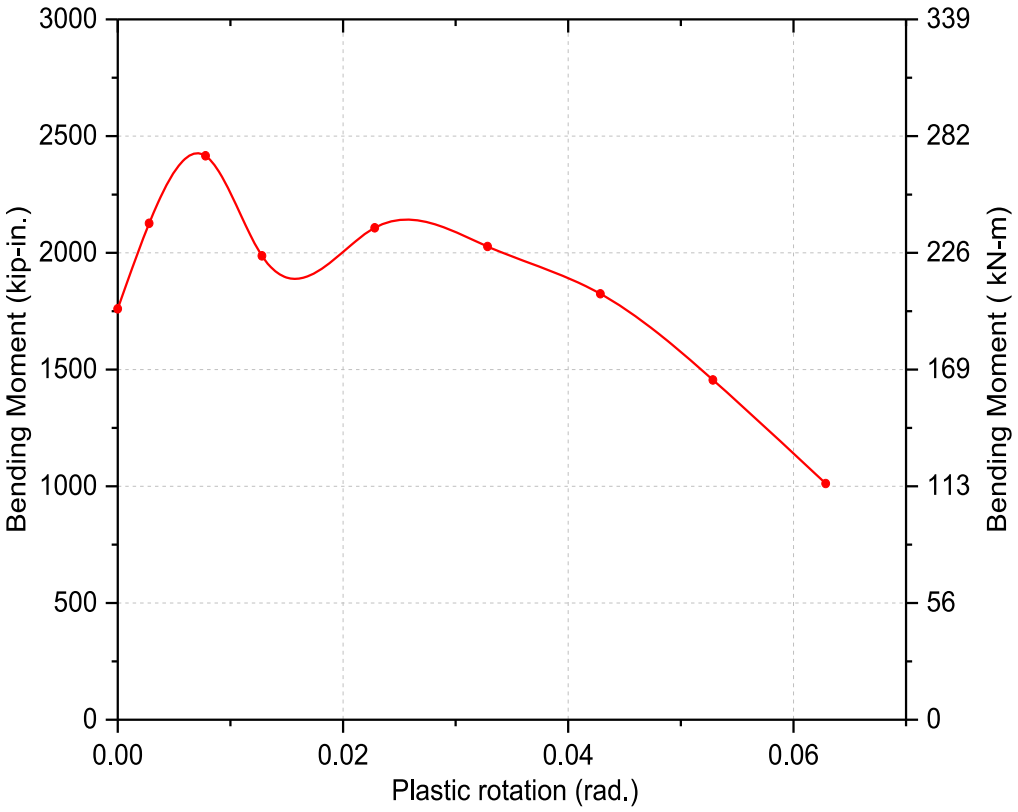

Figure 6.7 Plastic rotation plot of retrofitted specimen R2

6.3.3 Hysteretic Energy Dissipation of Specimen R2

Figure 6.4 shows hysteresis from the test of the CFRP NSM bars retrofitted specimen R2. Hysteresis loops are wide and stable, and a slow and gradual strength degradation occurred in the west (pull) direction, while a quick strength degradation was noticed in the east (push) direction. The test ended at the end of a 7% drift ratio with a 50% drop in lateral load capacity of the retrofitted specimen. Since the wall was wrapped with fiber sheets, it was impossible to record the different damage states. Instead of the damage states, bubbles on the jacketed wall and cracks on the footing were observed and marked using different color markers. The CFRP NSM retrofitted specimen dissipated 826.4 kip-in. (93.37 kN-m) of energy before ultimate failure at 7% drift ratio.

The cumulative hysteretic energy was obtained by adding the hysteretic energy of all the cycles and plotted against the drift ratio, as shown in Figure 6.8. The undulating curve signifies how the energy dissipates in each cycle. Variation in the undulation incorporates changes in the hysteresis due to bond failure between the CFRP NSM bars and epoxy in the footing.

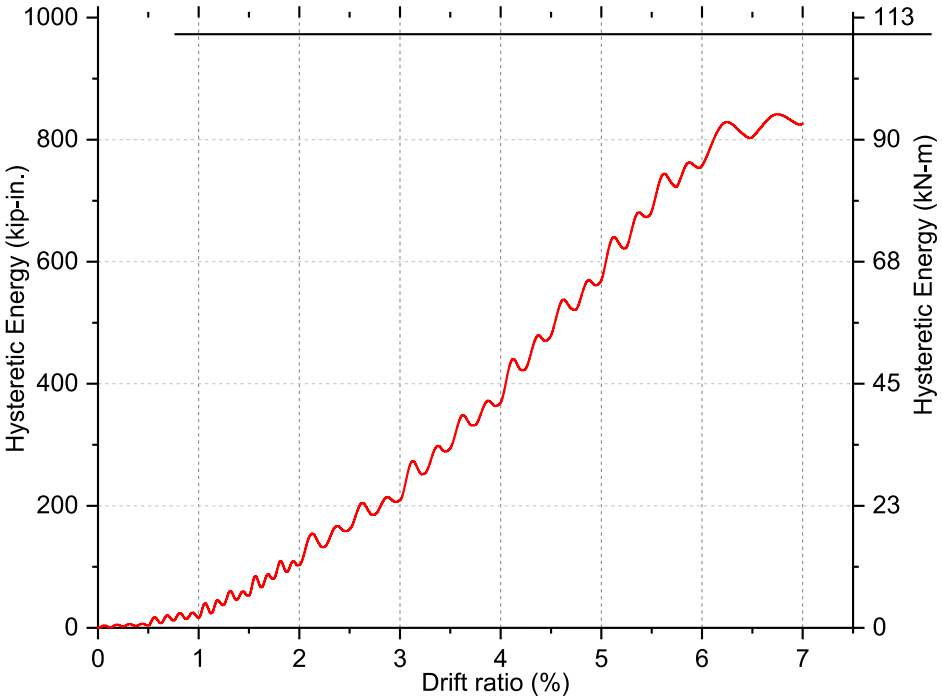

Figure 6.8 Cumulative energy dissipation of CFRP NSM retrofitted specimen R2

6.3.4 Stiffness Degradation of Specimen R2

The obtained stiffness deterioration is plotted against a drift ratio, as shown in Figure 6.9, which shows high initial stiffness of the specimen. This high initial stiffness is due to the addition of a stiff material such as CFRP NSM rods, CFRP wraps, and horizontal CFRP anchors as retrofit material. Bond failure between the CFRP NSM bars and adhesive in the footing resulted in high stiffness degradation after a 2% drift ratio.

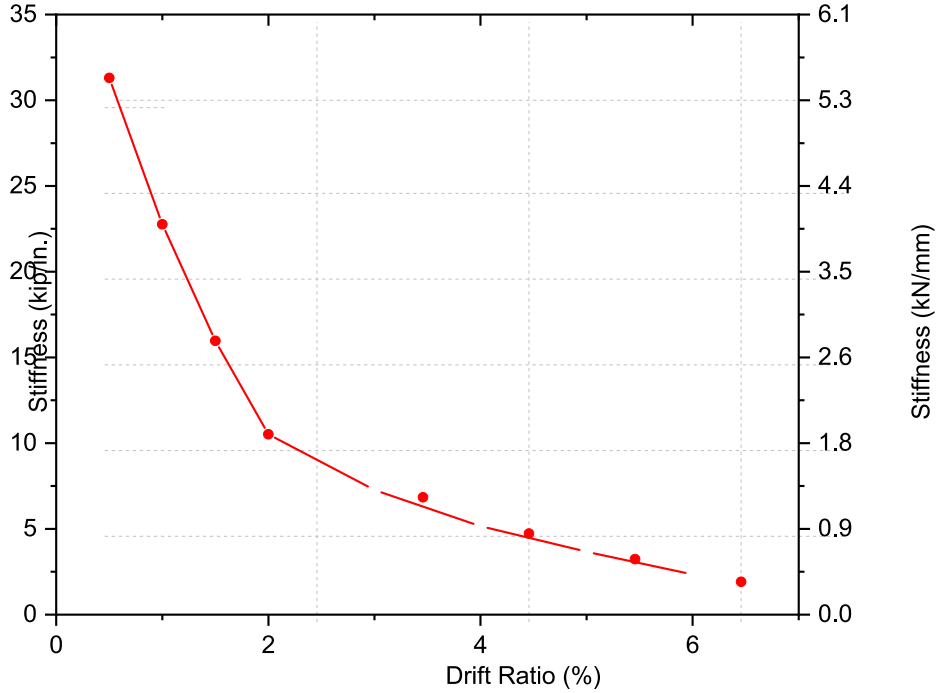

Figure 6.9 Stiffness deterioration of CFRP NSM retrofitted specimen R2

6.3.5 Curvature Profile of Specimen R2

The curvature profile obtained from the LVDT data of the retrofitted specimen is plotted in Figure 6.10. The retrofitted specimen was stiff, with low curvature values in comparison to the modern code-compliant specimen, which was expected.

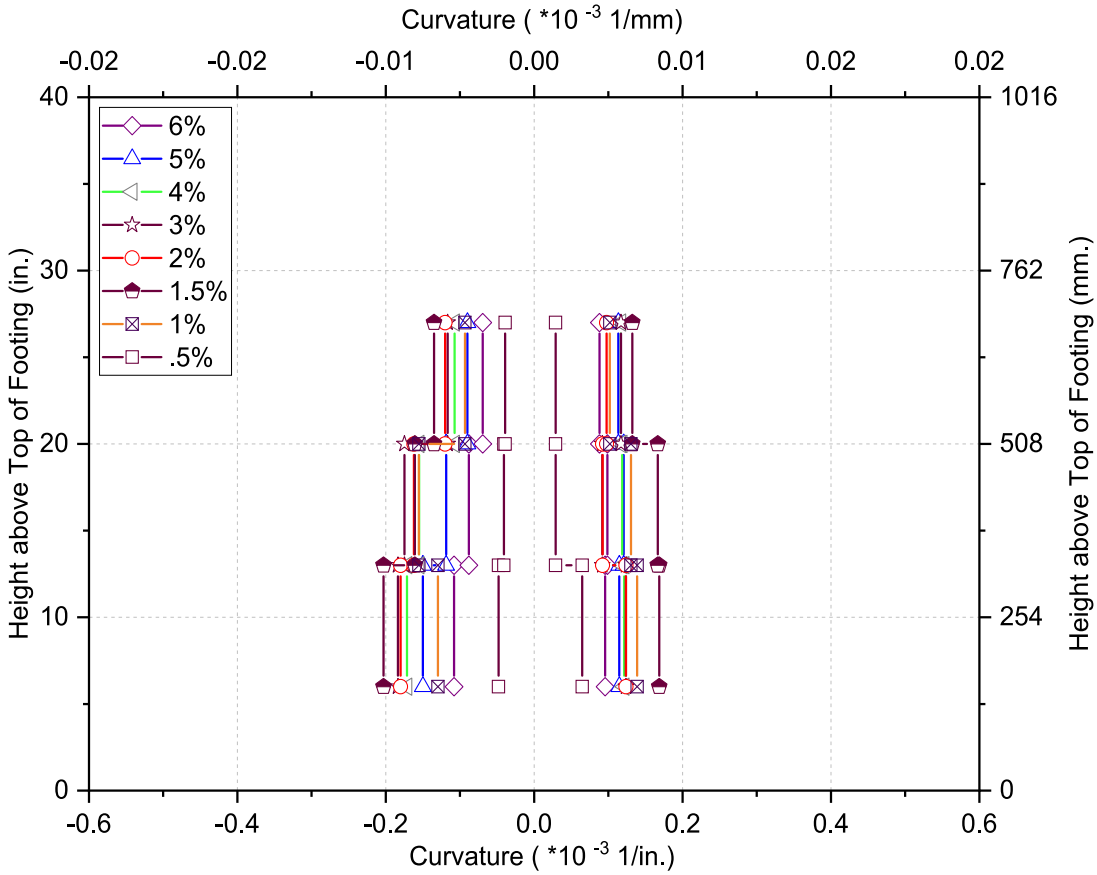

Figure 6.10 Curvature Profile for Specimen R2

6.3.6 Lap Splice Strain of Specimen R2

Lap splices of the longitudinal steel bars were present at the plastic hinge region of the retrofitted specimen. Strain gauges were attached at three levels for the starter and main bars in the lap splice region. The strain gauges were located at 1 in., 5 in., and 9 in. from the top of the footing. The length of the lap splice provided was 14 in. (37 bar diameter-db).

The lap splice performance was compared using the strain data from the strain gauges. The strain plot of the lap splices is shown in Figure 6.11. The middle level strain gauge pair plot shows the starter bar maximum strain is 1,000 μE, whereas the strain of the main bar at the same height is 2,500μE. While comparing the obtained strain data with rebar yield strain (i.e., strain % equals to the ratio of lap splice rebar strain to the steel bar yield strain), we can see that the main bar yields on increasing the drift.

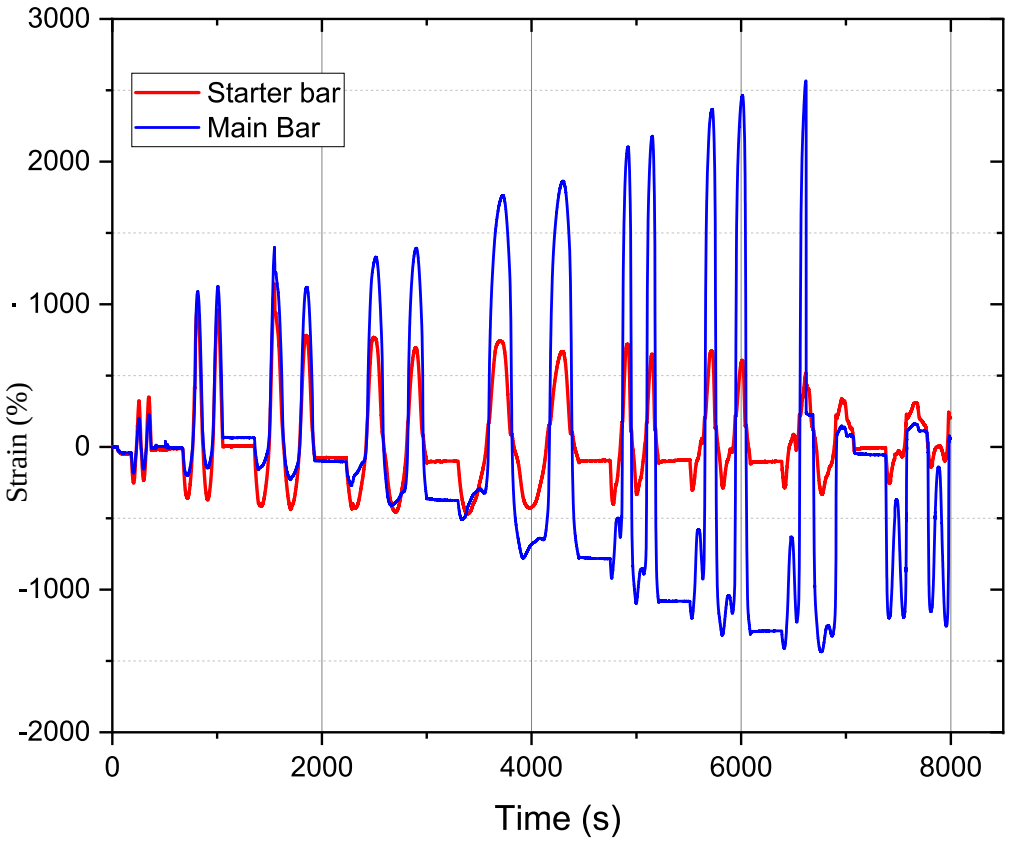

Figure 6.11 Strain at middle level of longitudinal steel bar lap splice of specimen R2

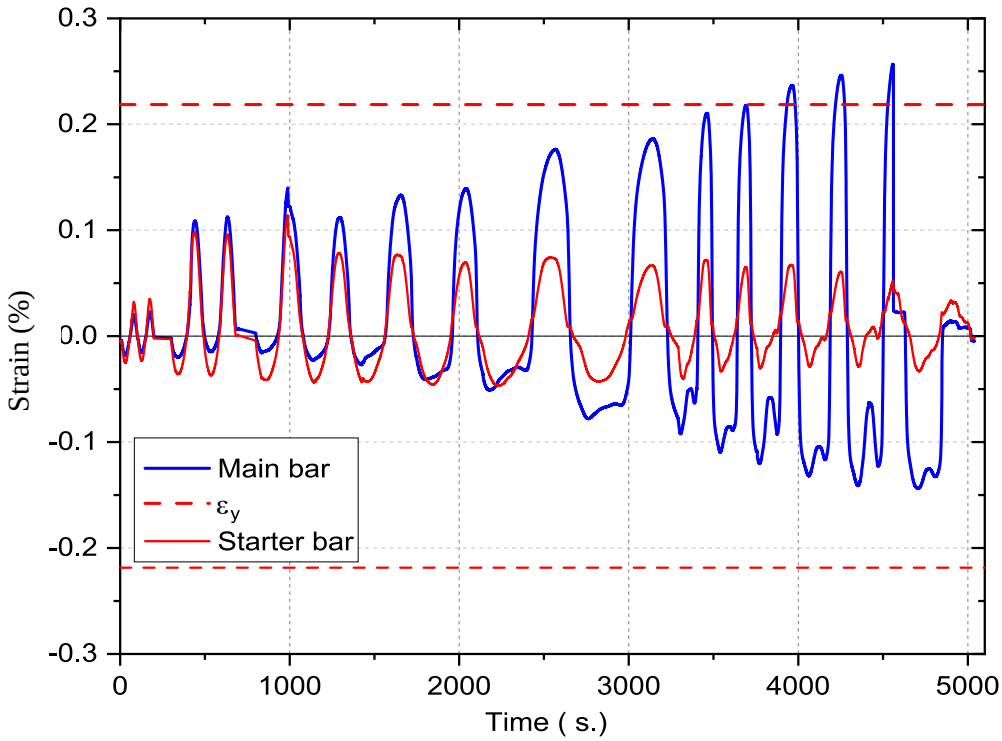

Figure 6.12 Comparison of lap splice bar strain with the yield point

From the above data, we concluded that the outside bar had more strain and yielded in comparison to the inside bar, which did not even yield. The above comparison concludes the lack of effective transfer of tension force generated in the wall to the footing. Even though the CFRP confinement prevented the early pullout failure and confined the NSM bars, Figure 6.12 shows that the NSM CFRP bar has more strain (%) reading in comparison to the steel bar, which implies the lap splice inability to transfer the generated tensile force. Hence, we concluded that the steel lap splice failed to work properly.

6.3.7 Performance of CFRP NSM bars in Specimen R2

The flexural strengthening of the deficient specimen was performed with CFRP NSM rods. This reinforcement transferred the tensile force generated through the applied lateral force to the footing. Three strain gauges were attached on both faces of the specimen on the CFRP NSM rods at 2 in. height from the top of the footing. According to the strain gauge data, the CFRP NSM rods on east and west faces were strained from 10% to 33% of the ultimate strain i.e., 1.58%. The strain plot versus drift ratio of the corresponding NSM CFRP rods is shown in Figure 6.12. The sudden drop in the strain capacity of the NSM rods shown in the figure may be the result of the two consecutive popping actions at 1.5% drift ratio. This popping occurred in both faces and showed that the CFRP NSM rods lost bond to the concrete inside the holes.

Figure 6.12b shows that the CFRP NSM fiber rod went to a maximum 0.5% strain in tension and to 0.34% strain in compression. Before failure, CFRP NSM rod went to 32% of its ultimate tensile strain capacity. In general, the CFRP NSM fiber rods do not take any compressive forces; however, in a retrofit, the CFRP NSM rods were jacketed with four layers of CFRP sheets, which enabled them to take some compressive force.

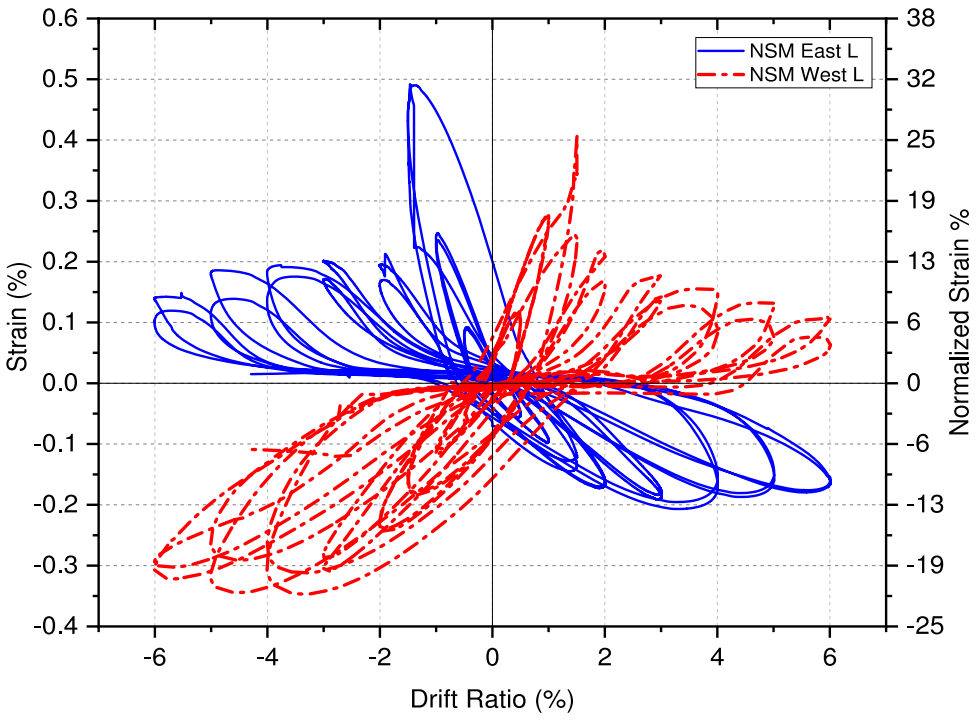

(a)

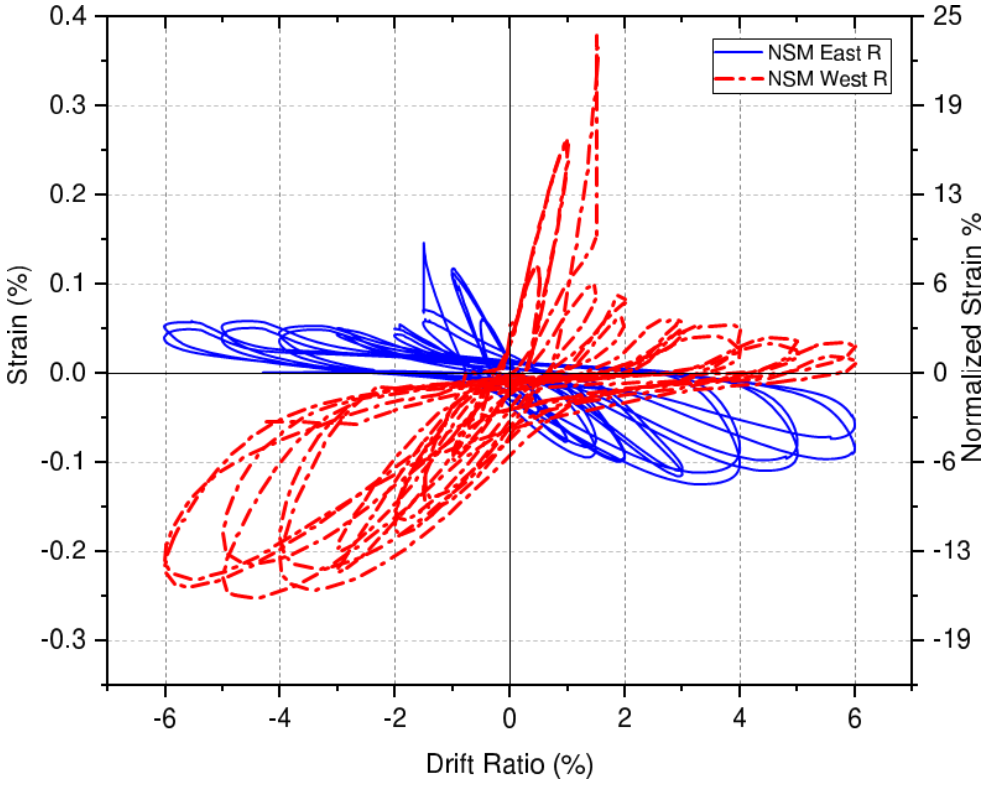

(b)

Figure 6.13 CFRP NSM rod performance: (a) West face and (b) East face of the wall of specimen R2

6.3.8 Physical Damage of Specimen R2

Before starting the test, air bubbles trapped in the CFRP jackets were marked. No cracking or fracture of fibers was heard or seen in the CFRP jacket in the first (0.5%) drift step. A new air bubble was observed on the east face of the wall at 12 in. height from the top of the footing. New hairline cracks were developed on top of the footing parallel to the installed NSM fiber rods. A new air bubble formed on the west face of the wall along the NSM rod at 2 in. height from the footing top. At the 1.5% drift ratio, minor hairline cracks that had formed at the 1% drift ratio increased their width to 0.007 in. Breaking of epoxy resin and splitting of CFRP fibers was heard during the 1% drift step. In the first pull cycle of 1.5% drift, a popping sound was heard at maximum drift. This did not have any significant impact on the hysteresis. However, on the first push cycle of the same drift step, two big popping sounds were heard, having a significant effect on the hysteresis curve. This action decreased the load capacity of the retrofitted specimen by 5 kips. Visual observation and Figure 6.5 obtained from the video recording during the experiment show consecutive popping or premature bond failure of two CFRP NSM rods on the west side of the specimen.

At a 2% drift ratio, the previously formed air bubbles increased in size, and more new air bubbles formed around the bottom 24 in. of the retrofitted specimen. The cracks on top of the footing joined to form a continuous loop around the wall. A new prominent crack was seen on the side of the footing at a 3% drift ratio. More severe concrete spalling was observed on the top of the footing. The size of the crack on top of the footing increased to 0.005 in. width at a 4% drift ratio. The lateral load capacity of the specimen was constant at 17 kips in the west (push) face while it was 25 kips in the east (pull) face. The lateral load capacity of the specimen started to degrade at the 5% drift ratio. The capacity of the specimen decreased to 21 kips in the pull and 16 kips in the push direction, respectively. Cracks in the footing were greater than 0.2 in. wide, and multiple popping sounds were heard during the second cycle of the 5% drift ratio.

Multiple popping sounds were heard in push and pull directions at 6% and 7% drift ratio, respectively. The lateral load capacity of the specimen rapidly degraded to 16 kips and 12 kips at 6% and 7% drift ratio, respectively. The test was stopped at the 7% drift ratio, since the lateral load capacity of the specimen was only half of the maximum load capacity.

Besides formation of some air bubbles, no damage was seen on the CFRP jackets. From the initial visual inspection, no fracture was visible on the CFRP NSM rods or on the interface between the wall and footing. Several popping sounds were heard before the drop in the load capacity of the specimen. From these observations and Fig. 6.5, obtained from the video documentation, we concluded that the wall failed due to improper bonding of at least two CFRP NSM rods and the silica mixed epoxy resin.

6.4 Numerical Model of Specimen R2

Numerical analysis was performed using the OpenSEES (Open System for Earthquake Engineering Simulation) software. The reinforced concrete bridge wall pier was modeled as a single *nonlinearBeamColumn* element with three integration points. In the OpenSEES model, the *Concrete04* material model was used to define cover and confined concrete of the wall pier. The proposed Popovics model defines the compressive stress-strain response. The *Steel02* material was used to model the longitudinal steel of the wall pier in OpenSEES and create a uniaxial steel material object with strain hardening. The CFRP NSM FRP rods were simulated as linear elastic uniaxial brittle material until rupture. The material properties, as defined in the technical datasheet, were used as input for the material. The experimental data analysis shows minimal tensile force transfer from the lap spliced longitudinal steel bars. Therefore, CFRP NSM rods were assumed to withstand all the force, and for simplification in the pushover analysis, the lap splices among the longitudinal steel bars were ignored. Two pushover

models were developed for different criteria. The first model was developed considering the experimental results. From the experimental data, the maximum strain observed in one of the CFRP NSM fiber rods was 0.50% or 0.32 times the normalized strain (ratio of strain data from strain gauge to the ultimate strain the NSM rods can achieve). Hence, even though the bond failure between the NSM rod and epoxy was the main reason behind failure, due to the complexity, of the actual bond failure the CFRP NSM rod was modeled to fail after achieving this strain. The second model was considered as a prediction model, i.e., keeping in mind what would be the ideal performance of the specimen if the CFRP NSM rods had not debonded.

The first pushover model was analyzed, and its result presented in Figure 6.14. The figure shows a comparison between results obtained from pushover analysis and the average backbone curve obtained from the cyclic test. The maximum strain for CFRP NSM rods obtained from the experiment was 0.5%, which was used as input. As seen in the comparison, initially, the steel longitudinal bar did not play any role as the CFRP NSM rods provided the strength to the retrofitted specimen. However, after failure of the CFRP NSM rods around 2 in. displacement, which is marked by the steep fall in the load-carrying capacity of the model, the lap-spliced longitudinal bars and the remaining CFRP NSM rods, provided the strength until failure. Figure 6.14 shows the comparison between the results obtained from the first pushover model and the cyclic experimental result of the retrofitted specimen R2 and the as-built specimen. This figure gives an idea that after failure of the CFRP NSM rod, the model behaves closer to the as-built specimen and fails at a 6% drift ratio. From the above discussion and results, it is clear that the pushover curves obtained from OpenSEES analysis are in agreement with the experimental results.

The second CFRP pushover model was developed to predict the lateral load capacity of specimen R2, considering the CFRP NSM rods would last until failure. In addition to the tensile force, the CFRP NSM rod is exposed to bending and shear force. Therefore, to predict capacity of the specimen, conservatively half of the ultimate strain of the CFRP NSM rod, as described in the technical data sheet (i.e., 1.58%), was considered. The obtained result, as shown in Figure 6.15, was plotted against the experimental result of the retrofitted specimen R2 and the as-built specimen. The predictive model shows that the wall would resist 32 kips of lateral force before failure of the CFRP NSM rods. However, the displacement ductility and ultimate drift ratio would remain practically the same as the experimental results obtained for specimen R2.

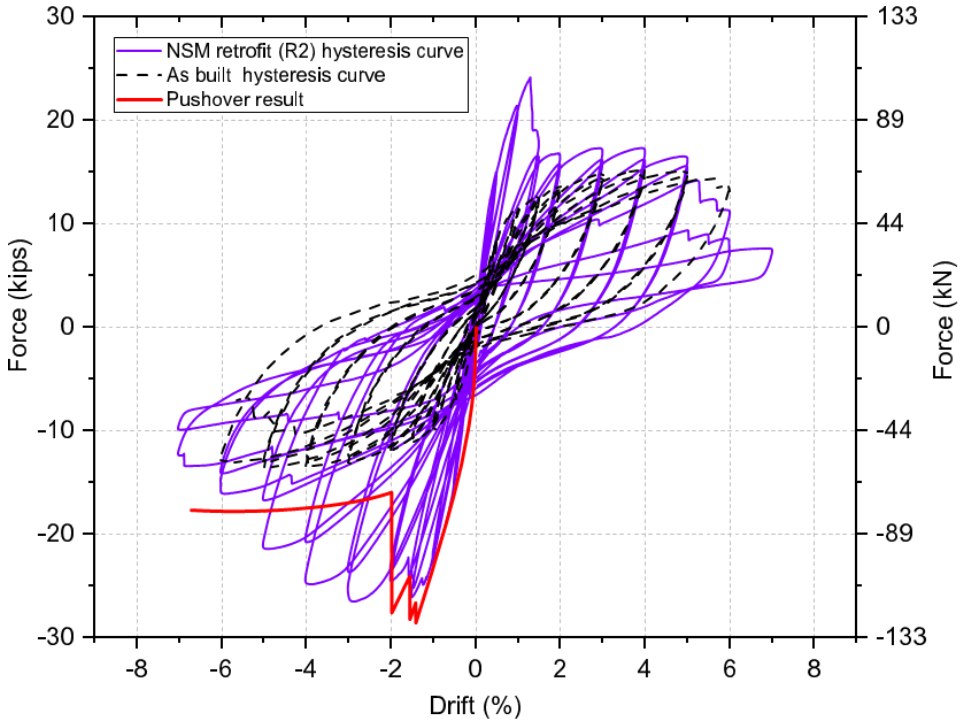

Figure 6.14 Comparison of pushover results in pull direction considering gradual debonding of CFRP NSM rods from OpenSEES with the experimental results of the retrofitted specimen R2 and the as-built specimen

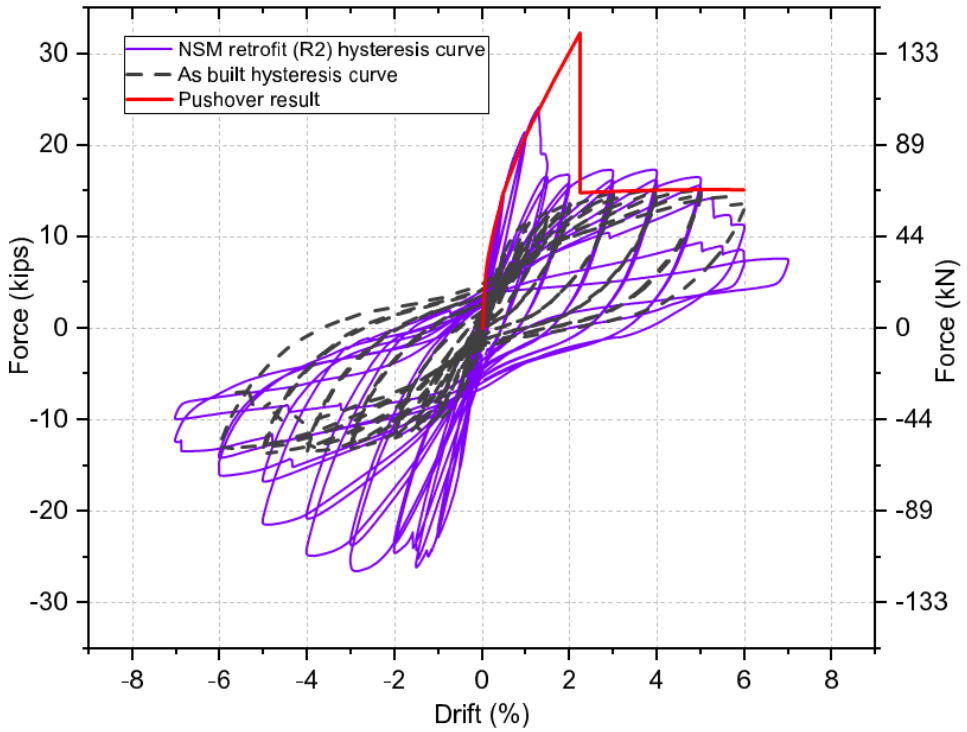

Figure 6.15 Comparison of numerically predicted pushover results from OpenSees with the experimental result of the retrofitted specimen R2 and the as-built specimen

6.5 Conclusion for Specimen R2

The retrofitted specimen was tested under reversed cyclic quasi-static lateral load with a constant axial load. An axial load of 120 kips (534 kN) was applied at the top of the wall for the duration of the experiment. The hysteresis curve shows that the specimen continued to resist lateral force until 1.5% drift ratio when a sharp loss in the lateral load-carrying capacity is observed in the push direction. Through video documentation and experimental observation, premature debonding failure of two of the CFRP NSM rods was observed, resulting in the loss of lateral load-carrying capacity of the specimen. The retrofitted specimen had enough strength to resist the applied lateral force in the pull direction. This premature bond failure resulted in ultimate failure of the specimen at a 5% drift ratio.

The larger drops in force in the hysteresis loops can be attributed to the loss of the bond of the CFRP NSM rods through debonding failure. The retrofit system (i.e., NSM CFRP rods, CFRP wrap) performed well in resisting the increased lateral force and displacement. The CFRP jackets and CFRP horizontal anchors were intact and did not experience any cracks or fracture until the end of the experiment. The failure of the wall was characterized as a 20% drop in total lateral force resistance. This occurred at a displacement of 4.8 in. (122 mm) or 5% drift ratio. The final results are shown in Table 6.1.

Table 6.1 CFRP NSM rods retrofit test summary for Specimen R2

Maximum Force (kip (kN))	25 (113)
Drift Ratio at Maximum Force (%)	1.5
Maximum Drift Ratio (%)	6.0
Maximum Displacement (in. (mm))	5.76 (146)
Number of Cycles	14
Energy Dissipation (kip-in. (kN-m))	827 (93.4)

7. REPAIR OF AS-BUILT WALL PIER USING MILD STEEL AND NSM BARS CFRP ANCHORS AND CFRP WRAPS SPECIMEN ABRP

7.1 Introduction

The control specimen built according to the old code was repaired using CFRP composites after initial testing. The repair included the use of both mild steel NSM bars, CFRP wraps in the hoop direction and CFRP horizontal anchors through the wall thickness. The specimen was tested under the same loading conditions as specified in Section 2.2. The repair was aimed at bringing the wall pier back to a safe and code-compliant condition, although it was apparent that it could not be repaired to perform to the same level as the as-built condition.

7.2 Repair Design of Specimen ABRP

The repair was designed using seven, 66 in. (1.68 m) long No. 4 (13 mm) mild steel rebar embedded in vertical grooves 0.75 in. (19 mm) into the wall on both sides, for a total of 14 steel bars. These were confined with unidirectional V-wrap C200H CFRP wraps oriented in the hoop direction; they included four layers of 24 in. (610 mm) segments at the base, two layers of 12 in. (305 mm) segments above that, and one layer for another 24 in. (610 mm) above those. After the first two CFRP layers were placed in the hoop direction at the base of the wall, 10 V-wrap HM 0.75 in. (19 mm) diameter CFRP anchors were placed through the wall to add confinement to the lap spliced region of the pier and increase the normal pressure to improve the shear friction capacity of the lap splice. These CFRP anchors were then confined by two additional layers of CFRP wraps in the hoop direction. The design of the repair is shown in Figure 7.1.

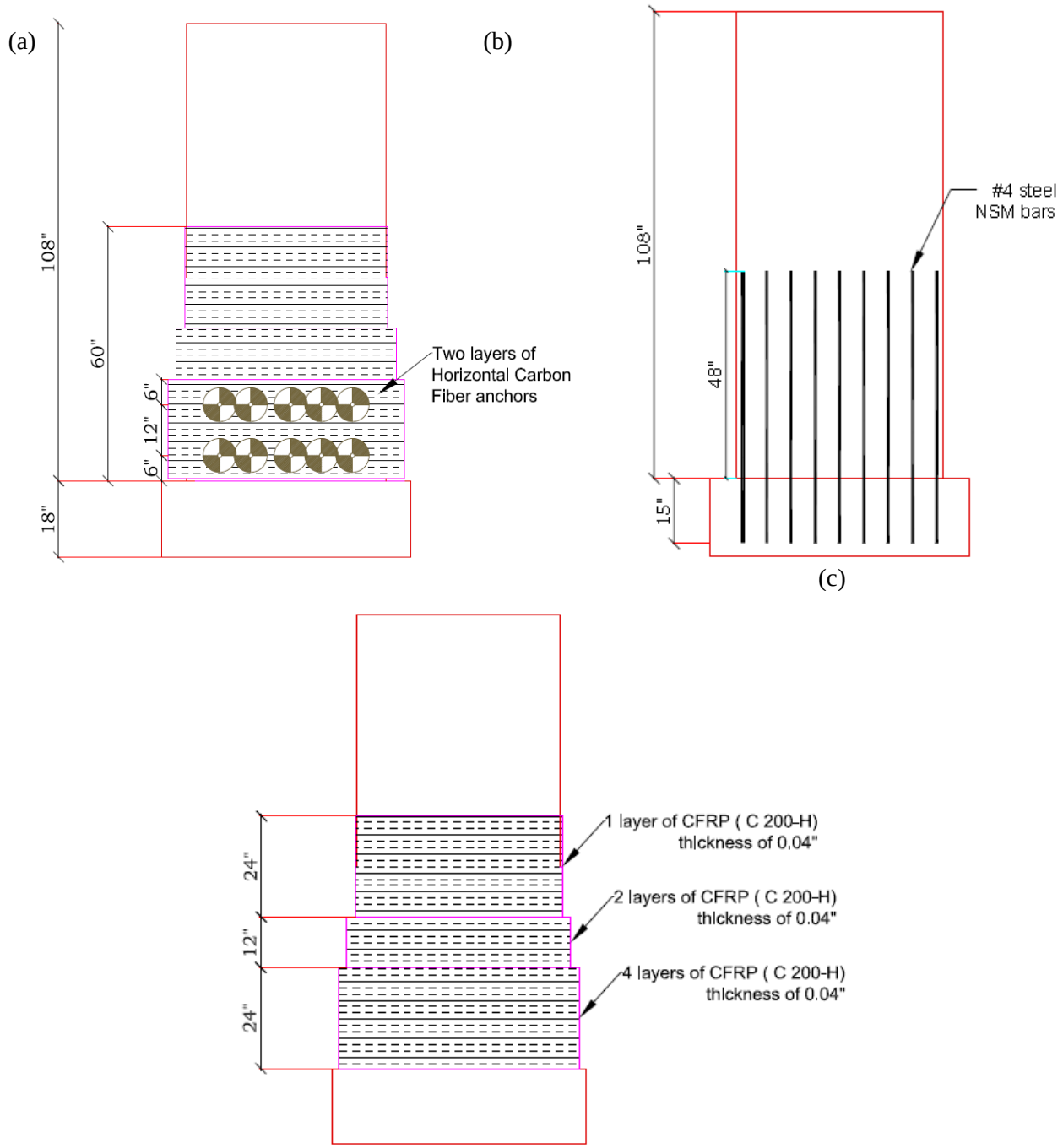

Figure 7.1 Retrofit design of specimen ABRP: (a) steel NSM bars (b) horizontal CFRP anchors, (c) hoop direction CFRP wraps

7.3 Repair Procedure of Specimen ABRP

The wall pier was first prepared by drilling 0.75 in. (19 mm) diameter holes horizontally through the wall for the placement of the CFRP anchors. Next, 0.75 in. (19 mm) square grooves, for the steel NSM bars, were drilled vertically up the wall 48 in. (1.22 m) beginning at the footing and extending down into the entire 18 in. (0.46 m) depth of the footing. Holes in the footing were then plugged with pieces of foam at the base and filled with Hilti HY 200 epoxy. To ensure complete filling of the orifices a float was used. The No. 4 (13 mm) steel NSM bars were then inserted into the epoxy-filled hole. This process is shown in Figure 7.2.

Figure 7.2 Mild steel NSM bar placement for specimen ABRP

Once the mild steel NSM bars had cur the wall was painted with a thin layer of V-wrap 770, a two-part epoxy to saturate the concrete in the wall pier. Part of the epoxy mixture was then combined with silica fume used to thicken the epoxy. This thickened paste was also applied to the wall in a thin layer to help keep the sheets of fibers in place before they had cured. The steel NSM steel bars were then moved to the side of the slots so the grooves could be filled with the paste. The steel bars were then pushed into the epoxy filled grooves and completely covered. This is shown in Figure 7.3.

Figure 7.3 Epoxy coverage of steel NSM bars of specimen ABRP

During this process, sheets of CFRP V-wrap were saturated with the original epoxy mixture. Each layer of the CFRP wrap was then carefully applied to the wall using metal rollers to ensure no air pockets could form under the layers. On completion of each layer application, the CFRP wrap was again covered in a thin layer of the thickened epoxy mixture. This process was repeated until all the CFRP wraps were applied. After the second layer of the CFRP sheets were applied in the hoop direction at the base, the fully saturated CFRP anchors were pulled through the wall and spread on both wall faces. The CFRP composite application is shown in Figure 7.4.

(a) (b)

Figure 7.4 Repair application process for specimen ABRP: (a) fiber saturation, (b) hoop direction CFRP wrap application, (c) horizontal CFRP anchors, (d) final wall repair

(c)

(d)

Figure 7.4 (continued)

7.4 Test Results of Specimen ABRP

The repaired specimen was tested under quasi-static loading with five-minute breaks in-between cycles. An axial load of 120 kips (534 kN) was applied at the top of the wall for the duration of the experiment. This load corresponds to 6% of the load-carrying capacity of the wall pier and simulates a bridge deck. Crack sizes and material degradation were observed throughout the test and were collected with various measured data to determine wall behavior. The hysteretic curve from the test is shown in Figure 7.5. The hysteresis curves exhibited general stability throughout the entire test until the first cycle of the 5% drift ratio when the lateral force dropped by 34% of the maximum. The rough edges of the hysteresis loops can be attributed to tensile failure and debonding of the CFRP sheets. The larger drops in force are due to debonding and tensile failure of the steel NSM bars.

7.4.1 Displacement Ductility of Specimen ABRP

The ductility of the wall pier was found following the procedure outlined in Section 2.7.1. The ultimate displacement indicated by a 20% drop in the ultimate lateral load strength of the pier wall was 4.8 in. (12.2 cm). Yield displacement was 0.74 in. (1.9 cm), resulting in a displacement ductility ratio of 6.5 for the system. Figure 7.6 shows the envelope, and idealized backbone developed using this procedure.

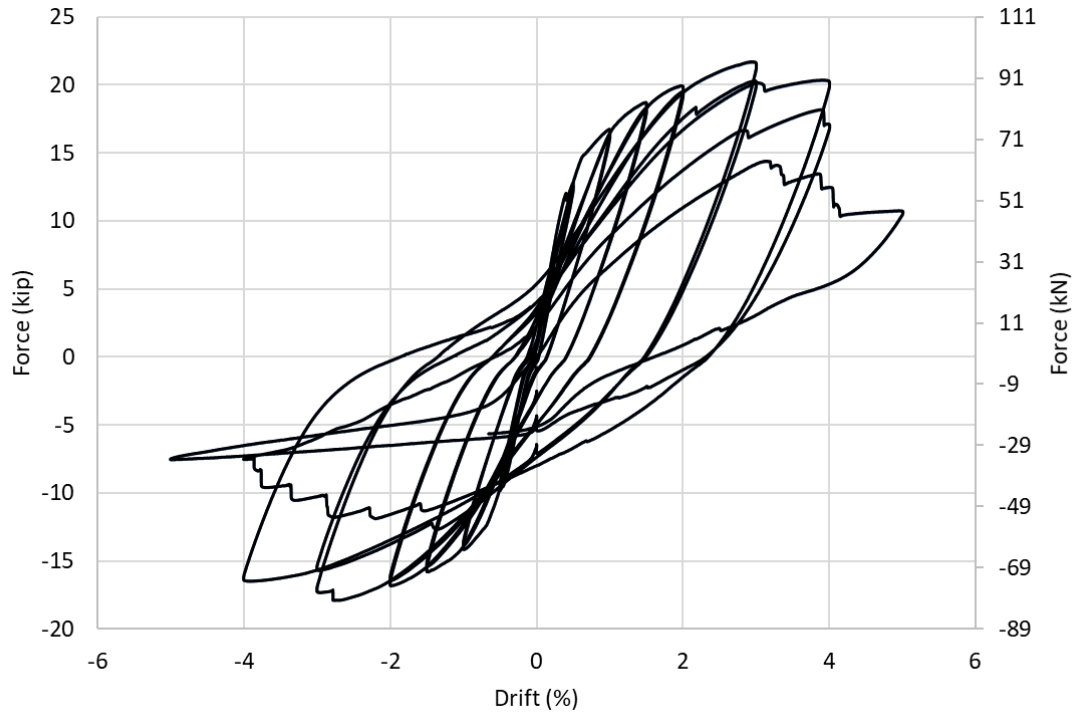

Figure 7.5 Hysteresis of as-built wall pier

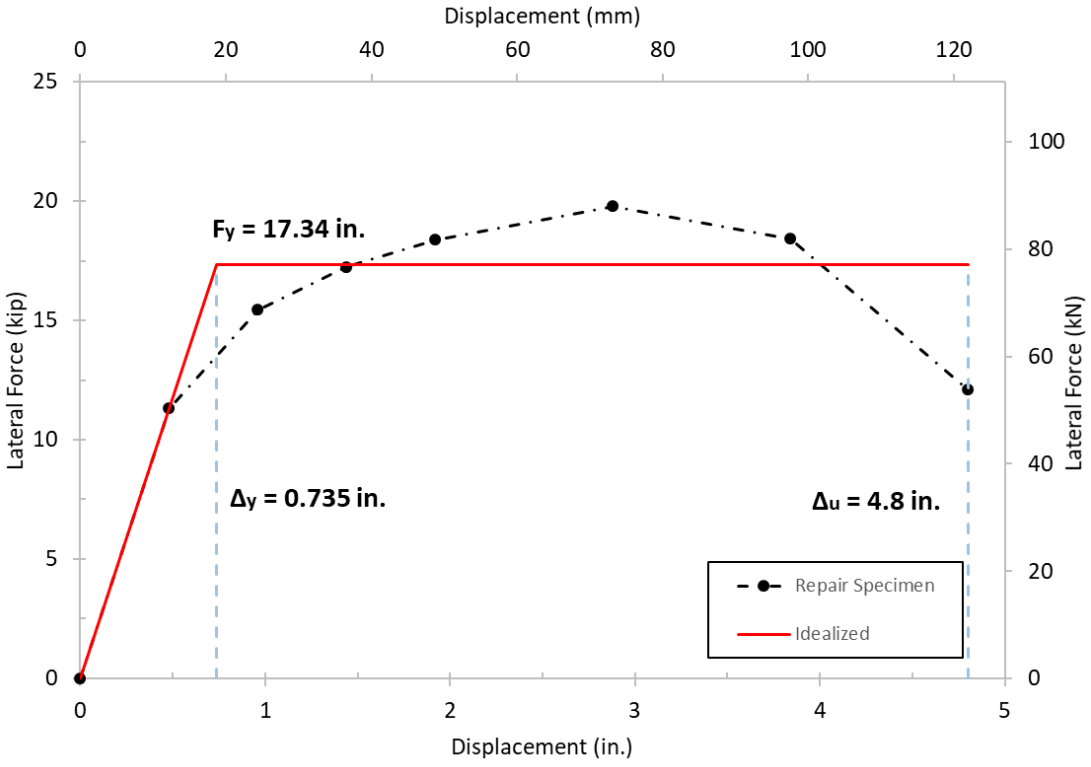

Figure 7.6 Displacement ductility plot of repaired specimen ABRP

7.4.2 Plastic Rotation of Specimen ABRP

The plot of plastic rotation of the seismically repaired wall pier was created using the procedure in Section 2.7.2. This plot is shown in Figure 7.7. From this plot, it can be seen that the specimen reached 0.031 rad of plastic rotation before ultimate failure at 4% drift. The plastic rotation of 0.031 rad combined with the displacement ductility ratio of 6.5 signifies a very good performance.

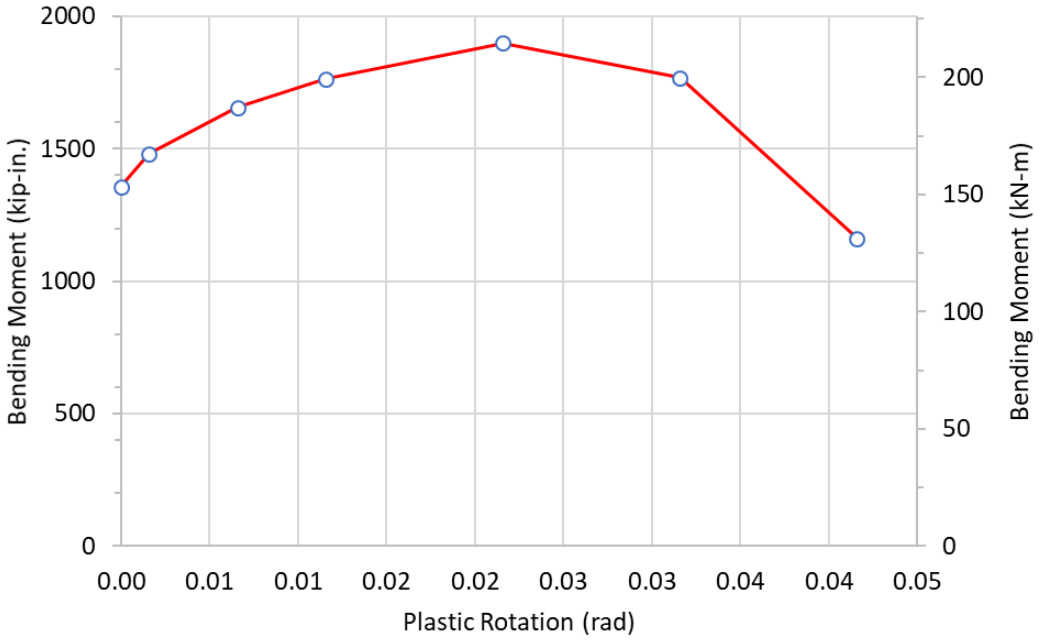

Figure 7.7 Plastic rotation plot or repaired specimen ABRP

7.4.3 Hysteretic Energy Dissipation of Specimen ABRP

The specimen hysteresis is shown in Figure 7.5. This plot exhibits overall behavior of the wall during testing. There is pinching in the center, which defines behavior of the plastic hinge formed at the base of the wall pier. The hysteretic curve displays the brittle nature of the CFRP system used to retrofit the wall, where large sporadic drops of force occur at multiple loading increments throughout the test. The cumulative hysteretic energy dissipation throughout the test is given in Figure 7.8. The total dissipated energy for the repaired specimen was 452.8 kip-in. (51.2 kN-m).

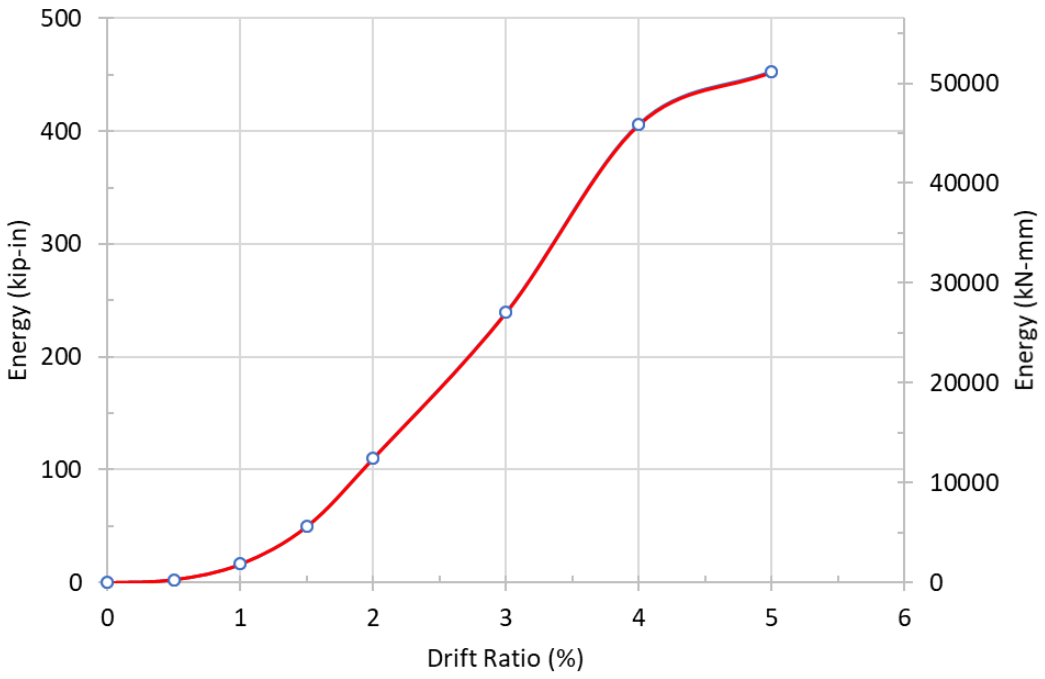

Figure 7.8 Cumulative hysteretic energy dissipation of specimen ABRP

7.4.4 Stiffness Degradation of Specimen ABRP

The average hysteretic stiffness was calculated as described in Section 2.7.4. Figure 7.9 shows the stiffness values plotted against the drift ratio of the specimen. The repaired specimen exhibited exponential stiffness degradation throughout the test. The initial stiffness of the repaired specimen was 24 kips/in., which is 1.5 times larger than the as-built specimen initial stiffness of 16 kips/in.

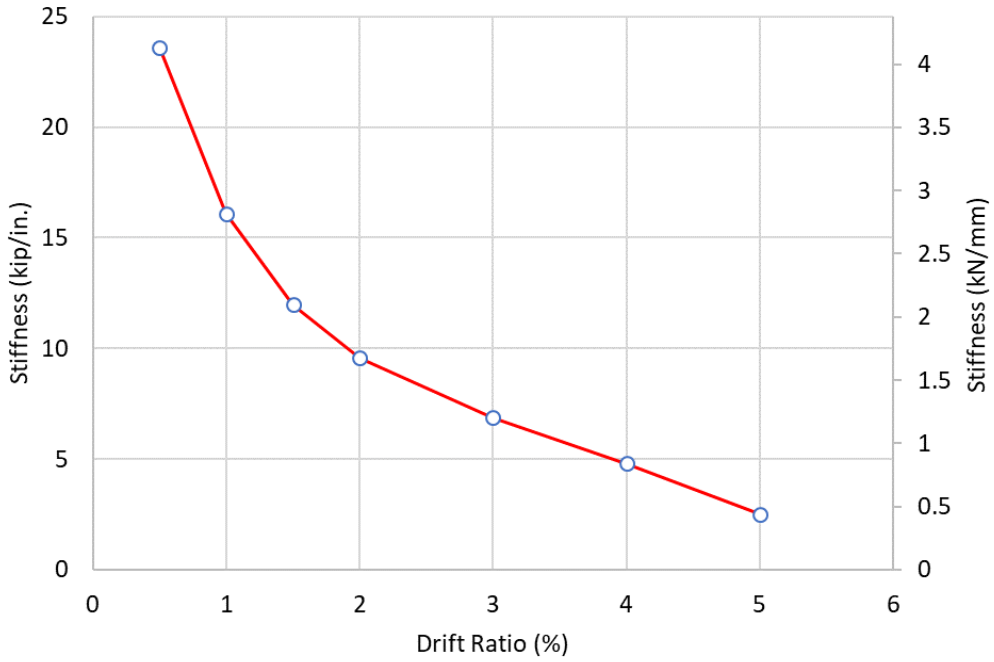

Figure 7.9 Stiffness deterioration of the repaired specimen ABRP

7.4.5 Damage Index of Specimen ABRP

The damage index discussed in Section 2.7.5 was applied to the repair test results, and the plot can be seen in Figure 7.10. This graph shows damage state of the wall pier at each drift ratio against the damage limit states of Table 2.2. The specimen reached moderate damage at the 1% drift ratio, and severe damage was seen at the 2% drift ratio. The collapse stage occurred when the wall reached 4% drift ratio. The repair specimen reached ultimate failure on the second cycle of 4% drift ratio. The plot accurately depicted this failure.

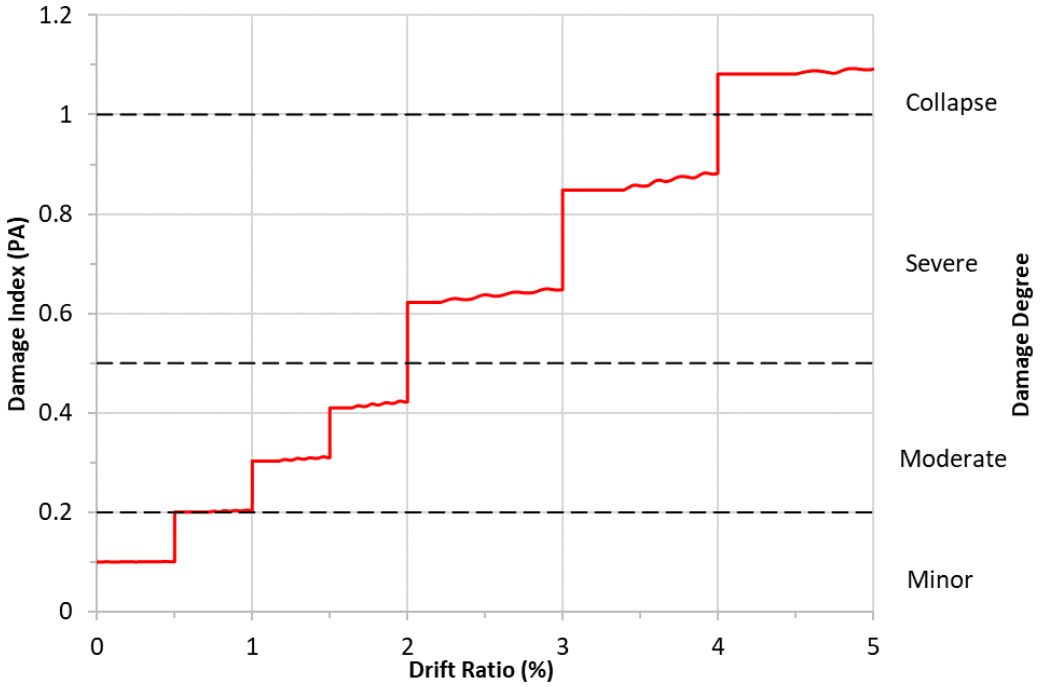

Figure 7.10 Damage Index of repaired Specimen ABRP

7.4.6 Physical Damage of Specimen ABRP

The experiment hysteresis is shown for the seismically repaired RC wall pier ABRP in Figure 7.5. The hysteresis loops show relative stability until the second cycle of the 3% drift ratio when we first saw a 1.6 kip (7.0 kN) drop in lateral load on the west ("push") side of the wall, and a 1.3 kip (5.9 kN) drop on the east ("pull") side of the wall. The lateral load resistance stayed relatively stable until ultimate failure. After the 4% drift cycle, the wall lost 7.8 kips (34.7 kN) of lateral resistance on the west wall face and 9.9 kips (44.4 kN) on the east face. This equated to a 36% drop in ultimate lateral load on the west and a 63% drop in ultimate lateral load on the east. Because these drops were larger than 20%, the 4% drift ratio was characterized as the point of failure. The lateral load on the east side of the wall never reached the same ultimate load as the west side. This can be attributed to the more extensive damage exhibited on the east side of the wall in the as-built wall pier test.

No visible cracking was exhibited in the wall pier or footing until the 1.5% drift ratio, when we began to see hairline cracks in the footing and at the interface of the wall and footing. The footing cracks are shown in Figure 7.11. At 2% drift ratio, the cracks at the interface of the wall and footing spread around the entire base of the wall. These cracks were too small to measure, but were visible as shown in Figure 7.12.

Figure 7.11 Footing cracks at 1.5% drift ratio for specimen ABRP

No debonding occurred on the CFRP wrap surface until the 3 % drift ratio. These debonded regions began to form at the base of the footing on the east wall face, and 8.0 in (3.14 cm) above the footing on the west side of the wall. The largest of the debonded regions measured about 15.0 in^2 (9670 mm^2). The majority of them were located at segments of the mild steel NSM bars underneath the CFRP jacket. At the 3% drift ratio, the east side of the wall also lost a lateral load of 1.3 kips (5.9 kN).

At the 4% drift ratio, the west side of the wall exhibited a significant force drop. At this point, 1.3 kips (5.9 kN) of lateral load resistance was lost. The east side also lost 9.9 kips (44.4 kN) of lateral load in the second cycle of 4% drift, which was 63% loss of ultimate strength on the east side of the wall and indicated failure of the wall. In addition, at 4% drift, debonding of the mild steel NSM bars had also spread on the west face of the wall pier, as shown in Figure 7.12. At this time, large portions of CFRP wrap debonded at the base of the wall. On the west face, this section measured about 4.0 in. (10.2 cm) high by 24.0 in (60.9 cm) wide, also shown in Figure 7.12. A large debonded region was also exhibited at the base of the east side of the wall but only measured 12.0 in (30.4 cm) by 3.0 in. (7.6 cm).

Figure 7.12 West face CFRP wrap debonding at 4% drift ratio for specimen ABRP

At the 5% drift ratio, the east side of the wall went through another significant force drop. At this point, 2.3 kips (10.6 kN) of the lateral load was lost. At the 5% drift ratio small regions of CFRP wrap debonding arose on the east face of the wall. These sections were no larger than 4.0 in^2 (25.8 cm^2) and were all located on top of the mild steel NSM bars. The debonded regions are shown in Figure 7.13. The wall test was terminated the at 5% drift ratio because of the substantial loss of lateral resistance seen on both sides of the wall in the second cycle of the 4% drift ratio.

Figure 7.13 East face CFRP wrap debonding at 5% drift ratio for Specimen ABRP

7.5 Conclusion for Specimen ABRP

The seismic repair of the as-built reinforced concrete wall pier built to deficient standards was tested under quasi-static cyclic loading. The pier failed in the second cycle of the 4% drift ratio due to debonding of the mild steel NSM bars. The west side of the wall pier exhibited more physical damage than the east side because the majority of damage from the as-built test was on the east wall face. Thus, the west side of the wall had to resist more lateral load as it had more strength before the repair test. The damaged region on the east transferred stress to the west side of the wall and allowed more damage to accrue throughout the remainder of the test.

The repaired specimen performed better than the as-built even though it lost 20% of its lateral force resistance after 4% drift. The energy dissipation of 452 kip-in. (51.2 kN-m) is 0.9 times that of the as-built wall pier, which reached 500 kip-in (56.5 kN-m). However, the repaired wall had a larger cumulative energy dissipation until the end of the 3% drift ratio. The repaired wall pier reached 4% drift ratio with increased stiffness and lateral force resistance. Although the repaired wall piers failure was categorized as brittle, it performed well until the point of failure. Results from the repaired specimen ABRP are shown in Table 7.1.

Table 7.1 Test summary for repaired specimen APRP

Maximum Force (kip (kN))	21.7 (96.5)
Drift Ratio at Maximum Force (%)	3.0
Maximum Drift Ratio (%)	5.0
Maximum Displacement (in. (mm))	4.8 (122)
Number of Cycles	13
Energy Dissipation (kip-in. (kN-m))	452.8 (51.2)

8. REPAIR OF MODERN CODE COMPLIANT WALL PIER USING CFRP DONUT-SPECIMEN MCRP

8.1 Introduction

After strong earthquakes, rather than a complete replacement, repair of damaged bridges is economical and has a beneficial impact on bringing traffic flow back to normal. This fact is related to the concept of seismic resiliency. A damaged reinforced concrete wall pier specimen meeting the current AASHTO code was repaired to restore its stiffness and load-carrying capacity. The specimen was repaired using the plastic hinge relocation technique. The primary objective of this technique is to strengthen the original damaged region so it can withstand additional shear and bending moments generated from a future earthquake.

8.2 Repair Design for Specimen MCRP

The modern code-compliant specimen lost its stiffness with the force transferring mechanism in the plastic hinge region after the original cyclic test. The main reason behind this loss was the severe concrete spalling and fracture of longitudinal rebar. The objective of the repair was to restore the stiffness and load-carrying capacity of the wall pier. The plastic hinge region was relocated to a new, undamaged region using a plastic hinge relocation technique with similar methods developed for columns (Parks et al. 2016; Rutledge et al. 2014; Wu and Pantelides 2017a). To move the plastic hinge to a new location, the damaged section of the wall pier was enlarged to an elliptical shape using a prefabricated CFRP shell. The modified wall section consisted of epoxy anchored headed steel bars with the void filled between the wall pier and shell with expansive cement concrete. The CFRP shell provided confinement and acted as formwork for the additional cast concrete.

8.2.1 Repair Height and Cross Section for Specimen MCRP

The first step in the seismic repair required selection of the repair height for the damaged specimen. The repair height must be long enough to relocate the plastic hinge to the less damaged region. However, before choosing a repair height, it is important to consider that the higher the repair height, the higher is the bending moment demand to reach a similar displacement capacity as the current code-compliant specimen. The bending moment capacity of the repaired specimen, as shown in Figure 8.1, was extrapolated at the new plastic hinge location. The bending moment resulting in the plastic hinge formation of the modern code-compliant specimen (Mp) must be developed in the new plastic hinge location and is given by:

$$\mathrm{M}_H = M_p \,/\, (1 - H_R / H_W) \tag{8.1}$$

where M_H = bending moment capacity of the section at the base of the column; H_R = height of repair; H_W = height of wall specimen from the base of the footing to the point of lateral load application. The rectangular cross-section of the wall pier at the repaired region was converted to an elliptical section with a 30 in. minor axis and 60 in. major axis length.

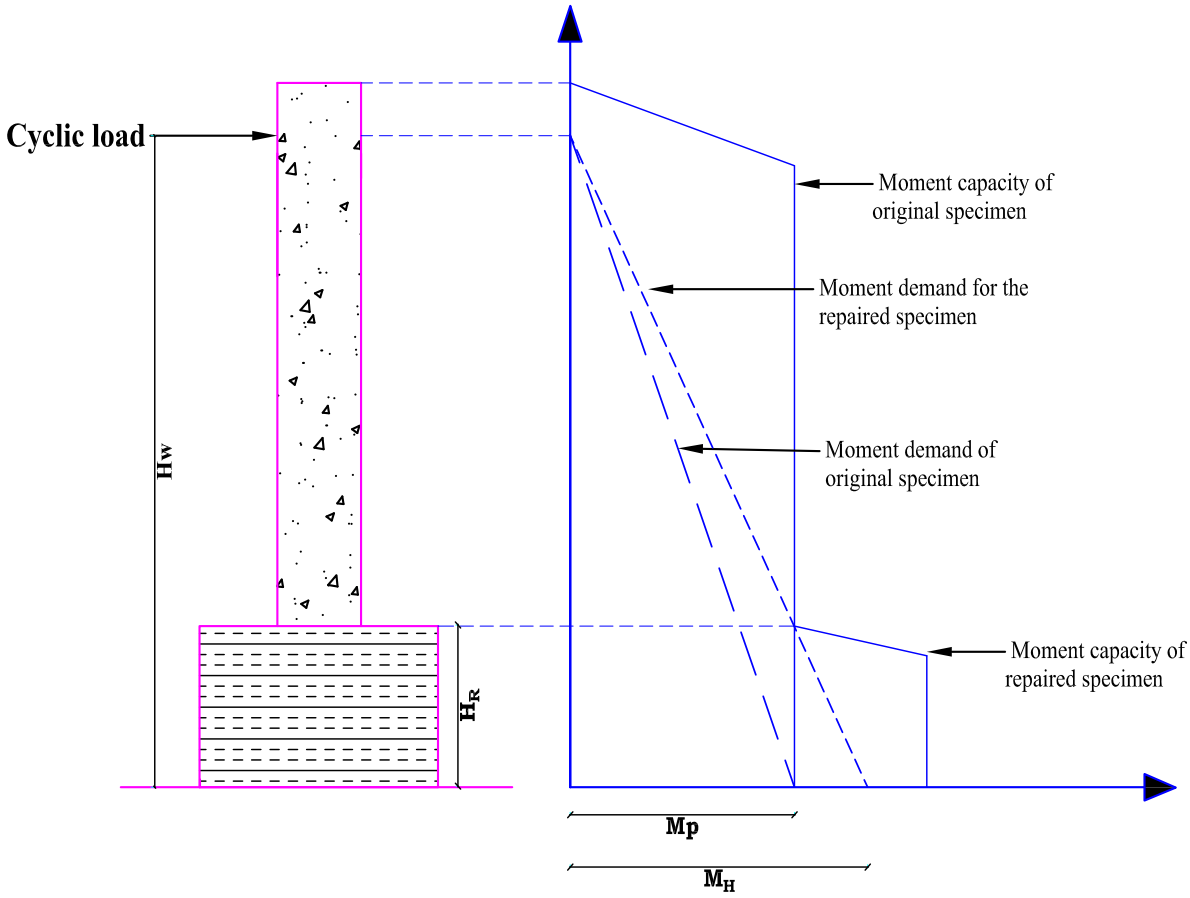

Figure 8.1 Moment demand and moment capacity of the repaired specimen

Figure 8.2 shows the cross section of the repaired specimen with the combination of an elliptical CFRP shell and a number of headed steel bars. The elliptical CFRP shell provided shear strength and concrete confinement of the repaired section and the headed steel bars provided flexural strength. Guidelines for providing an optimal shape of the CFRP shell for confinement were developed by (Yan and Pantelides 2011) and were followed here.

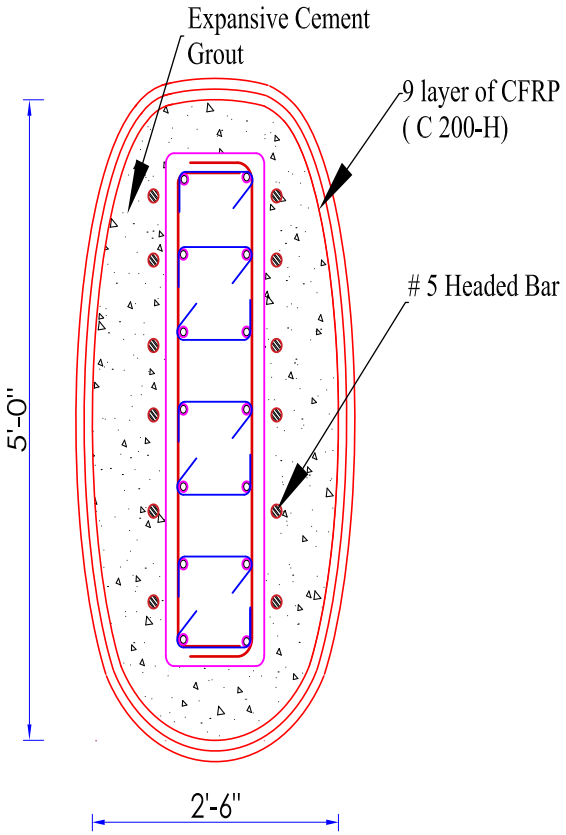

Figure 8.2 Elliptical cross-section of the repair region for specimen MCRP

8.2.2 Headed Steel Rebar for Specimen MCRP

The current code-compliant specimen failed fracture of the longitudinal steel bars. Additional steel bars in the form of headed steel bars were used to reestablish the flexural strength and tension transfer between the wall pier and footing. Since most of the rebars yielded in the first cyclic test, only 25% of the rebar present in the original wall was assumed to provide flexural strength in the repaired region. The headed steel bars were evenly spaced on the side of the wall, as shown in Figure 8.3. The ultimate tension in the post-installed headed bar was obtained using the equation.

$$T_u = M_H / (j_d) \tag{8.2}$$

where jd = effective depth of the repaired section. The headed steel bars were assumed to be at a distance of 2 in. from the face of the wall, and depth ‘d’ is considered from the outside face of the CFRP shell to the center of the headed bars. With the assumption of j equal to 0.9 and d equal to 23 in. the ultimate tension in the headed steel bars equals 196 kips. For a successful repair, the nominal tensile capacity of the post-installed steel bars in the repaired region should be greater than 196 kips. The nominal tensile capacity of the section is given by

$$T_n = 1.3\, f_y\, A_s \tag{8.3}$$

where fy = yield stress of the headed steel bar; As = area of the required headed steel bars.
The ultimate tensile capacity of the steel bar was assumed as 1.3 times the yield capacity (Parks et al. 2016). With six #5 headed steel bars, and a conservative estimate of 25% contribution from the bars

inside the wall, Eq. (8.3) gives a tensile capacity of the section of 205 kips, which is higher than the required capacity. The minimum embedment length to develop the ultimate strength is given as

$$L_d = 1.3\, A_b f_y / (d_b \pi\, \tau_{bond}) \tag{8.4}$$

where Ab=Area of rebar, 0.31 in2; fy= yield strength of the bar, 58,000 psi; db= diameter of the bar, 0.625 in; τ_{bond}= epoxy bond strength, 1,700 psi. From Eq. (8.4) the minimum embedment length was 7 in. However, to prevent the pullout and smooth transfer of the force, a 12 in. embedment length was provided.

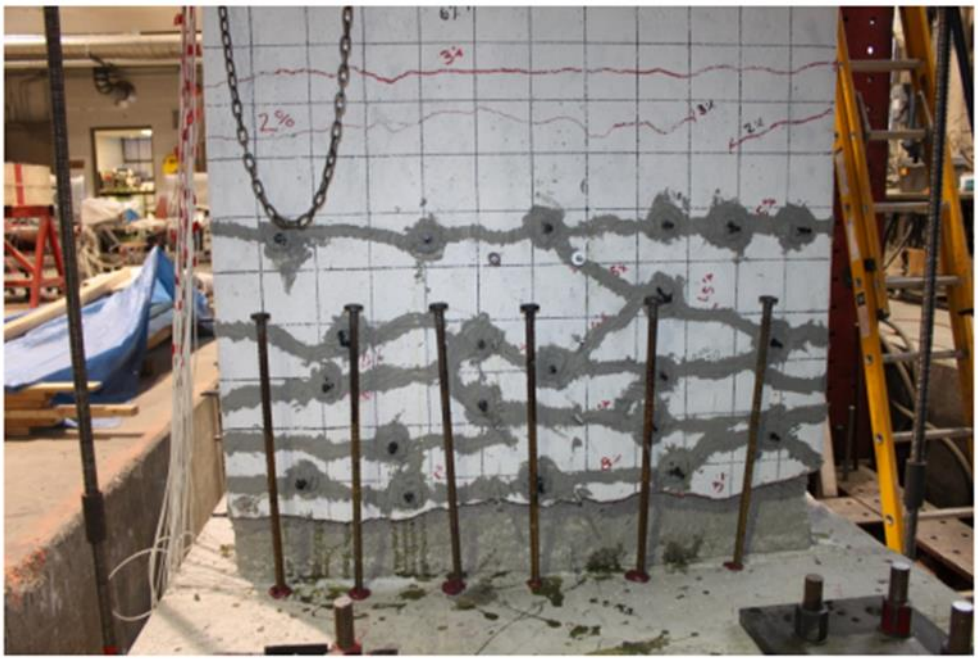

Figure 8.3 Installed headed steel bars for repaired specimen MCRP

8.2.3 Nonshrink Concrete Mix Design for Specimen MCRP

Nonshrink concrete with a compressive strength of 4,000 psi was provided in the CFRP shell. The compressive strength of the concrete chosen was lower than the compressive strength of the wall pier concrete. Komponent cement was added in the concrete mix to control the expansion of the CFRP shell. A quantity of 15% by volume of Portland cement was replaced with Komponent expansive cement to minimize shrinkage (Wu and Pantelides 2017b) and to provide active confinement in the repair concrete.

8.2.4 Steel Collar Design for Specimen MCRP

To increase bond between the wall pier concrete and expansive cement concrete, a steel collar consisting of steel plates and steel studs was installed on the wall perimeter inside the CFRP shell. The steel plate used for the collar was 0.375 in. thick and 6 in. in height. The shear force demand along the collar region was determined using the following equation (Wu and Pantelides 2017a):

$$Q_D = R\, L_r / w \tag{8.5}$$

where R = predicted lateral force capacity, 42.08 kips; w = width of the cross-section, 12 in., L_r = vertical distance between the lateral force and centroid to shear studs, 75 in. The shear force demand obtained from the Eq. (8.5) was 263 kips. The nominal shear strength of one steel stud Q_n can be determined as (AISC 2016):

$$Q_n = 0.5\, A_{sa}\sqrt{(f'_{cR}\, E_c)} \tag{8.6}$$

where A_{sa} = area of headed steel studs, 0.78 in2 ; f'_{cR}= repair concrete strength, 4,100 psi.; E_c= modulus of elasticity of repair concrete, 3,650 ksi. The nominal shear strength of one steel stud obtained from Eq. (8.6) is 48 kips. Hence, six shear studs were required on each face as shown in Figure 8.4.

Figure 8.4 Steel collar with welded studs for specimen MCRP

8.2.5 CFRP Wrap Design for Specimen MCRP

Using Eq. (2.7) to Eq. (2.12), we obtain the required thickness of 0.032 in. to provide adequate shear capacity in the repaired region. One additional layer of CFRP wrap was provided for shear strengthening of the repaired section. From the above calculation, nine layers of CFRP wraps with the given properties were used to form a CFRP shell. In addition, one vertical CFRP layer was provided to prevent the cracking and splitting of the fibers in the hoop direction.

8.3 Repair Procedure for Specimen MCRP

All cracks were sealed using a sealant. The injection points were installed along the cracks with this sealant at a 5 in. spacing. Epoxy was injected from all entry points, as shown in Figure 8.5, starting from the bottom and was allowed to set for two days to reach full strength.

Figure 8.5 Epoxy injection of cracks for specimen MCRP

Six holes on each side of the wall were drilled into the footing for the post-installed headed steel bars. The drilled holes were 13.5 in. deep. The vacuumed hole was injected up to half the depth of the drilled hole, and the headed bar was slowly twisted and inserted into the epoxy injected hole. Figure 8.6 shows the headed bar installation process. The steel collar was placed around the wall starting at 12 in. from the top of the footing to ensure the grout and original concrete of the wall pier would act in a composite manner.

Figure 8.6 Headed steel bar installation process: (left) drilling holes;
(right) headed bar placement for specimen MCRP

The CFRP shell was created using unidirectional V-wrap C200H fibers oriented along the hoop direction and was cured with epoxy resin. The formwork for the CFRP composite shell was created with a combination of precut plywood and 24-gauge aluminum foil. To create the CFRP composite shells, nine hoop layers and one vertical layer using the precut sheets of CFRP impregnated with resin were applied over the formwork. The first eight hoop layers of CFRP sheets were applied, followed by a single vertical layer and finished with the outer one final hoop layer. After curing, the aluminum foil and plywood were removed.

Once the CFRP composite shell fully cured, it was centered according to its position and was prepared for casting concrete. The non-shrink concrete was cast to fill the space between the CFRP shell and wall pier. The specimen was left to cure for at least 28 days. The details of the elliptical cross section and the repaired wall pier specimen are shown in Figure 8.2 and Figure 8.7, respectively.

Figure 8.7 CFRP donut formation: (left) shell formation with precut aluminum foil; (right) CFRP wrapped around the aluminum form

8.4 Test Results for Specimen MCRP

The repaired specimen was tested under quasi-static loading with five-minute breaks between cycles. An axial load of 120 kips (534 kN) was applied at the top of the wall for the duration of the experiment. The repair system performed well in relocating the plastic hinge. No failure was observed in the repair system. The CFRP shell was intact and did not experience any cracking until the end of the experiment. A good bond was developed due to the effective performance of the shear studs and the steel collar confined by the CFRP shell. The lateral force capacity of the repaired specimen reached 36.25 kips (161.248 kN) before failure at 6% drift ratio. The repaired specimen failed at the relocated plastic hinge region due to unexpected brittle buckling failure above the “CFRP Donut.”

8.4.1 Displacement Ductility for Specimen MCRP

An idealized elastoplastic curve was obtained through the method described in Section 2.7.1 and plotted with the average backbone curve, as shown in Figure 8.8. The yield displacement and corresponding yield force were 1.792 in. (45.52 mm) and 33.80 kips (150.35 kN), respectively. The ultimate displacement was 5.653 in. (143.59 mm), corresponding to a displacement ductility of the system equal to 3.15.

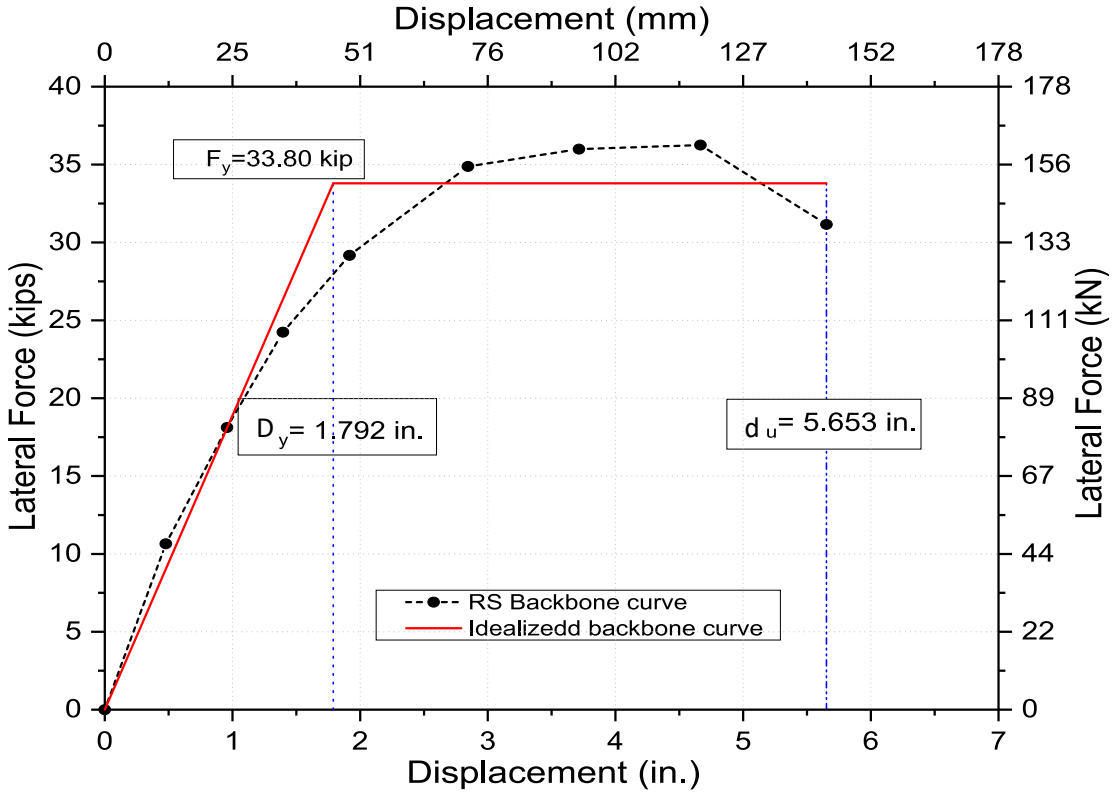

Figure 8.8 Modern code repaired (MCRP) displacement ductility

8.4.2 Plastic Rotation for Specimen MCRP

The plot of plastic rotation of the repaired wall pier was found using the procedure outlined in Section 2.7.2 and is shown in Figure 8.9. From this plot, it can be seen that the specimen reached 0.04 rad of plastic rotation before ultimate failure at 6% drift. The lateral load resistance is high; however, due to early unexpected brittle failure of the repaired specimen, we were unable to observe the true performance.

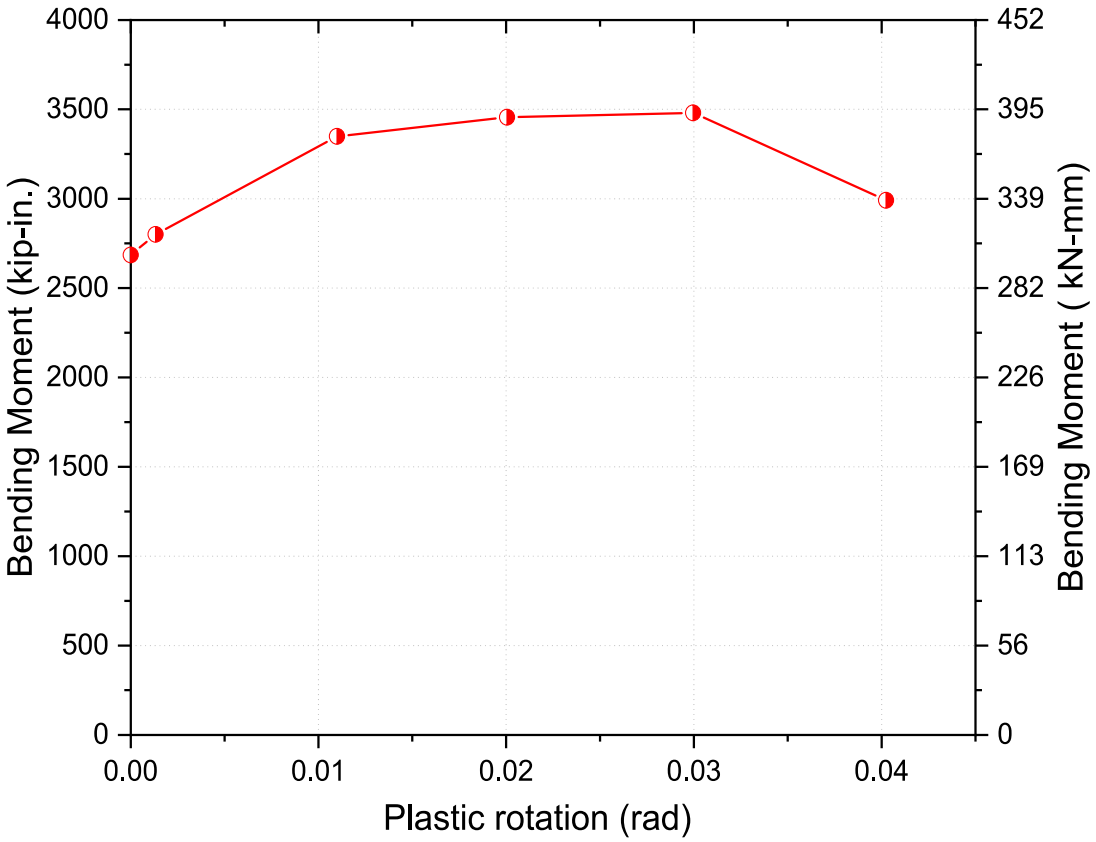

Figure 8.9 Plastic rotation plot of repaired specimen MCRP

8.4.3 Hysteretic Energy Dissipation for Specimen MCRP

Hysteresis loops are wide and stable without major strength degradation until the 6% drift ratio. The test ended at the end of the 6% drift ratio with a 37% drop in lateral force capacity of the specimen. Until 6% drift ratio, the hysteresis is symmetric in both directions dissipating a large amount of energy with wide hysteretic loops. Figure 8.10 shows the hysteresis obtained from the experiment.

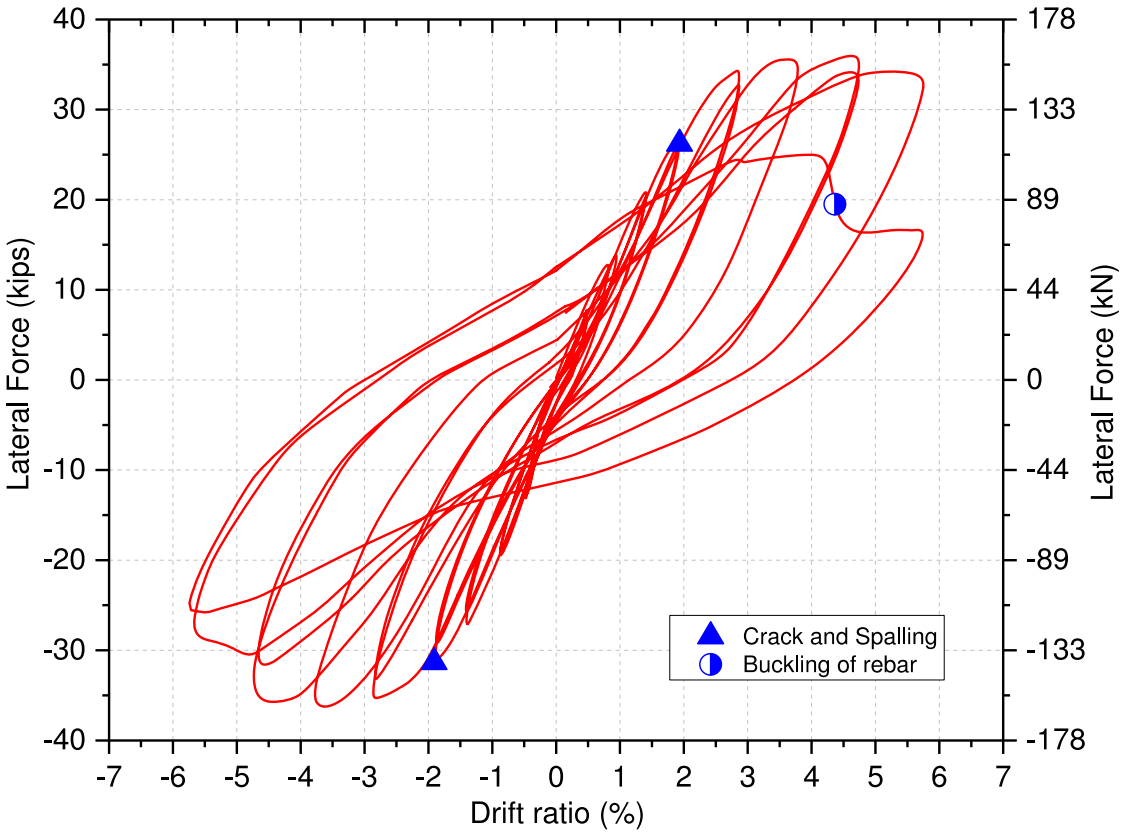

Figure 8.10 Hysteresis of repaired specimen MCRP

The cumulative hysteretic energy is obtained by adding the calculated hysteretic energy of all cycles and plotted against the drift ratio, as shown in Figure 8.11. The undulating curve signifies how energy is dissipated in each cycle. The specimen dissipated 1106.8 kip-in. of energy before failure at 6% drift ratio.

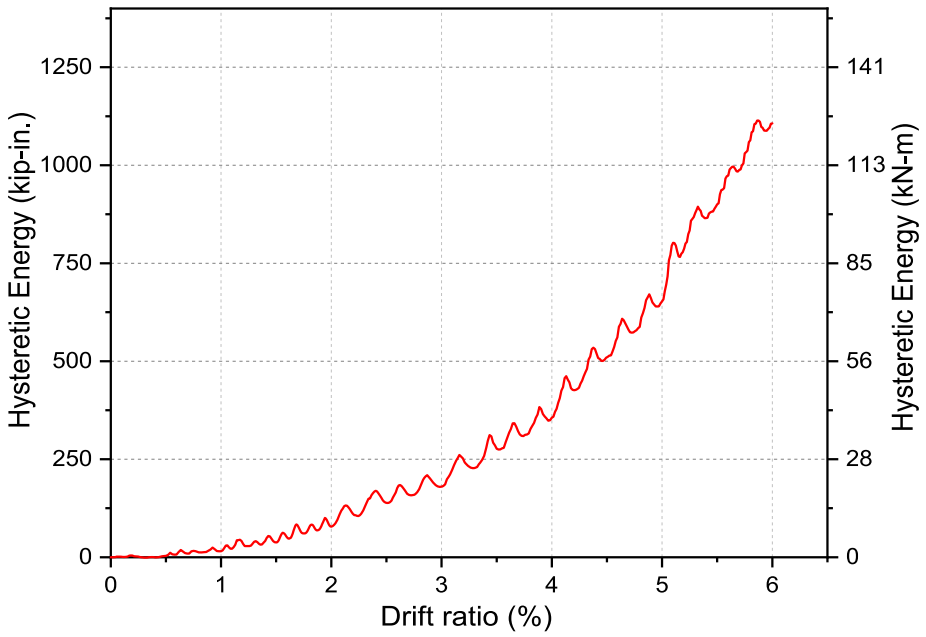

Figure 8.11 Cumulative energy dissipation of repaired specimen MCRP

8.4.4 Stiffness Degradation for Specimen MCRP

The obtained stiffness deterioration is plotted against drift ratio, as shown in Figure 8.12. The repaired specimen has high initial stiffness due to the added repair region.

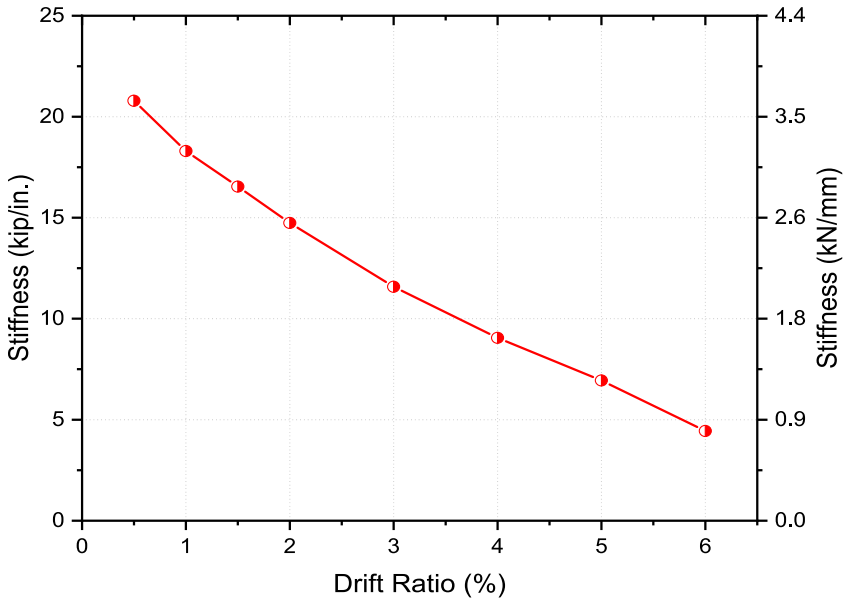

Figure 8.12 Stiffness deterioration of repaired specimen MCRP

8.4.5 Damage Index for Specimen MCRP

Damage assessment was performed according to the description in Section 2.7.5, The damage index was plotted against different damage levels, as shown in Figure 8.13. The obtained plot shows moderate damage degree after the 1% drift ratio. The repaired specimen was severely damaged after the 2% drift ratio. The specimen reached near collapse at 5% drift ratio and completely failed at 6% drift ratio.

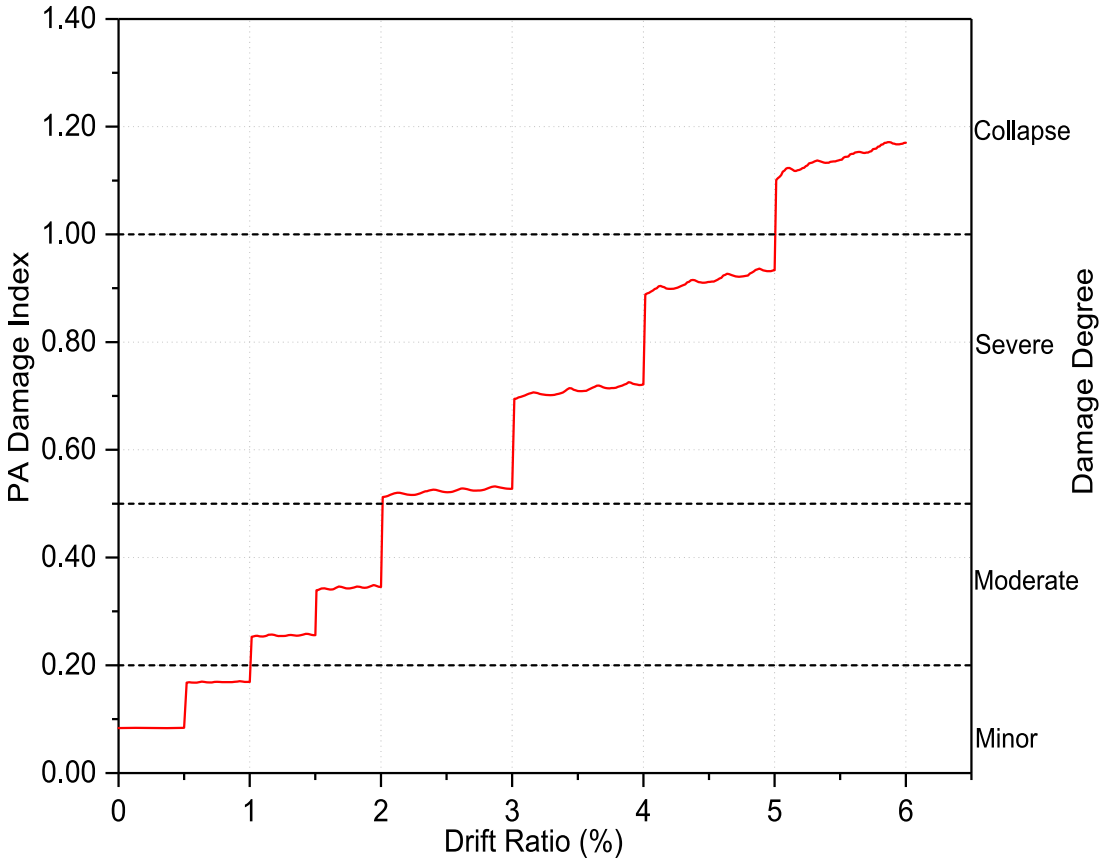

Figure 8.13 Damage Index of MCRP specimen

8.4.6 Physical Damage for Specimen MCRP

In the first load step of the 0.5% drift ratio, cracks of width 0.007 in. started to develop 2 in. from the top of repair along both faces of the wall. The cracks that developed previously started to widen up to 0.013 in. along the west face and to 0.01 in. along the east face of the wall in the second load step of the 1% drift ratio. At the 2% drift ratio, a new crack .003 in. wide was developed on the east face of the wall. The cracks present 2 in. from the top of the repair widened to 0.015 in. At 3% drift ratio, bottom cracks presented 2 in. above the CFRP shell widened to 0.025 in. along both faces of the wall pier. Concrete spalling started at the 4% drift ratio. Major structural cracks developed at this stage, and the cracks began to form a continuous loop around the wall pier.

At the 5% drift ratio, severe spalling started along both faces of the wall, as shown in Figure 8.14. Major cracks of width more than 0.05 in. were observed at 2 in., 6 in., and 10 in. from the top of the repair. In the first cycle of the 6% drift ratio, a slight drop in strength was observed in the pull direction. As a result, in the second cycle, the specimen failed by the buckling of the vertical bars in the push direction. This failure is shown in Figure 8.15. No damage was seen in the original plastic hinge location. The wall failed at a certain height above the repair region.

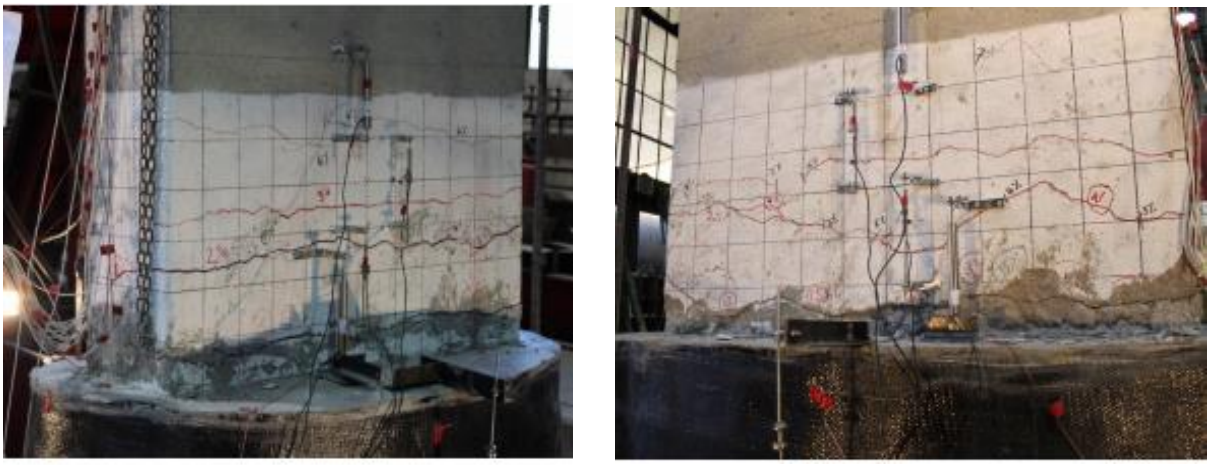

Figure 8.14 Experimental observation of specimen MCRP at a 5% drift ratio: (a) east side (b) west side

Figure 8.15 Experimental observation of specimen MCRP at a 6% drift ratio:
(a) east side and (b) west side

8.5 Performance of the Repair System for Specimen MCRP

8.5.1 Headed Steel Rebar Performance for Specimen MCRP

The headed steel bars were used to transfer the tensile force between the wall pier and footing. Strain gauges were placed on headed steel bars at 2 in. height from the top of the footing on both sides of the repaired specimen. According to the strain gauge data, the headed steel bars on the east face were strained more than those at the west face. At a 3.7% drift ratio, the middle headed steel bar on the east side reached a maximum 55% of the yield strain, whereas the middle headed rebar on the west side could only reach a maximum 36% of the yield strain.

8.5.2 CFRP Shell Performance for Specimen MCRP

The CFRP sheet composite wrap around the repair region provides the confinement and shear strength to the repair concrete and wall piers. The strain gauges were placed at 3 in., 8 in., 15 in., and 20 in. from the top of the CFRP shell to measure the hoop strain. Figure 8.16 shows that the hoop strain recorded on the east side of the wall pier is 0.07%, which is double in comparison to the west side whose reading shows 0.03%, showing more circumferential stress acting in the east side of the specimen. The major reason behind this is due to the difference in the tensile strain obtained by the headed bars in the respective face. The strain gauge placed at the top of the CFRP shell was located at a similar height to the top of the headed steel bars. Thus, it recorded the highest hoop strain in comparison to the strain gauges placed at other levels. This shows the CFRP shell contribution in obtaining the circumferential tension and shear strength of the repair region.

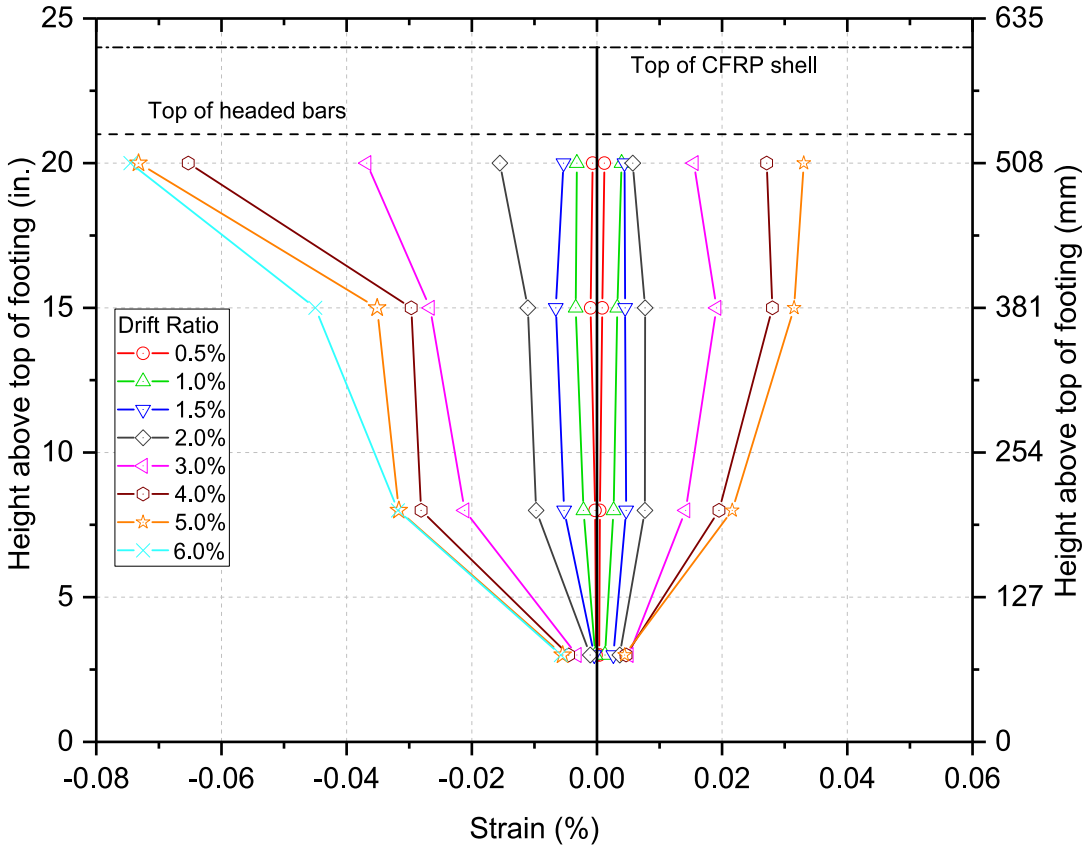

Figure 8.16 Hoop strain profile of CFRP donut shell of specimen MCRP

8.5.3 Performance of Steel Collar and Shear Studs for Specimen MCRP

No measured data was obtained from the steel collar and shear studs to study its performance. However, from a previous study (Wu and Pantelides 2017a), it can be said that the steel collar in association with the shear studs increased the bond between the original column concrete and repair grout inside the CFRP shell. This test confirms those findings since no failure was observed between original concrete and the repair grout.

8.6 Conclusion for Repaired Specimen MCRP

A rapid seismic repair method previously developed for reinforced concrete columns was used to repair the damaged concrete wall pier specimen. This method used a plastic hinge relocation technique. In the past, this method was successfully used to repair columns of circular or octagonal shape for low cross-section aspect ratio. For the first time, such a repair method has been successfully applied to restore the load-carrying capacity and stiffness of a damaged reinforced concrete wall pier with a cross-section aspect ratio of four. However, due to unexpected brittle buckling failure, the repaired specimen was unable to match the ductility of the undamaged specimen.

The repair system performed well in relocating the plastic hinge. No failure was observed in the repair system. However, once the plastic hinge was relocated above the original position, the specimen became less reinforced for the extra bending moment generated in the newly formed plastic hinge region. Hence, this was the major reason behind the relatively early brittle buckling failure of the repaired specimen. Even though the repaired specimen did not match the displacement capacity and energy dissipation of the modern code-compliant specimen, and considering the overall performance, the repair technique was successful in restoring the major characteristics of the modern code-compliant specimen.

Additional measures should be taken to prevent buckling failure. Additional CFRP wraps around the modern code-compliant wall pier specimen in the region above the relocated plastic hinge should be applied for buckling prevention. The experimental results are tabulated in Table 8.1.

Table 8.1 Performance for repaired specimen MCRP

Maximum Force (kip (kN))	36.42 (162)
Drift Ratio at Maximum Force (%)	5%
Maximum Drift Ratio (%)	6%
Maximum Displacement (in. (mm))	5.65 (143.51)
Number of Cycles	15
Energy Dissipation (kip-in. (kN-m))	1106.8 (125.05)

9. SUMMARY AND CONCLUSIONS

Four half-scale reinforced concrete bridge wall pier specimens were designed and built in the structures laboratory at the University of Utah. One specimen was designed according to modern seismic code guidelines (i.e., AASHTO LRFD Bridge Design Specifications and LRFD Seismic Bridge Design) and was named the "modern code compliant specimen." The other three specimens were a half-scale model of the as-built bridge wall pier and were named the "as-built specimens." The as-built specimens were built with seismic deficiencies, such as inadequate lap splices of longitudinal steel bars, inadequate transverse and longitudinal reinforcement, and inadequate seismic detailing to simulate the performance of the old reinforced concrete bridge wall piers.

The main aim of the research was to determine and compare performance of the modern code compliant and as-built deficient wall pier and to develop retrofit and repair methods to mitigate the seismic deficiencies either before or after a seismic event. One of the walls piers among the as-built specimens was tested in the as-built condition under quasi-static cyclic lateral loading and a constant axial load of 6% of the wall pier's axial load capacity. The performance of the as-built wall pier was then used for comparison to the retrofitted and repaired specimens. Also, under the same loading condition, the modern code compliant specimen was tested, and its performance was used to compare the effectiveness of the seismic repair of the modern code compliant specimen and retrofit of the as-built specimens. The performance of the specimens was evaluated under different seismic parameters such as ductility, energy dissipation, lateral load capacity, curvature profile, and stiffness degradation.

9.1 As-built Specimen

The as-built wall pier specimen had multiple deficiencies that resulted in the poor performance of the wall pier. These included inadequate length and confinement of lap splices of longitudinal reinforcement in the plastic hinge region, inadequate longitudinal and transverse steel reinforcement, and a lack of seismic detailing. The primary failure of the wall was slip and failure of the longitudinal lap splices in the plastic hinge region at the base of the wall. The as-built wall pier failed in the second push cycle of 6% drift ratio due to failure of the lap splices on the east side of the wall. The east side exhibited more damage than the west side of the wall pier because the test began with a "pull", stressing the east side of the wall first.

The as-built wall pier behaved poorly, and although it made it through 15 cycles of testing up to 6% drift, the energy dissipation of 500 kip-in. (56.54 kN-m) is 17.5% of the energy exhibited by the modern code compliant wall pier, which reached 2857 kip-in. (322.8 kN-m). The wall degraded its load resisting capacity rapidly and would have performed poorly, potentially collapsing, in the case of a strong earthquake. Although the ductility of the wall was 7.1, the wall was unable to resist more than 15.2 kips (67.6 kN), which is 50% of the modern code compliant wall pier's capacity of 31 kip (137.9 kN).

9.2 Modern Code Compliant Specimen

The modern seismic bridge design code clearly defines the design criteria for designing wall piers and columns. Bridge structures are designed such that under cyclic lateral load, the structural component undergoes concrete cracking, cover spalling, and reinforcement yielding with a significant amount of rotation in the plastic hinge regions. The modern AASHTO code prevents the splicing of longitudinal steel bars at the end regions where plastic hinges may develop during seismic activity. In addition, the minimum amount of transverse and longitudinal reinforcements is provided with proper seismic detailing. The provided opposite longitudinal steel bars are held together with seismic hooks, and the plastic hinge regions are confined with closely spaced transverse steel ties.

The modern code compliant specimen failed on the first push cycle of the 10% drift ratio. Failure was due to fracture of a single longitudinal steel bar on the west face of the wall. Low-cycle fatigue was the main reason for fracture of the longitudinal bar. The specimen dissipated a large amount i.e., 2857 kip-in. (323 kN-m) of energy and achieved a displacement ductility of 5.3 with 31 kip (138 kN) of lateral load capacity. A smooth curvature profile and gradual degradation of stiffness were observed through data analysis. A finite element model was created using OpenSees to predict lateral load capacity and match the cyclic hysteresis obtained from the experiment. The pushover and cyclic hysteretic models closely matched the experimental results. This specimen performed very well under reverse cyclic lateral loads regarding different seismic parameters such as energy dissipation, ductility, lateral load capacity, and stiffness degradation. The failure mode was a ductile failure with fracture of a single longitudinal steel bar at the 10% drift ratio.

9.3 Retrofitted As-built Specimen Using CFRP Vertical Anchors (R1)

The second as-built wall pier was retrofitted using a combination of CFRP anchors applied vertically into the footing to increase flexural resistance, and horizontally into the wall face to increase shear resistance and confinement of the lap splices. The anchorage performance was enhanced by the application of CFRP jacketing in both the vertical and hoop direction to further increase confinement and distribute the flexural demand across the wall face.

The pier lost load in the first cycle of 2% drift ratio due to failure of multiple CFRP vertical anchors on the west side of the wall. The east side exhibited more physical damage than the west side of the wall pier because the anchor failures began on the east side, which transferred stress to the west side and allowed more damage to accrue throughout the remainder of the test. The retrofit specimen performed better than the as-built, even though it lost 20% of its lateral force resistance after 2% drift ratio. The retrofit wall piers' energy dissipation of 816 kip-in. (92.2 kN-m) is 1.6 times more than the as-built wall pier, which only reached 500 kip-in. (56.5 kN-m). The wall reached 2% drift with double the stiffness and 48% more lateral load resistance compared to the as-built specimen.

9.4 Retrofitted As-built Specimen Using CFRP NSM Rods (R2)

The third as-built wall pier was retrofitted using a combination of CFRP Near Surface Mounted (NSM) rods, horizontal CFRP anchors, and CFRP jacket layers. The main objective of the retrofit was to strengthen the as-built specimen so that its seismic performance including flexural capacity, lateral load carrying capacity, and stiffness would be improved and be comparable to the modern code compliant specimen.

The initial bond failure between two of the CFRP NSM rods and adhesive on the west face of the retrofitted specimen in the first cycle of 1.5% drift ratio was the starting cause of loss of lateral load, which ultimately led to failure of the specimen at 5% drift ratio. The silica fume-added epoxy adhesive was manually applied to the drilled holes and CFRP NSM rods, instead of using the pressurized silicone gun. This resulted in the variable application of adhesive on at least two of the CFRP NSM rods, which resulted in premature bond failure at 1.5% drift ratio. The lateral load-carrying capacity of the retrofitted specimen was 25 kips (113kN), which was175% and 84% of the lateral capacity of the as-built and modern code compliant specimens, respectively. The curvature profile of the retrofitted specimen was small, showing the higher stiffness of the retrofitted specimen. In addition, before failure, the retrofitted specimen dissipated 827 kip-in. (93.4 kN-m) of hysteretic energy, which is 166% and 29% of the total hysteretic energy dissipated by the as-built and modern code compliant specimens, respectively.

9.5 Repaired As-built Specimen Using Steel NSM Bars and CFRP Anchors and Wraps (ABRP)

The first as-built wall pier was repaired after damage from testing. This repair used steel NSM bars embedded vertically into the footing and up the wall face to increase flexural resistance. CFRP anchors were also used horizontally through, the wall face to increase shear resistance and confinement of the lap-splices. The anchors and steel NSM bars performance were enhanced by application of CFRP jacketing in the hoop direction to further increase confinement of the lap-splices and ensure debonding did not occur.

The repaired wall pier failed in the second cycle of the 4% drift ratio due to debonding of the steel NSM bars. The west side of the wall pier exhibited more physical damage than the east side because the majority of damage from the as-built test was on the east wall face. Therefore, the west face of the wall had to resist more lateral load as it had more strength resistance prior to the repair test. The repaired specimen performed better than the as-built even though it lost 20% of its lateral force resistance after 4% drift. The energy dissipation of 452 kip-in. (51.2 kN-m) is 0.9 times that of the as-built wall pier, which reached 500 kip-in. (56.5 kN-m). However, the repaired wall had a cumulative energy dissipation of 239 kip-in. (27.0 kNm) at the end of the 3% drift ratio, which is two times larger than the as-built 120.7 kip-in. (13.6 kN-m) energy dissipation at the end of 3% drift. The repaired wall reached 4% drift with 128% the stiffness and 127% the lateral force resistance compared to the as-built specimen. Although the retrofit pier walls' failure is categorized as brittle, it performed better than the as-built until failure. Overall, the steel NSM bars in conjunction with the CFRP system worked well.

9.6 Repaired Modern Code Compliant Specimen Using CFRP Donut (MCRP)

The modern code-compliant damaged wall pier was repaired using a plastic hinge relocation technique. This technique relocates the plastic hinge from the damaged region to an undamaged region of the wall pier. The damaged region was strengthened with a prefabricated CFRP shell with epoxy-anchored headed steel bars, a steel collar with embedded steel studs, and the void in between the shell and wall filled with expansive cement concrete. The major objective of the repair was to restore stiffness and lateral load-carrying capacity of the damaged region of the wall pier.

Due to brittle buckling failure of longitudinal steel bars above the relocated plastic hinge region, the repaired specimen failed on the second push cycle of the 6% drift ratio. The repair system performed very well in relocating the plastic hinge, and no failure was observed in the repair system. The relocation of the plastic hinge to the undamaged region reduced the moment arm, which resulted in the extra bending moment and shear force in that region. Considering the confinement reinforcement of the relocated plastic hinge region, the repaired specimen had wide-spaced and insufficient transverse reinforcement in comparison to the extra bending moment generated and was the major cause behind the buckling failure. Before failure, the repaired specimen dissipated 1107 kip-in. (125 kN-m) of hysteretic energy, which is 39% of the total energy dissipated by the undamaged current code compliant specimen. The repaired specimen achieved a displacement ductility of 3.2, which is greater than the minimum local displacement ductility capacity of 3.0 set by Caltrans.

Hence, the damaged modern code compliant wall pier specimen could be repaired using the column plastic hinge relocation technique to restore stiffness and lateral load carrying capacity. However, considering the failure mechanism, the confining pressure and spacing of the transverse reinforcement above the relocated plastic hinge region should be checked to improve performance from the repair and to avoid brittle failure.

REFERENCES

AASHTO. (1973). Standard Specifications for Highway Bridges. American Association of State Highway and Transportation Officials, Washington, DC.

AASHTO. (2011). AASHTO Guide Specifications for LRFD Seismic Bridge Design. American Association of State Highway and Transportation Officials, Washington, DC.

AASHTO. (2012). AASHTO LRFD Bridge Design Specifications, 6th Edition. Transportation, American Association of State Highway and Transportation, Atlanta, GA.

Aboutaha, R. S., Engelhardt, M. D., Jirsa, J. O., and Kreger, M. E. (1999). "Experimental investigation of seismic repair of lap splice failures in damaged concrete columns." ACI Structural Journal, 96(2), 297–306.

American Concrete Institute Committee 318 (2014). Building Code Requirements for Structural Concrete (ACI 318-14) and Commentary (ACI 318R-14). American Concrete Institute, Farmington Hills, MI.

American Concrete Institute 440 (2004). "Guide for the design and construction of externally bonded FRP systems for strengthening existing structures." ACI 440, Farmington Hills, MI: ACI.

American Institute of Steel Construction. (2016). ANSI / AISC 360-16, specification for structural steel buildings. American Institute of Steel Construction.

Bournas, D. (2011). "Bond strength of lap-spliced bars in concrete confined with composite jackets." Journal of Composites for Construction, 15(2), 156-167.

Bournas, D. A., and Triantafillou, T. C. (2009). "Flexural strengthening of reinforced concrete columns with near-surface-mounted FRP or stainless steel." ACI Structural Journal, 106 (4), 495-505.

Bournas, Dionysios A., Pavese, A., and Tizani, W. (2015). Tensile capacity of FRP anchors in connecting FRP and TRM sheets to concrete. Engineering Structures, 82, 72–81. https://doi.org/10.1016/j.engstruct.2014.10.031.

Bousias, S., Spathis, A. L., and Fardis, M. N. (2007). "Seismic retrofitting of columns with lap spliced smooth bars through FRP or concrete jackets." Journal of EarthquakeEngineering, 11(5), 653–674.

De Lorenzis, L., and Nanni, A. (2002). "Bond between near-surface mounted fiberreinforced polymer rods and concrete in structural strengthening." ACI Structural Journal, 99(2), 123–132.

De Lorenzis, L., and Teng, J. G. (2007). "Near-surface mounted FRP reinforcement: An emerging technique for strengthening structures." Composites Part B: Engineering, 38(2), 119–143.

Elsanadedy, H. M., and Haroun, M. A. (2005). "Seismic design criteria for circular lapspliced reinforced concrete bridge columns retrofitted with fiber-reinforced polymer jackets." ACI Structural Journal, 102(3), 354-362.

Faustino, P., and Chastre, C. (2016). "Damage effect on concrete columns confined with carbon composites." ACI Structural Journal, 113(5), 951–962.

Galati, D., and De Lorenzis, L. (2009). “Effect of construction details on the bond performance of NSM FRP bars in concrete.” Advances in Structural Engineering,12(5), 683–700.

Ghosh, K. K., and Sheikh, S. A. (2007). “Seismic upgrade with carbon fiber reinforced polymer of columns containing lap-spliced reinforcing bars.” ACI Structural Journal, 104 (2), 227-236.

Hantouche, E. G., Harajli, M., Haddadin, F., and Elsouri, A. (2015). “Seismic strengthening of bond-critical regions in wall-type bridge piers using active confinement.” Journal of Bridge Engineering, 20(11), 1–12.

Harajli, M. H. (2009). “Bond strengthening of lap spliced reinforcement using external FRP jackets: An effective technique for seismic retrofit of rectangular or circular RC columns.” Construction and Building Materials, 23 (3), 1265-1278.

Harajli, M. H., and Dagher, F. (2008). “Seismic strengthening of bond-critical regions in rectangular reinforced concrete columns using fiber-reinforced polymer wraps.” ACI Structural Journal, 105 (1), 68-77.

Harries, K. A., Ricles, J. R., Pessiki, S., and Sause, R. (2006). “Seismic retrofit of lap splices in nonductile square columns using carbon fiber-reinforced jackets.” ACI Structural Journal, 103(6), 874-884.

Hassan, T., and Rizkalla, S. (2004). Bond mechanisms of near surface mounted FRP bars and strips for flexural strengthening of concrete structures.” ACI Structural Journal,101(6) 830-839.

Hawkins, N. M., Gamble, W. L., Shkurti, F. P., & Lin, Y. (2000). Seismic Strengthening of Inadequate Length Lap Splices. Proc. 12th World Conference on Earthquake Engineering, Auckland, New Zealand, Paper No., 1–7.

Hose, Y.D., Priestley, M.J.N., and Seible, F. (1997). “Strategic relocation of plastic hinges in hinge columns.” Caltrans Report No. SSRP-97/05. Division of Structural Engineering, Univ. of California, San Diego, La Jolla, CA.

Jiang, S. F., Zeng, X., Shen, S., and Xu, X. (2016). “Experimental studies on the seismic behavior of earthquake-damaged circular bridge columns repaired by using combination of near-surface-mounted BFRP bars with external BFRP sheetsjacketing.” Engineering Structures, 106, 317–331.

Kim, I., Jirsa, J. O., and Bayrak, O. (2009). Use of CFRP anchors to strengthen lap splices of rectangular RC columns. Frprcs - 9, 60(July), 1–5.

Kim, I. S., Jirsa, J. O., and Bayrak, O. (2011). “Use of carbon fiber-reinforced polymer anchors to repair and strengthen lap splices of reinforced concrete columns.” ACI Structural Journal, 108(5), 630–640.

Mahini, S. S., and Ronagh, H. R. (2011). “Web-bonded FRPs for relocation of plastic hinges away from the column face in exterior RC joints.” Composite Structures, Elsevier Ltd, 93(10), 2460–2472.

Mander, J. B., and Priestley, M. J. N. (1989). “Theoretical stress-strain model for confined concrete.” Journal of Structural Engineering, 114(8), 1804-1826.182

McKenna, F., Fenves, G., and Scott, M. (2014). “Open System for Earthquake Engineering Simulation (OpenSees).” Univ. of California, Berkeley, CA. (http://opensees.berkeley.edu).

Mitchell, D., Sexsmith, R., and Tinawi, R. (1994). Seismic retrofitting techniques for bridges - a state-of-the-art report. Canadian Journal of Civil Engineering, 49(6), 881–898.

Moran, D. A., and Pantelides, C. P. (2012). “Elliptical and circular FRP-confined concrete sections: A Mohr-Coulomb analytical model.” International Journal of Solids and Structures, Elsevier Ltd, 49(6), 881–898.

Moran, D. A., Pantelides, C. P., and Reaveley, L. D. (2019). “Mohr-Coulomb model for rectangular and square FRP-confined concrete.” Composite Structures, 209,889–904.

Nye, T. K., Pantelides, C. P., and Alkhradji, T. (2018). “Bidirectional GFRP-composite connections between precast concrete wall panels under simulated seismic load.” Journal of Composites for Construction, 22(4), 1–13.

Pantelides, C.P., and Gergely, J. (2002). “Carbon-fiber-reinforced polymer seismic retrofit of RC bridge bent: design and in-situ validation.” J. Compos. Constr., 6(1), 52-60.

Park, Y., and Ang, A. H. -S. (1985). “Mechanistic seismic damage model for reinforced concrete.” Journal of Structural Engineering, 111(4), 722–739.

Parks, J. E., Brown, D. N., Ameli, M. J., and Pantelides, C. P. (2016). “Seismic repair of severely damaged precast reinforced concrete bridge columns connected with grouted splice sleeves.” ACI Structural Journal, 113(3), 615–626.

Perrone, M., Barros, J. A. O., and Aprile, A. (2009). “CFRP-based strengthening technique to increase the flexural and energy dissipation capacities of RC columns.” Journal of Composites for Construction, 13(5), 372–383.

Popovics, S. (1973). “A numerical approach to the complete stress-strain curve of concrete.” Cement and Concrete Research, 3(5), 583-599

Priestley, M. J., Seible, F., & Calvi, G. M. (1996). Seismic Design and Retrofit of Bridges. https://doi.org/10.1002/9780470172858

Rabbat, B. G., & Russell, H. G. (2008). Friction Coefficient of Steel on Concrete or Grout. Journal of Structural Engineering, 111(3), 505–515. https://doi.org/10.1061/(asce)0733-9445(1985)111:3(505)

Rutledge, S. T., Kowalsky, M. J., Seracino, R., and Nau, J. M. (2014). “Repair of reinforced concrete bridge columns containing buckled and fractured reinforcement by plastic hinge relocation.” Journal of Bridge Engineering, 19(8), A4013001.183

Seible, F., Priestley, M. J. N., Hegemier, G. A., and Innamorato, D. (1997). Seismic Retrofit of RC Columns with Continuous Carbon Fiber Jackets. Journal of Composites for Construction, 1(2), 52–62. https://doi.org/10.1061/(asce)1090-0268(1997)1:2(52)

Seifi, A., Hosseini, A., Marefat, M. S., and Khanmohammadi, M. (2018). “Seismic retrofitting of old-type RC columns with different lap splices by NSM GFRP and steel bars.” Structural Design of Tall and Special Buildings, 27(2), 1–21.

Sharaky, I. A., Torres, L., Baena, M., and Vilanova, I. (2013). “Effect of different material and construction details on the bond behaviour of NSM FRP bars in concrete.” Construction and Building Materials, 38(June), 890–902.

Vrettos, I., Kefala, E., and Triantafillou, T. C. (2013). Innovative flexural strengthening of reinforced concrete columns using carbon-fiber anchors. ACI Structural Journal, 110(1), 63–70.

Wu, R. Y., and Pantelides, C. P. (2017a). “Rapid seismic repair of reinforced concrete bridge columns.” ACI Structural Journal, 114(5), 1339–1350.

Wu, R. Y., and Pantelides, C. P. (2017b). “Rapid repair and replacement of earthquakedamaged concrete columns using plastic hinge relocation.” Composite Structures, 180, 467–483.

Yan, Z., and Pantelides, C. P. (2011). “Concrete column shape modification with FRP shells and expansive cement concrete.” Construction and Building Materials, 25(1), 396–405.